UNIVERSITY OF CALIFORNIA, SAN DIEGO

Distinct Functions of Negative Regulators of NF-kappaB

A dissertation submitted in partial satisfaction of the
requirements for the degree of Doctor of Philosophy

in

Chemistry

by

Jeffrey D. Kearns

Committee in charge:

Professor Alexander Hoffmann, Chair
Professor Michael Burkart
Professor Daniel J. Donoghue
Professor Jeff Hasty
Professor Robert Tukey

2009

The dissertation of Jeffrey D. Kearns is approved, and it is acceptable in quality and form for publication on microfilm and electronically

_____

_____

_____

_____

_____

Chair

University of California, San Diego

2009

DEDICATION

This thesis is dedicated to my family.

To my mother and father who taught me, much to the detriment of their sanity and patience, to ask "Why?" To my brothers who showed me that you need to excel to get any attention. And most of all, to my wife and daughter. To Mayumi who has stood by my side for almost a decade and without whom these five years in graduate school would not have been possible. To Emi who teaches me a little more everyday about how to be a better person and whose picture on my computer desktop is a constant source of comfort and motivation.

EPIGRAPH

We don't get a chance to do that many things,
and every one should be really excellent…

So this is what we've chosen to do with our life…

So it better be [darn] good. It better be worth it.

And we think it is.

Steve Jobs, CEO Apple Inc.

TABLE OF CONTENTS

LIST OF ABBREVIATIONS

50:50	p50:p50 NF-κB homodimer
A:A	RelA:RelA NF-κB homodimer
A:50	RelA:p50 NF-κB heterodimer
A20	TNF-associated interacting protein 3
C1	Tumor Necrosis Factor Receptor Signaling Complex Type 1
CHX	Cyclohexamide
DMEM	Dulbecco modified essential media
DTT	Dithiothreitol
EDTA	Ethylenediamenetetracetic acid
EMSA	Electromobility Shift Assay
IκBα	Inhibitor of kappaB alpha
IκBβ	Inhibitor of kappaB beta
IκBε	Inhibitor of kappaB epsilon
IκBδ	Inhibitor of kappaB delta
IKKα	Inhibitor of kappaB kinase α (synonymous with IKK1)
IKKβ	Inhibitor of kappaB kinase β (synonymous with IKK2)
IKK1	Inhibitor of kappaB kinase 1 (synonymous with IKKα)
IKK2	Inhibitor of kappaB kinase 2 (synonymous with IKKβ)
IKKK	Inhibitor of kappaB kinase (IKK) kinase
IL-1β	Interleukin-1 beta
LPS	Lipopolysaccharide
LTβR	Lymphotoxin beta receptor (TNFR superfamily member3)
MEF	Murine Embryonic Fibroblast
NEMO	NF-κB Essential Modulator
NEMO/IKK2	IKK complex consisting of NEMO and IKK2/2 or IKK2/1 dimer
NF-κB	Nuclear Factor kappaB
NIK	NF-κB-Inducing Kinase
NIK/IKK1	IKK complex consisting of NIK and IKK1 homodimer
ODE	Ordinary Differential Equation
PMSF	Phenylmethylsulfonyl fluoride
RPA	RNase Protection Assay
TNF	Tumor Necrosis Factor
TNFR1	TNF Necrosis Factor Receptor Type 1
TNFR2	TNF Necrosis Factor Receptor Type 2
TRADD	TNFR-Associated Death Domain
TRAF	TNFR-Associated Factor
RIP	Receptor Interacting Protein
WT	Wild type

LIST OF FIGURES

LIST OF TABLES

ACKNOWLEDGEMENTS

I arrived in San Diego in the September of 2003 with the expectation that I would lab tech for two years while my wife attended graduate school and then move elsewhere for my own graduate school training. Much has happened between now and then and there are many people who I would like to acknowledge.

I would like to express my thanks to Professor Alexander Hoffmann. He hired me, a recent B.S. graduate with no lab experience, as a lab tech even though I pulled a bonehead move by showing up for the interview with his 2002 Science paper stapled out of order. With Alex's help, I applied for the graduate program and then joined his lab. Over the years Alex has provided invaluable mentorship and I am thankful for the opportunities that he made available to collaborate with others within and outside the lab.

As a founding member of the Signaling Systems Laboratory (SSL), I have a special appreciation for those who have been my colleagues since the first year. Our esteemed 'Senior Postdoc,' Soumen Basak, deserves particular recognition. We were the first two members of the lab and he took it upon himself to teach an unlearned lab tech how to be a scientist. Soumen continued to provide guidance and friendship throughout my graduate career and I am grateful to him for his efforts. I only hope he can find a good hamburger after he moves back to India. Shannon Werner was the first graduate student to join the lab and was a fellow transplant from the tropical paradise of the Commonwealth of Massachusetts. In addition to years of banter, I also had a great deal of fun during our collaboration on the 2008 G&D paper.

Some later members of the SSL also deserve personal acknowledgement. Derren Barken, the lab's first Ph.D. student to graduate, helped me to transition from molecular to mechanistic/kinetic modeling and provided critical assistance in the early years. Ellen O'Dea, a fellow Class of 2004 biochemistry graduate student, was a great labmate who could be counted on to supply scientific knowledge and inappropriate jokes in equal measures. She is also to be commended for being the only experiment-focused lab member to dip her toes in the computational modeling field. Vincent Shih, I fear, is forever traumatized by my attempts to teach him American-style slang in his first 6 months here. He recovered enough sanity by his third year in graduate school to form a productive collaboration with me for his 2009 PNAS article. The members of the SSLSO (aka, the Signaling Systems Laboratory Siberian Outpost in NSB 4318) made my last year more enjoyable—Paul Loriaux, Marcelo Behar, and Benedicte Mengel. My thanks to all of the other "Hoffmorons" (hey, it worked for the Baltimore lab!) who provided guidance or at the very least made my time in the lab just a little more interesting.

Life does in fact exist outside of the SSL and I'd like to thank some other UCSD people for their support. Professors Gouri Ghosh and Betsy Komives were always excellent sounding boards as I teetered between the fields of biochemistry and biophysics. My appreciation to professors Donoghue, Burkart, Tukey, and Hasty for their guidance as members of my thesis committee. Erika Mathes, Olga Savinova, and Jessica Ho were great lab neighbors. The Molecular Biophysics Training Grant (professors Susan Taylor, Andrew McCammon, *et al.*) provided 2 years of research funding as well as pizza dinner every month while we listened to some really

interesting biophysics seminars. My gratitude also extends outside of the UCSD community to the American Heart Association (Western States Affiliate) who provided the remaining 2 years of funding and inspired me to look outside the basic science bubble.

The SSL integrates computational/mechanistic modeling with experimental studies to study the dynamics of cell signaling. As such, our work is often highly collaborative. The research described in my dissertation is published or in preparation for submission and my collaborators are cited in both the text and acknowledgements of each chapter. Permission has been extended to include this material. My thanks to all of these collaborators. I'd like to acknowledge my colleagues with whom I share authorship. Alexander Hoffmann provided insightful discussions, research direction, and contributed to the writing of each of these manuscripts. Chapter 1 is adapted from work published in the Journal of Biological Chemistry (2009) on which I was the primary author. Chapter 3 is based upon work published in the Journal of Cell Biology (2006) for which I was primary author. Soumen Basak, Shannon Werner, and Christine Huang contributed experimental data. A section of Chapter 3 is based upon work in preparation for submission for which I contributed experimental data. Diane Longo is primary author and professors Jeff Hasty and Lev Tsimring contributed research direction. Chapter 4 is based upon work published in Genes and Development (2009) on which I share co-primary authorship with Shannon Werner. Victoria Zadorozhnaya, Candace Lynch, and Elen O'Dea contributed experimental data. Professors Mark Boldin, Averil Ma, and David Baltimore contributed reagents. Chapter 5 is based upon two published studies—the first in Cell (2007) on which

Soumen Basak is primary author and the second in Proceedings of the National Academy of Sciences on which Vincent Shih is primary author. I contributed computational simulations to both manuscripts. For the *Cell* manuscript, Hana Kim, Ellen O'Dea, Shannon Werner and professors Vinay Tergaonkar, Chris Benedict, Carl Ware, and Inder Verma provided experimental data, critical insights, and/or reagents. For the *PNAS* manuscript, Olga Savinova provided experimental data and Professor Gouri Ghosh provided insightful discussions. Chapter 6 is based upon work in preparation for submission. Candace Lynch, Soumen Basak, and Kim Ngo provided experimental data. Soumen Basak provided critical discussions as well.

This dissertation is dedicated to my family, and they deserve an acknowledgement as well. Thank you for years of love and support. Mayumi and Emi, my two favorite ladies, I can't wait to start our new adventure together in Boston!

VITA

2003 Bachelor of Science, Biology. Haverford College.

2006 Master of Science, Chemistry. University of California, San Diego.

2009 Doctor of Philosophy, Chemistry. University of California, San Diego.

PUBLICATIONS

Barken D (*), Wang CJ (*), **Kearns JD**, Cheong R, Hoffmann A, Levchenko A. (2005) "Comment on 'Oscillations in NF-κB signaling control dynamics of gene expression'" Science. **308**:52

Kearns JD, Basak S, Werner SL**,** Huang CS, Hoffmann A. (2006) "IκBε provides negative feedback to control NF-κB oscillations, signaling dynamics and inflammatory gene expression." J Cell Biol. **173:** 659-664

Basak S, Kim H, **Kearns JD**, Tergaonkar V, O'Dea E, Werner SL, Benedict CA, Ware CF, Ghosh G, Verma IM, Hoffmann A. (2007) "A fourth IκB protein within the NF-κB signaling module." Cell. **128:** 369-381

O'Dea EL, Barken D, Peralta RQ, Tran KT, Werner SL, **Kearns JD**, Levchenko A, Hoffmann A. (2007) "A homeostatic model of IκB metabolism to control NF-κB constitutive activity." Mol Syst Biol. **3: 111**:1-7

Fusco AJ, Savinova OV, Talwar R, **Kearns JD**, Hoffmann A, Ghosh G. (2008) "Stabilization of RelB requires multidomain interactions with p100/p52." J Biol Chem. **283**:12324-12332

O'Dea EL, **Kearns JD**, Hoffmann A. (2008) "UV as an amplifier rather than inducer of NF-κB activity." Mol Cell. **30**:632-641

Werner SL (*), **Kearns JD** (*), Zadorozhnaya V, Lynch C, O'Dea E, Boldin MP, Ma A, Baltimore D, Hoffmann A. (2008) "Encoding NF-κB temporal control in response to TNF: distinct roles for the negative regulators IκBα and A20." Genes and Dev. **22:** 2093-2101

Kearns JD and Hoffmann A. (2009) "Integrating computational and biochemical studies to explore mechanisms in NF-κB signaling." J Biol Chem. **284:** 5439-5443

Shih VF-S, **Kearns JD**, Basak S, Savinova OV, Ghosh G, Hoffmann A. (2009) "Kinetic control of negative feedback regulators of NF-κB determine pathogen- and cytokine-receptor signaling specificity." Proc Natl Acad Sci USA (*in press*)

Wuerzberger-Davis SM (*), Chen Y (*), Tang DT (*), **Kearns JD**, Bates PW, Lynch C, Ladell NC, Yu M, Podd A, Zeng H, Wen R, Hoffmann A, Wang D, Miyamoto S. "*In vivo* role of IκBα nucleocytoplasmic shuttling." (Submitted)

Kearns JD, Lynch C, Basak S, Ngo K, Hoffmann A. "IκB isoforms regulate the generation of distinct RelA/NF-κB Dimers." (In Preparation)

Longo D, **Kearns JD**, Hoffmann A, Hasty J, Tsimring LS. "Dual-delayed feedback provides sensitivity and robustness to the NF-κB signaling module." (In Preparation)

(*) These authors contributed equally to this work

ABSTRACT OF THE DISSERTATION

Distinct Functions of Negative Regulators of NF-kappaB

by

Jeffrey D. Kearns

Doctor of Philosophy in Chemistry

University of California, San Diego, 2009

Professor Alexander Hoffmann, Chair

The Nuclear Factor kappaB (NF-κB) signaling pathway is central to cellular responses to a diverse set of stimuli and stresses. It has been shown that much of this pleiotropic capacity is encoded within the activation dynamics of the upstream IκB Kinase (IKK), which acts as a central hub for NF-κB signaling. To account for how regulatory mechanisms impart specific NF-κB dynamics in response to IKK activity, I utilized a multidisciplinary approach that integrated mechanistic mathematical modeling with laboratory experimentation. Herein, I describe four pair wise comparisons between NF-κB inducible IκBα protein, the predominant regulatory mechanism, with others mediated by IκBβ, IκBε, IκBδ and A20. IκBε and A20 are shown to primarily regulate the second phase of TNF responsive NF-κB activity by

dampening oscillatory behavior and tuning the amplitude, respectively. Differences in inducible synthesis and stimulus-responsive degradation kinetics are determined to impart specific functionalities for IκBα and IκBδ negative feedback in acute/inflammatory versus chronic/pathogenic NF-κB signaling. In the final study, the role of IκBβ, a constitutive regulator, is delineated as mediating the distribution of RelA/NF-κB dimers in the resting cell but not their dynamics following cellular stimulation. These studies reveal the individual role of each mechanism, and collectively, the sources and functionalities of the emergent systems properties observed in cells in which these regulators act combinatorially.

Chapter 1

Introduction

DECIPHERING THE DYNAMICS OF CELLULAR SIGNALING

Signal transduction networks regulate cellular function and respond to changes in intra- and intercellular environments. They control both homeostatic and stimulus-induced responses. However, the role and importance of individual network components in the function of the network are often difficult to discern. This is evident when a genetic deletion or mutation does not show an expected phenotype or when a pharmacological treatment has surprising effects.

Computational simulations with networks reconstructed *in silico* as mathematical equations enable functional analysis of network behavior and are well suited to complement *in vivo* and *in vitro* studies (Alon, 2007; Eungdamrong and Iyengar, 2004; Kholodenko, 2006; Palsson, 2006). The utility of integrating experimental and computational methodologies derives from the iterative application of each approach to inform the other. Experimental analyses provide critical insight to select the components and reactions to include in the computational model and to constrain the simulation parameters. In turn, the computational analyses provide mechanistic insights to generate hypotheses and drive further experimental analyses. Studies of the *lac* operon in *E. coli* are often cited as original examples of this integrated approach wherein a simple set of mathematical equations was sufficient to account for the transcriptional negative feedback of the *lac* operon (Novick and Weiner, 1957). In eukaryotic systems, developmental, cell-cycle control, and circadian rhythm processes in several organisms have been examined and validated *in silico* (Davidson *et al*, 2002; Fuss *et al*, 2005; Ingolia, 2004; Leloup and Goldbeter, 2003;

Robertson *et al*, 2007). Models of protein kinase cascades have produced important insights such as amplification and temporal fidelity, bistability, and signaling crosstalk (Heinrich *et al*, 2002).

More recently, advances in the newly minted field of Systems Biology have produced increasingly complete cellular *parts lists* that have enabled statistical modeling to reconstruct large scale molecular interaction networks (Beyer *et al*, 2007; Ng *et al*, 2006). However, the resulting models are largely non-quantitative and do not consider the temporal dimension, although these aspects are essential to biological regulation (Kholodenko, 2006). With *Top-Down* network reconstruction efforts identifying functional modules, biochemical *Bottom-Up* approaches are critical for providing mechanistic detail. This is where kinetic computational modeling of molecular networks may function as an important bridge for these distinct approaches.

THE NF-κB TRANSCRIPTION FACTOR SIGNALING NETWORK

The NF-κB family of transcription factors are central mediators of cellular responses to inflammatory, developmental, and stress cues (Hoffmann and Baltimore, 2006a)(Figure 1.1). Misregulation of NF-κB signaling has severe health consequences and untangling the combinatorial complexity of the NF-κB network is likely to have broad biomedical impact in understanding disease and devising therapeutic strategies (Tergaonkar, 2006). For instance, persistent elevated NF-κB activity is associated with chronic inflammatory diseases such as rheumatoid arthritis, asthma, heart disease, and multiple forms of cancer (Barnes and Karin, 1997; Karin and Greten, 2005; Laberge *et al*, 2005).

There are five NF-κB monomer subunits, all containing a conserved Rel homology region—RelA, RelB, cRel, p50, p52— that associate to generate up to fifteen NF-κB transcription factor dimers (Ghosh *et al*, 1998; Hoffmann *et al*, 2006a)(Figure 1.2). In unstimulated cells, these dimers are held in a latent form in the cytoplasm by stoichiometric associations with ankyrin-repeat-containing inhibitor proteins—IκBα, IκBβ, IκBε, and the recently identified IκBd/p100 isoform (Basak *et al*, 2007)—which act to inhibit NF-κB DNA binding activity and prevent its nuclear accumulation. Activation of NF-κB requires proteasome-mediated degradation of the IκBs initiated by stimulus-responsive IκB Kinase (IKK) complexes. Developmental stimuli signal via a complex consisting of NF-κB Inducing Kinase (NIK) and IKK1 homodimer while other stimuli signal via a complex of NF-κB Essential Modulator (NEMO) and an IKK2-containing IKK dimer. Upon subsequent nuclear translocation of free NF-κB, each dimer activates overlapping but distinct gene expression programs (Hoffmann *et al*, 2003) that include the genes for some NF-κB monomers and IκB inhibitor proteins (Hoffmann *et al*, 2006b). Thus, NF-κB is regulated via combinatorial complexity that arises from the temporal, stimulus, and cell-type specific expression of dimers, their activation, and their control via both negative and positive feedback mechanisms (Ghosh *et al*, 1998; Hoffmann *et al*, 2006b).

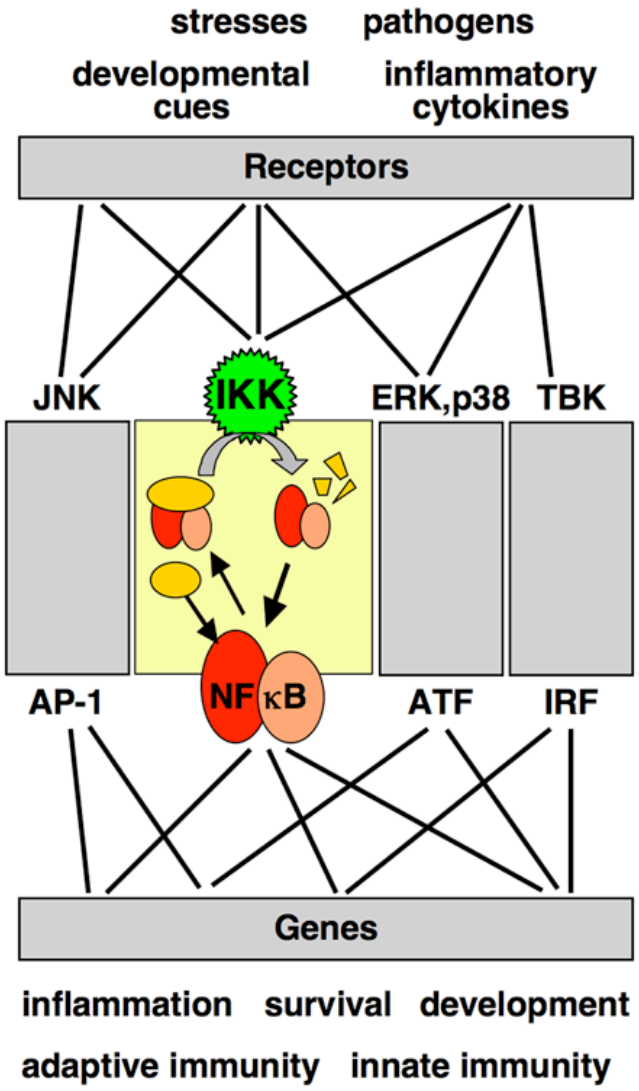

Figure 1.1 Important mammalian signaling modules

The cell responds to external and internal stimuli through complex signal transduction networks that utilize distinct signaling modules to exact specific cellular responses. The NF-κB signaling module is one such key mediator. IκB Kinase (IKK) complexes are activated in response to cellular stimuli and causes accumulation of NF-κB transcription factor in the nucleus that drives stimulus-specific gene expression programs. Similar modules have been described for signaling induced transcription factor activity by Janus kinase (JNK) for Activator Protein 1 (AP-1), Extracellular Signal-Regulated Protein kinase (ERK) for Activating Transcription Factor (ATF), and TANK-binding kinase (TBK) for Interferon Regulatory Factor (IRF). Some of the many connections between stimuli, discrete signaling modules, and cellular responses are shown and are illustrative of the combinatorial complexity inherent in the cellular signal transduction network.

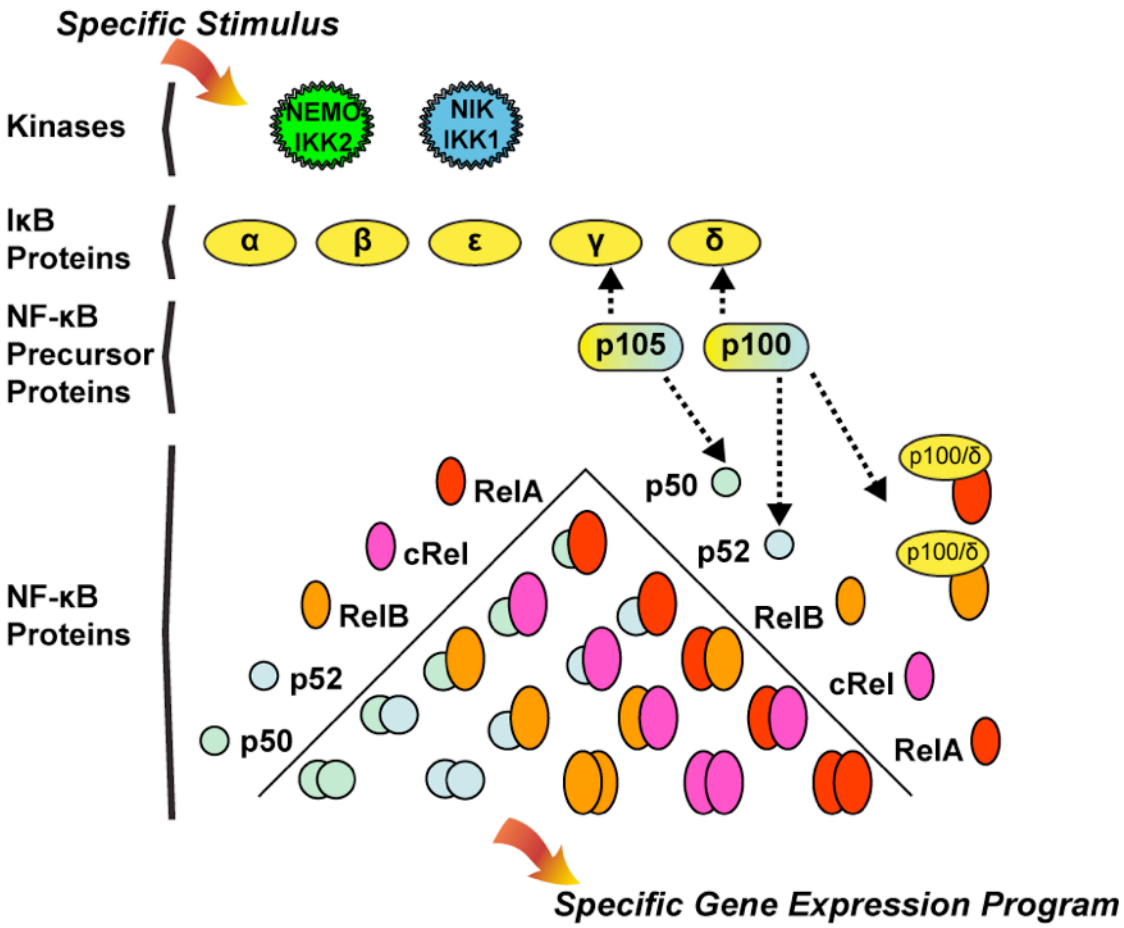

Figure 1.2 Combinatorial complexity in the NF-κB module

NF-κB proteins are dimeric associations of five protein monomers. Up to fifteen NF-κB dimers are generated and the abundance of each is cell type and stimulus-dependent. These dimers are regulated via stoichiometric associations with IκBα, -β, -ε, -δ/p100, and -γ/p105 inhibitor proteins. The NF-κB precursor proteins, p105 and p100, form homodimers with IκB activity or are proteolytically processed to generate p50 and p52 NF-κB monomers, respectively. Recent experiments suggest that RelA and RelB are also contained within high molecular weight complexes with p100 (shown, right) with unknown stimulus-responsive characteristics (Savinova *et al*, 2009). Cellular stimuli and stresses activate NEMO-dependent IKK2 or NIK-dependent IKK1 complexes that drive IκB protein degradation and subsequent NF-κB dimer activity to elicit specific gene expression programs.
(Adapted with permission from (Hoffmann *et al*, 2006b))

CONSTRUCTION OF AN NF-κB COMPUTATIONAL MODEL

A computational model was constructed to examine the dynamical control of NF-κB signaling (Hoffmann *et al*, 2002) and ascertain the individual roles of the three canonical IκB proteins (IκBα, IκBβ, IκBε) in regulating NF-κB activity in response to the inflammatory cytokine TNF. The construction of the computational model required consideration of several questions. (1) What should be the scope of the model? (2) How much molecular detail should the model contain? (3) Which computational modeling technique is best suited? (4) What are the values of the parameters that govern the network reactions?

Model Scope

The most basic utility of a model is in exploring the relationship between a network stimulus or perturbation (input) and the resulting cellular response or network behavior (output). As NF-κB is a pleiotropic transcription factor that responds to numerous intra- and intercellular signaling events, the boundaries of the module were selected to allow for experimentally measurable *input* and *output* activities (Figure 1.3). With only a few exceptions, the varied upstream inflammatory activation pathways all converge on the NEMO/IKK2 complex and thus the activity of NEMO/IKK2 was used as the model input. The output of the model is defined as the presence of free NF-κB dimer in the nucleus (*NF-κB activity*). While much quantitative data exists for the expression of NF-κB responsive genes (microarray, qPCR, etc), the mechanisms that translate NF-κB activity to gene expression are

promoter-specific and are not yet well enough understood to be included in a computational model. By limiting the scope of the model to nuclear NF-κB activity, the model is relevant for NF-κB responsive genes in general. The model, as constructed, is therefore a predictive tool to relate specific stimulus-induced NEMO/IKK2 activities to specific NF-κB responses.

Model Graininess

Model graininess defines which reactions and which components are described in the model; with a very detailed model being *fine-grained* and a simplified model being *coarse-grained*. Even small biological networks can lead to insurmountable complexity if too much detail is included and it is critical to select the minimum level of detail that allows the questions that drive the project to be addressed.

As the IκB proteins are the key mediators of NF-κB nuclear localization, the model describes reactions that govern IκB metabolism including synthesis, degradation, cellular localization, and association/dissociation with NF-κB (Figure 1.3). To reduce complexity, some multi-step biochemical events were combined into single reaction mechanisms based on prior biochemical knowledge. For example, IκB proteins are known to be rapidly degraded via the ubiquitin-dependent proteasome pathway following NEMO/IKK2-mediated phosphorylation. As only the NEMO/IKK2-mediated phosphorylation had been found to be rate limiting, the model employed a single NEMO/IKK2-dependent protein degradation reaction in lieu of multiple explicit reactions governing the ubiquitin-mediated proteasome pathway. Similar reductions were made in removing transport machinery for cellular shuttling

events, combining mRNA synthesis, processing, and cytoplasmic localization into a single reaction, and treating protein translation as a single-step process.

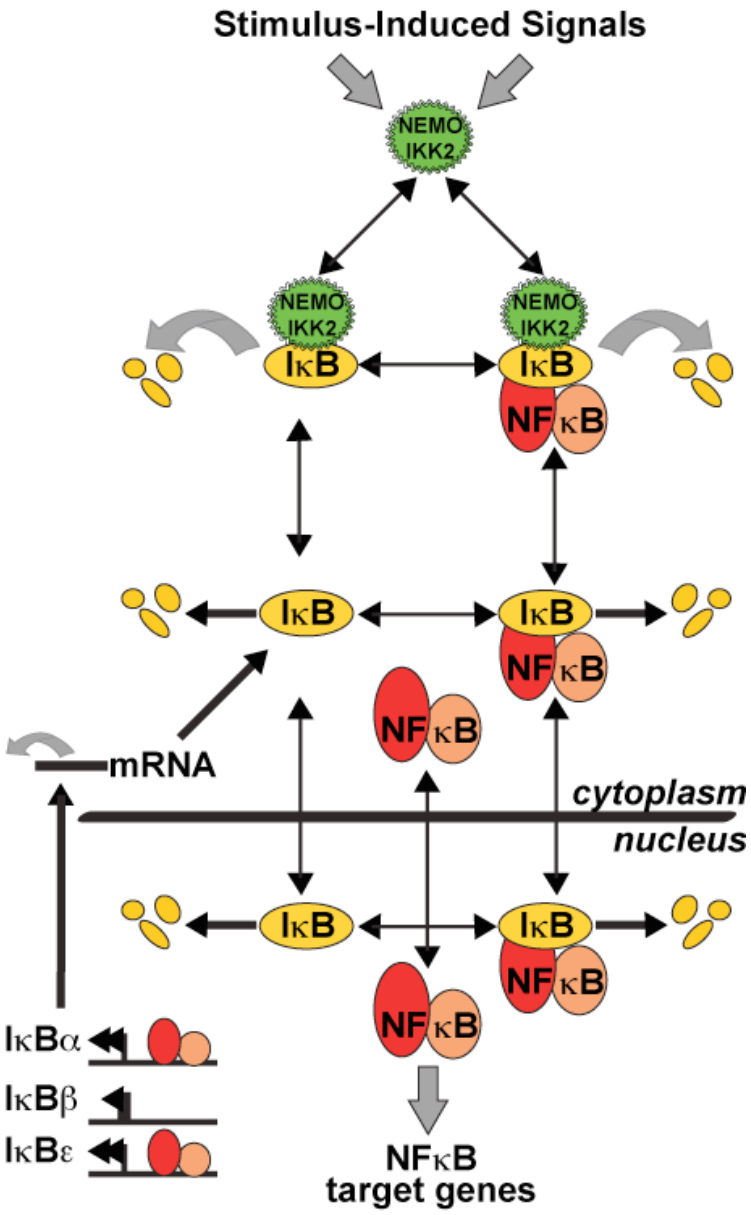

Figure 1.3 NF-κB module reaction map

Schematic diagram of the components and reactions that are described within the NF-κB computational model. Distinct reactions exist for each IκB isoform (α, β, ε) and are controlled by isoform-specific reaction rate constants. Reactions control synthesis and degradation of the IκBs, association and dissociation of IκBs, NF-κB, and IKK, and cellular localization. NF-κB is a product or reactant in multiple reactions and, for clarity, is included once in the middle of the diagram. The temporal profile of IKK activity is used as the model input.

Mathematical Modeling Methodology

There are several mathematical approaches that have been found useful for modeling biochemical reaction networks. Boolean modeling based on the application of electronics AND and OR gates (and many others) is useful when analyzing how multiple inputs cooperate to produce an output, as for example in the combinatorial transcription factor control of gene expression (Buchler *et al*, 2003). Flux balance analysis (FBA) has been used to predict how networks alter their steady state behavior to achieve a particular physiological objective, as in metabolism controlling bacterial cell growth (Covert *et al*, 2004). In cell signaling, however, responses to stimuli are often non-steady state (e.g. transient) events and therefore necessitate a mathematical approach that can calculate the time-dependent changes in the concentration or activity of network components. Ordinary differential equations (ODEs) that utilize mass action kinetics and rate constants are often used to describe dynamical cell signaling. Further, in some regulatory networks, when molecule numbers are low, the mathematical model must account for the fact that molecular processes are not graded, but are essentially stochastic. Such molecular noise can play significant roles as exemplified by cell fate decision-making and the viral latency/lysis switch (Rao *et al*, 2002; Raser and O'Shea, 2005).

In modeling NF-κB activity, both homeostatic and stimulated states are of interest. Since the molecule numbers are high (over 100,000 NF-κB dimers per cell), a system of ODEs rather than the more computationally demanding stochastic approach was chosen to describe mass action kinetics (Hoffmann *et al*, 2002). Examples of the ODEs that represent the rate of change in the IκBα mRNA and the nuclear NF-κB

activity are shown in Figure 1.4. Each ODE represents the flux for one component as a function of time, and the model contained 24 components and ODEs.

These mathematical equations can be written and solved with the help of programs such as Mathematica® (Wolfram Research) or MATLAB® (The Mathworks, Inc.) that offer suites of numerical solvers for solving systems of ODEs. Models may also be written using Systems Biology Markup Language (SBML) via one of the many software packages that permit construction and simulation of these models, like MATLAB SimBiology® (The Mathworks, Inc.), CellDesigner™ (The Systems Biology Institute, Tokyo, Japan), and others (www.sbml.org). Some of these tools also have graphical interfaces that enable model construction simply by drawing a reaction network and entering rate constants. These applications represent a step towards making modeling as user-friendly as other bioinformatic tools, such as those for nucleotide and peptide alignment (Altschul *et al*, 1997).

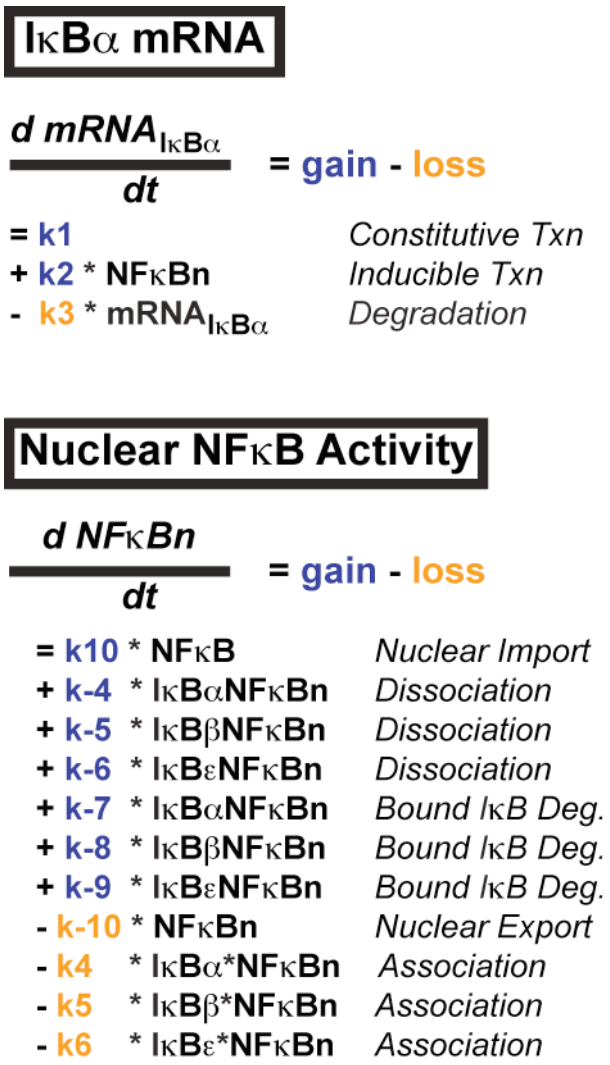

Figure 1.4 Examples of model ordinary differential equations

Two examples of the 24 ordinary differential equations (ODEs) that are contained within the NF-κB model. The flux for each component is calculated via mass action kinetics by subtracting the sum of the reactions that remove the component from the sum of the reactions that produce the component. Shown first is the equation governing IκBα mRNA expression, which contains the reactions of constitutive and NF-κB-inducible transcription and mRNA degradation. Shown second is the equation governing the amount of free NF-κB protein in the nucleus, which is controlled by association and dissociation with IκB proteins, protein degradation of NF-κB-bound IκBs, and cellular localization reactions.

Model Reaction Rate Constants

The equations of a model constitute the model structure as they define the connectivity between components. The rate constants quantify the connectivity, and *parameteriz*ing a model (defining the values of the rate constants) is the final and often the most difficult step in model construction. Ideally, all values would be measured, but in practice this is not always feasible and models contain rate constants that are measured, experimentally constrained, or estimated/fit. For instance, the rate constants governing protein-protein interactions, cellular localization, and protein half-lives are measurable quantities. Other values are difficult to directly measure or are composite parameters as a result of a coarse-grained model structure. Related experiments can constrain the values of some of these rate constants. For example, measurements of mRNA and protein abundances can constrain the values of synthesis parameters when coupled to measurements of degradation rates. Finally, the module input:output relationship can be used as a constraint to *fit* the remaining parameter values such that the model recapitulates this relationship.

A balance must be achieved during the parameterization process to avoid *under-* or *over-constraining* the model. If too few values are experimentally determined there may be several possible parameter sets that recapitulate network behavior, but conversely when too many experiments are done the model may be incapable of doing so. In these cases, the data that cannot be accounted for by the model may motivate subsequent studies and in turn result in a revised version of the model.

In the case of the NF-κB signaling module, a rich literature of biochemical rate constants derived from *in vitro* measurements and quantitative cell biology meant that one third of the 73 parameters were known with a high degree of confidence, one third were significantly constrained by literature data, and only the remaining third had to be derived from parameter fitting. To this end, experimental data from three cell lines, each expressing only one of the three IκB proteins (double knockouts) were used as fitting constraints. The online supplementary material contained an extensive accounting of the sources for each reaction rate constant (Hoffmann *et al*, 2002).

THE UTILITY OF COMPUTATIONAL MODELING

There have been numerous studies that have expanded upon and/or refined the original NF-κB model (Barken *et al*, 2005; Basak *et al*, 2007; Cheong *et al*, 2006; Hoffmann *et al*, 2002; Kearns *et al*, 2006; Lipniacki *et al*, 2004; Nelson *et al*, 2004; O'Dea *et al*, 2007; Werner *et al*, 2005). In addition, other studies have reduced the complexity of the model to focus only on critical reactions (Cho *et al*, 2003; Hayot and Jayaprakash, 2006; Krishna *et al*, 2006). From the biochemist's perspective, each modification ought to be motivated by specific biological questions. In this context, the following considers the utility of computational modeling more generally.

Sufficiency Test

In its simplest form, a mathematical model is the summary of our molecular or mechanistic knowledge of a biological process. A model that fails to recapitulate the

cellular response (network behavior) indicates that our knowledge of the molecular mechanisms is insufficient to account for the observed biology. Indeed, further simulations can inform experimental studies to look for missing mechanisms. In this way, the modeling process is integrated with experimental analyses and iterative tests of sufficiency can be used to increase the scope and detail both of the model and of our biochemical understanding.

Emergent Properties

A network of molecular reactions has functional characteristics that are not evident from studying a single reaction. These characteristics are called network emergent properties. Network behaviors such as dose responses, dynamic negative feedback regulation, compensation between redundant or overlapping mechanisms, crosstalk between stimuli, and functional memory are examples of emergent properties that can be addressed through mathematical modeling.

Perturbation Studies

One of the advantages of having a virtual representation of the biochemical network is that virtual experiments, in contrast to biological experiments, can be done systematically, cheaply and fast. One simple strategy is to use simulations of knockouts, in which specific components are removed from the model, to discern the effects (phenotypes) and reveal emergent properties, including compensation mechanisms. For example, by removing IκBα from the model, its role in post-induction repression of NF-κB was assessed (Hoffmann *et al*, 2002).

Similarly, parameter sensitivity analysis involves simulating the model repeatedly with a range of values for one or more rate constants to identify the contribution each reaction makes to the network behavior. Unlike for linear reaction pathways where rate-limiting step is the slowest reaction, complex signaling networks may have non-obvious rate-limiting steps. In particular, the rate-limiting step often depends on the homeostatic state of the cell and the stimulus used. The application of parameter sensitivity analyses to biomedical sciences can identify which reactions are sensitive to modulation within the ranges achievable by genetic or pharmacological tools. Further, it may also provide insight into how a drug with a known molecular target within the network will affect the network response. Simulations of the model with the drug-induced perturbation(s) that do not recapitulate observed experimental results may suggest that the drug has unknown targets within the cell.

SPECIFIC RESEARCH FINDINGS

The temporal dynamics of NEMO/IKK2 activity are critical for providing stimulus-specific cellular responses (Werner *et al*, 2005). The broad theme of my dissertation research is the identification and exploration of the regulatory mechanisms that act combinatorially to mediate these dynamics to NF-κB. First, I explore the interplay between IκBα and IκBε negative feedback mechanisms to show how differences in their NF-κB inducible synthesis kinetics provide specific functionalities for these two redundant IκBs (Chapter 3). Second, I extend the NF-κB computational model upstream to the inflammatory cytokine TNF receptor (TNFR) to find why the

NF-κB-inducible negative regulators IκBα and A20 deubiquitinase are not redundant, but rather impart specific regulation (Chapter 4). Third, in two related projects, I contrast IκBα and IκBδ negative feedback to delineate the functions of IκBδ as mediating crosstalk between inflammatory (NEMO/IKK2-induced) and developmental (NIK/IKK1-induced) NF-κB responses and discriminating between transient and persistent inflammatory signaling (Chapter 5). Fourth, I examine the role of IκBβ in regulating NF-κB, and thereby reveal a novel role for IκBβ in determining the composition of the RelA/NF-κB dimer pool that is responsive to inflammatory stimuli (Chapter 6).

ACKNOWLEDGEMENTS

Some text and figures are adapted from a *JBC* mini-review article for which I am the primary author (Kearns and Hoffmann, 2009). Professor Alexander Hoffmann is the corresponding author.

Chapter 2

Materials and Methods

Cell Culture and Reagents

Primary MEF cells were cultured at 37°C at 5% CO_2 in Dulbecco modified essential media (DMEM, CellGro) containing 10% fetal calf serum (FCS, ThermoScientific Hyclone), 1% penicillin + streptomycin (CellGro), and 1% L-Glutamine (CellGro). Prior to stimulation, cells were starved 24 h in reduced media containing 0.5% FCS. 3T3 immortalized MEF were cultured similarly but with media containing bovine calf serum (BCS, ThermoScientific Hyclone). Stimulations were performed with recombinant TNF (Roche Diagnostics), LPS (Sigma Aldrich, B5:055), or murine IL-1β (EMD Biosciences) at indicated concentrations. Cells transiently stimulated (pulse stimulation) were washed twice with 1x PBS following stimulation and returned to untreated media. Cells treated with the translational inhibitor cyclohexamide (CHX, Sigma Aldrich) were pre-treated 30 min with 100ng/mL final concentration before addition of stimulus. At indicated time points, cells were harvested according to one of the following conditions. Protein samples were then normalized by Bradford or Lowry assay before use according to the manufacturer's instructions (BioRad). RNA samples were normalized by 260/280nm absorbance readings from an UV/Vis spectrophotometer (Eppendorf).

Cytoplasmic and Nuclear Protein Lysates:

Media was aspirated and cold phosphate buffered saline (PBS) + 1mM EDTA was added before scraping cells into a 1.5mL epi-tube. Cells were pelleted in a picofuge for 1 min, resuspended in a pellet-equivalent volume of cytoplasmic lysate buffer (10mM HEPES-KOH pH 7.9, 60nM KCl, 1mM EDTA, 0.5% NP40, 1mM DTT, 1mM

PMSF), incubated on ice for 2 min, vortexed for 30 sec, and then pelleted in a picofuge for 30 sec. Supernatant was then transferred to a fresh tube (Cytoplasmic Lysate) and stored at -80°C. The pellet was then washed once with the same volume of cytoplasmic lysate buffer and then resuspended in a pellet-equivalent volume of nuclear lysate buffer (250mM Tris-HCl pH 7.5, 60mM KCl, 1mM EDTA, 1mM DTT, 1mM PMSF).

SDS-RIPA Protein Lysates

Media was aspirated and cold phosphate buffered saline (PBS) + 1mM EDTA was added before scraping cells into a 1.5mL epi-tube. Cells were pelleted in a picofuge for 1 min, resuspended in a pellet-equivalent volume of SDS Radio Immunoprecipitation Assay (RIPA) buffer (50mM Tris-HCl pH 7.5, 150mM NaCl, 1mM EDTA, 0.1% SDS, 1% TritonX-100, 1mM DTT, 1mM PMSF), and stored at -80°C.

RNA isolation

Media was aspirated and the plates were washed with cold PBS and total cellular RNA was isolated with Trizol Reagent according to the manufacturer's instructions (Invitrogen). The RNA was stored at -80°C in 10mM Tris-HCl pH 7.9.

Western Blot

3x SDS sample buffer (189mM Tris-HCl, 30% glycerol, 5% SDS, 15% beta-mercaptoethanol) was diluted to 1x with normalized protein extract and then boiled at

95°C for 5 min. Samples and a pre-stained protein marker (New England Biolabs) were run on an SDS-PAGE gel for ~1 h at 200V and transferred (5 min at 12V followed by 1 h at 18 V) onto a PVDF membrane (GE Healthcare). The membrane was then washed in TBS-T, incubated at room temperature 1 h in 5% milk in TBS-T to block, and incubated at 4°C overnight in 5% milk in TBS-T + primary antibody. TBS-T was then used to repeatedly wash the membrane (rinse, 2, 5, 5, 10, 15 min) before 1 h room temperature incubation with secondary antibody in 5% milk in TBS-T and then a second round of TBS-T washes. ECL-Plus reagent (GE Healthcare) was added and the protein bands visualized on a Typhoon 9400 Variable Mode Imager (GE Healthcare). The data was then quantitated using ImageQuant software (version 5.2, GE Healthcare).

Electromobility Shift Assay (EMSA)

2.5μL of nuclear lysate sample was incubated at room temperature for 15 min with 3μL of 2X binding buffer (20mM Tris-HCl pH 7.5, 100mM NaCl, 20% glycerol, 2% NP-40, 2mM EDTA, 0.1 mg/mL PolyIdC) and 0.5μL (0.01pmol) of P^{32}-labeled oligonucleotide probe (GCTACAA*GGGACTTTCC*GCTG*GGGACTTTCC*AGGGAGG, the two NF-κB binding sites are denoted in italix). Samples were then run on a gel containing 5% acrylamide (30:0.8) and 5% glycerol in 1X TGE buffer (24.8mM Tris-HCl, 190mM glycine, 1mM EDTA) at 200V for 2 h. The gel was dried for 1 h at 80°C and placed overnight in a Storage Phosphor screen (GE Healthcare) before scanning with a

Typhoon 9400 Variable Mode Imager (GE Healthcare). The data was then quantitated using ImageQuant software (version 5.2, GE Healthcare).

RNase Protection Assays (RPA)

Transcript levels were monitored with [α-^{32}P] UTP-labeled probes using a RiboQuant kit (BD Biosciences) according to the manufacturer's instructions. Data was obtained using a Storage Phosphor screen and a Typhoon 9400 Variable Mode Imager (GE Healthcare). Data was quantitated using ImageQuant software (version 5.2, GE Healthcare) by normalization to L32 and/or GAPDH housekeeping mRNA following local background subtraction. Probes for IκB and NF-κB mRNA were generated according to Table 2.1. G-CSF, LIF, MIP-2, TNF, L32, and GAPDH probes were obtained from RiboQuant sets (BD Biosciences).

Computational Modeling

Models were constructed and simulated using MATLAB software (The Mathworks, Inc.). Using graphical wiring schematics containing the list of species (proteins and mRNA), cellular compartments (nucleus and cytoplasm), reactions, and reaction rate constants as guides, three MATLAB files were generated for each specific model—a 'Run' file containing simulation parameters, a 'Simulation' file containing the specific ordering of the simulations, and an 'ODE' file containing the set of ordinary differential equations. Initial concentrations for each species were heuristically assigned and the model was allowed to simulate repeatedly until a steady state condition was reached. IKK activity (either in the form of a numerical input

curve or a step-function) was then used to perturb the model system from the steady state. The simulations produced numerical results (concentrations of each species per unit time) that were then used as inputs to model analysis functions (line plots, bar plots, etc.). There are tables in the *Methods* section of each chapter denoting the specifics of each computational model as well as the methodology of the analysis functions used. Further, the Introduction (Chapter 1) discusses the general strategies employed during model construction.

Table 2.1 RNase Protection Assay Probes

IκB probes were designed to select for mature mRNA species by spanning exon-exon junctions. The following primer pairs, containing flanking EcoR1 (5') and HindIII (3') restriction enzyme sequences, were used to amplify fragments from reverse-transcribed RNA isolated from murine embryonic fibroblast cells (MEF). Fragments were then cloned into empty vector (RiboQuant, BD Biosciences) containing a T7 transcription initiation site and an ampicillin-resistance marker.

TARGET	**PRIMERS (FORWARD, REVERSE)**	**PROBE (bp)**
cRel (*rel*)	GGAATTCATTGAACAGCCAAGGCAGAG CCCCAAGCTTTGAGGTCGCAGTCTTCAATG	400
IκBε (*nfkbie*)	GGAATTCGGCAGACAGCTTTCTCATCC CCCCAAGCTTTCCTGGGGTGTCTCATCTTC	365
p100/p52 (*nfkb2*)	GGAATTCAGATTGAGGTGGACCTGGTG CCCCAAGCTTTCGAAGGAAAGCTGAGAAGC	329
Bcl3 (*bcl3*)	GGAATTCTGGAGAACAACAGCCTGAAC CCCCAAGCTTAGTTGGTGGCACTTTGGTCT	294
p105/p50 (*nfkb1*)	GGAATTCCTACGGATTTCCTCCCTACG CCCCAAGCTTCTGAAATCCCATGTCCTGCT	262
IκBβ (*nfkbib*)	GGAATTCGCCCTTAGTCTTTGGCTACG CCCCAAGCTTTCTCAGCCACCAACACTCCT	233
RelB (*relb*)	GGAATTCTGATCCACATGGAATCGAGA CCCCAAGCTTATCATAGGCAAAGCCATCGT	205
IκBζ (*nfkbiz*)	GGAATTCTGCTACACATCCGAAGCAAC CCCCAAGCTTAACAGAGCTGGCCTCTTGC	178
RelA (*rela*)	GGAATTCACTTGTGGGGAAGGACTGC CCCCAAGCTTGGGGTTATTGTTGGTCTGGA	154
IκBα (*nfkbia*)	GGAATTCTCGCTCTTGTTGAAATGTGG CCCCAAGCTTTGGAGATTTTCCAGGGTCAG	134
L32	*Housekeeping probe from RiboQuant set* (shown here for probe size reference)	113
GAPDH	*Housekeeping probe from RiboQuant set* (shown here for probe size reference)	96

Chapter 3

IκBε provides negative feedback to control NF-κB oscillations, signaling dynamics and inflammatory gene expression

ABSTRACT

NF-κB signaling is known to be critically regulated by the NF-κB-inducible inhibitor protein IκBα. The resulting negative feedback has been shown to produce propensity for oscillations in NF-κB activity. Integrated experimental and computational studies demonstrate that another IκB isoform, IκBε, also provides negative feedback on NF-κB activity, but with distinct functional consequences. Upon stimulation, NF-κB -induced transcription of IκBε is delayed relative to that of IκBα, rendering the two negative feedback loops to be in anti-phase. As a result, IκBε has a unique role in dampening IκBα-mediated oscillations during long lasting NF-κB activity. Further, both of these distinct negative feedback regulators are required for the termination of NF-κB activity and NF-κB-mediated gene expression in response to transient stimulation. These findings extend the capabilities of a computational model of IκB-NF-κB signaling and reveal a novel regulatory module of two anti-phase negative feedback loops that allows for fine-tuning of the dynamics of a mammalian signaling pathway.

INTRODUCTION

Temporal control of NF-κB activity has been shown to mediate stimulus-specific gene expression programs in response to different inflammatory stimuli (Werner *et al*, 2005), and understanding the dynamic regulation of NF-κB by IκB proteins is of critical importance. Negative feedback mediated by IκBα was shown to confer the propensity for oscillatory NF-κB nuclear activity, when examined biochemically in gene knockout cells containing only the IκBα isoform (Figure 3.1B, Hoffmann et al., 2002) or by microscopy using transiently transfected IκBα and RelA proteins fused to fluorescent moieties (Figure 3.1D, Nelson et al., 2004). The oscillations are not apparent in cells containing all three IκB proteins at normal expression levels (Figure 3.1C and A, (Barken *et al*, 2005; Hoffmann *et al*, 2002)).

These observations suggested that IκBβ and/or IκBε proteins play a role in dampening IκBα-mediated oscillations and determining the dynamics of NF-κB activity. The mechanism that confers dampening of oscillations in NF-κB activity was proposed to involve the nuclear accumulation of newly synthesized IκBβ that binds nuclear and promoter-bound NF-κB and shields it from IκBα-mediated nuclear export (Phillips and Ghosh, 1997; Suyang *et al*, 1996). This mechanism was included in the original computational model that recapitulates NF-κB activation in response to TNF stimulation (Hoffmann *et al*, 2002), but later studies in our laboratory (C. Aguilera, unpublished results) were unable to observe the IκBβ effect in murine embryonic fibroblasts, the cells for which the model was constructed. Removal of the mathematical term for this mechanism from the model resulted in highly oscillatory

NF-κB responses (Figure 3.1E, F). While genetic evidence points to important roles of IκBβ and IκBε in regulating the dynamics of NF-κB signaling, the mechanisms by which they function remained unclear.

This study investigates the dynamic behavior of all three canonical IκB isoforms, in particular, contrasting IκBε and -β functions with that of IκBα. This work revealed that IκBε expression is in fact highly NF-κB inducible, and that it mediates functional negative feedback on NF-κB activity, however in anti-phase to that of IκBα. Two anti-phase negative feedbacks emerge as an important regulatory module that may be present for the dynamic control of signaling in other pathways as well.

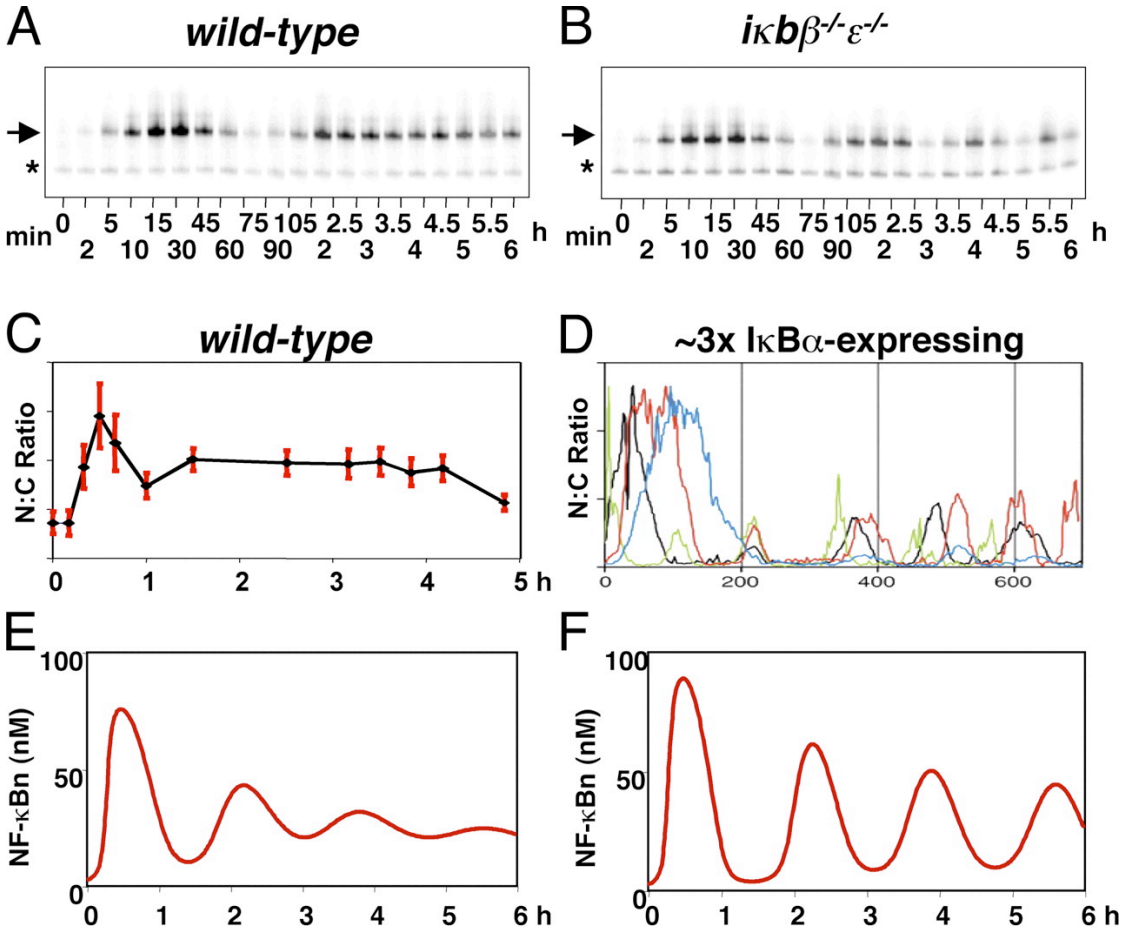

Figure 3.1 Oscillations in NF-κB nuclear localization

(A) Electrophoretic mobility shift assays (EMSAs) show nuclear localization of NF-κB in wild-type and
(B) *iκbβ*$^{-/-}$*ε*$^{-/-}$ MEF cells stimulated with TNF (adapted from (Hoffmann *et al*, 2002)). Arrows indicate specific nuclear NF-κB binding activity while asterisks indicate nonspecific DNA binding complexes.
(C) Quantitation of immunohistochemical analysis of individual cells stimulated with TNF (adapted from (Barken *et al*, 2005)).
(D) Recordings from live individual cells transduced with overexpressing RelA and IκBaα fusion proteins and stimulated with TNF, where each colored line represents the recording from one cell (adapted from (Nelson *et al*, 2004)).
(E) NF-κB nuclear localization predicted by a computational model (Hoffmann *et al*, 2002) with and (F) without the IκBβ-mediated protective mechanism described in (Phillips *et al*, 1997).

RESULTS

IκBε is TNF inducible via NF-κB

A library of probes for RNase Protection Assays (RPA) was constructed that allowed for the simultaneous quantitative monitoring of all three IκB mRNAs to characterize the regulation of IκBε and IκBβ gene expression in response to stimulation (Table 3.1). Analysis of the mRNA levels in murine embryonic fibroblasts (MEFs) stimulated with TNF confirmed that IκBα was strongly induced (Figure 3.2A). IκBβ showed only weak induction, which suggests that it is not a strong NF-κB-responsive gene in this cell type. Remarkably, IκBε transcription was highly induced by TNF stimulation and quantitation of these results showed that IκBε was induced to a higher degree than IκBα (Figure 3.2B). While the exact induction folds varied in replicate assays using separate MEF cell stocks (data not shown), IκBε fold induction was consistently higher than that for IκBα. Further, IκBε expression was also induced in response to LPS and in the macrophage cell line RAW264.7 and 70Z B-cells (data not shown) indicating that the dynamic control of its synthesis is not specific to TNF or to fibroblasts. Analysis of IκB mRNA levels in MEF cells deficient in NF-κB showed no induction of any of the three IκBs (Figure 3.2A).

The temporal profile of IκBα transcript induction during chronic TNF stimulation is well described (Scott *et al*, 1993)—it shows rapid activation as early as 15 min, a peak within 1 h, and a slow attenuation over many hours. A similar activation profile for IκBε induction was observed but I was surprised to note a

distinct 45 min onset delay (Figure 3.2A, B). This suggests that the IκBε promoter may involve a delay mechanism such as a requirement for the activation of an NF-κB-responsive transcription factor (feed-forward regulation). However, the inhibition of protein synthesis by cycloheximide (CHX) did not attenuate transcriptional activation of either IκBα or IκBε (Figure 3.2D, Figure 3.3) and thus does not support the notion of feed-forward regulation.

It has been previously shown that transient TNF stimulation leads to transient nuclear NF-κB activity lasting about 60 min only (Hoffmann *et al*, 2002). To determine whether short stimulation would efficiently induce IκBε expression, an RPA was performed on MEF cells stimulated for 15 min with TNF. The results show that IκBε transcription is still activated with an onset delay, and with an induction profile similar to that of chronically stimulated cells (Figure 3.2C, Figure 3.3). As NF-κB activity is diminished when IκBε mRNA levels are still rising and as CHX treatment precludes a feed-forward mechanism, this suggests that the time delay in the activation of IκBε transcription occurs post NF-κB recruitment to the promoter. Further study is required to elucidate the mechanism of this delay.

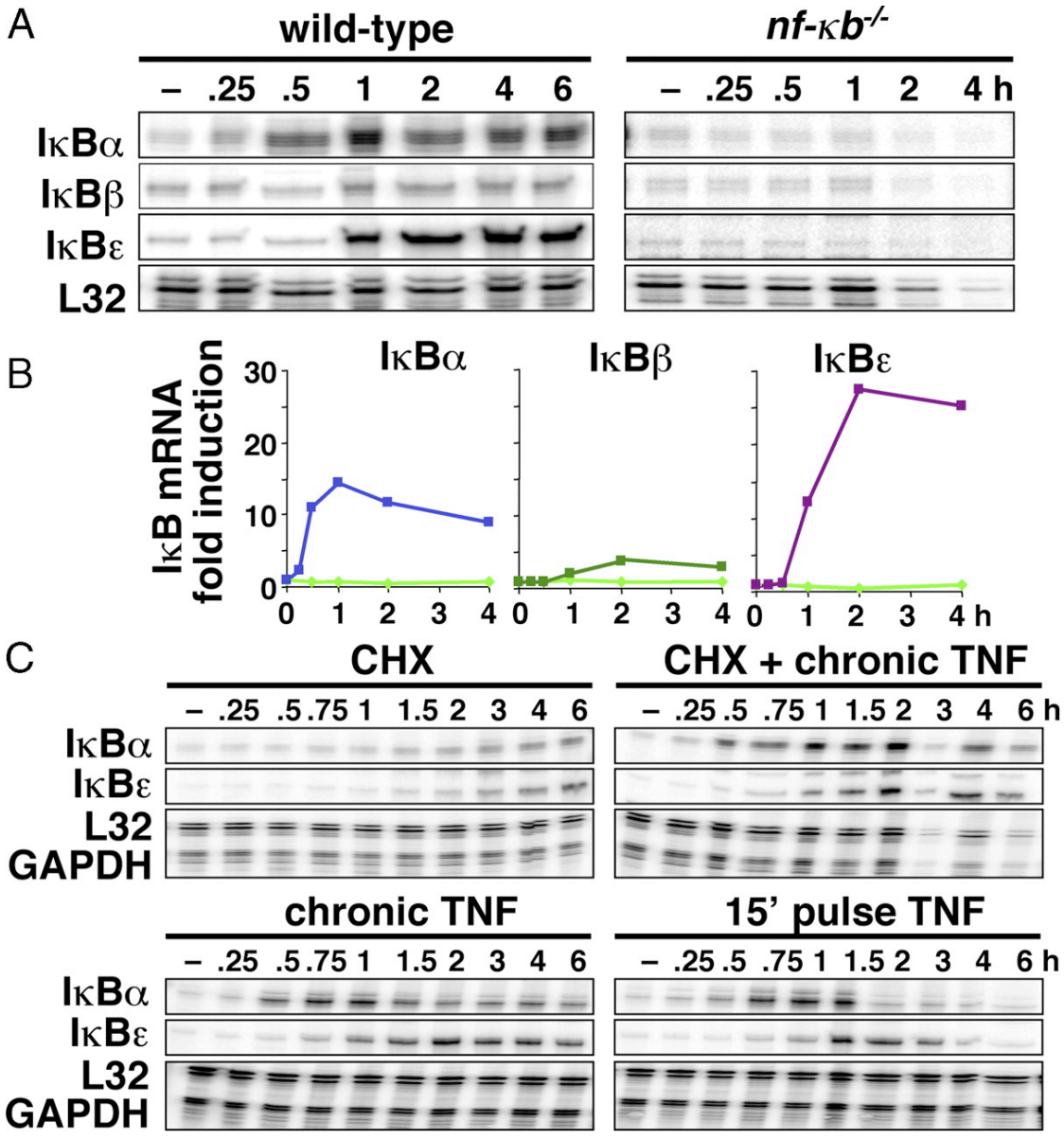

Figure 3.2 IκB gene transcription in response to inflammatory stimulation

(A) RNase Protection Assay (RPA) revealing IκB mRNA levels in wild type and NF-κB-deficient cells following chronic TNF stimulation.
(B) IκB mRNA fold induction in wild type (blue, green, and purple) and NF-κB-deficient (light green) stimulated cells normalized to L32 housekeeping gene expression.
(C) IκB mRNA levels in wild-type cells in response to chronic treatment by cycloheximide and/or TNF and 15 min transient stimulation with TNF.

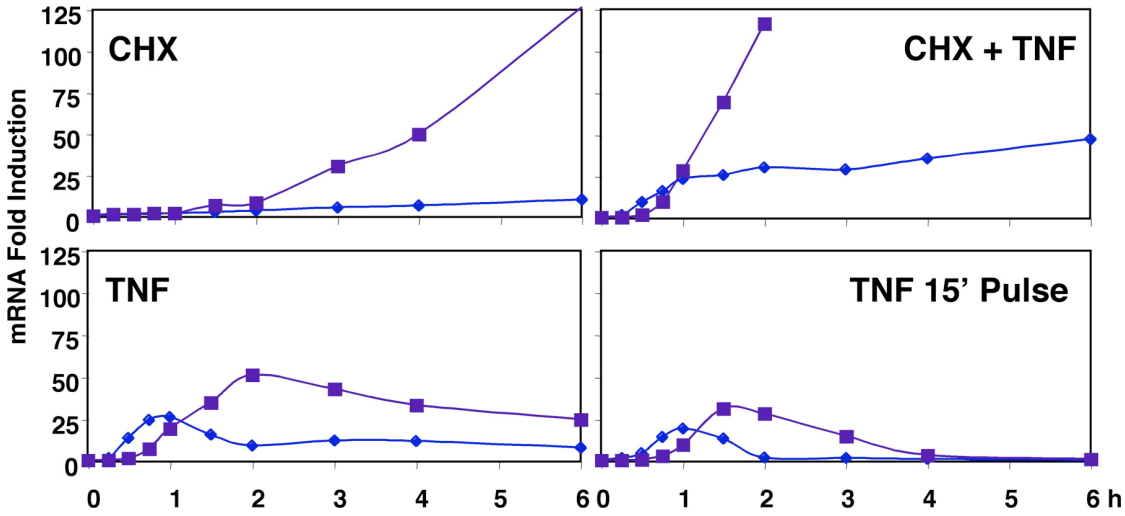

Figure 3.3 Quantitation of IκBα and -ε gene expression.

Induction folds of IκB mRNA levels as measured by RNase protection assay in wild type cells in response to chronic treatment by cyclohexamide and/or TNF and a 15-min transient stimulation with TNF. RPA results were quantitated by local background subtraction and normalization to L32 and GAPDH housekeeping genes. IκBα, blue diamonds; IκBε, purple squares.

Computational modeling reveals dynamic control mechanisms

NF-κB responsive syntheses of IκBε and IκBβ were added to the mathematical model (Table 3.1, Table 3.2) in order to explore the functional consequences imparted by these negative feedback regulators upon NF-κB activity. To determine the kinetic parameter values for the inducible transcription of each isoform, the temporal responses of IκB transcription in the model were constructed such that the mRNA induction profiles calculated by the model correlated with the RPA data (Figure 3.4A). This required the fitting of parameters defining transcription and translation rates and mRNA stability. The new model also includes revised IκB protein degradation parameters from earlier studies (O'Dea *et al*, 2007).

The revised model recapitulates IκBα protein degradation immediately following NEMO/IKK2 activation and rapid synthesis in response to NF-κB nuclear localization (Figure 3.4B, C). Chronic stimulation results in repeated IκBα protein degradation and synthesis (Figure 3.4B). In addition, the model shows delayed induction of IκBε and IκBβ protein syntheses. The low inducibility of IκBβ transcription results in very low IκBβ protein synthesis, while the high inducibility of IκBε transcription results in notable accumulation of IκBε protein (Figure 3.4B).

Earlier studies revealed oscillatory NF-κB activity in cells lacking IκBβ and IκBε (Hoffmann *et al*, 2002) and in cells in which NF-κB-inducible IκBα was overexpressed (Nelson *et al*, 2004), while in wild type cells late NF-κB activity (beyond 2 h) was remarkably steady (Hoffmann *et al*, 2002). However, the underlying dampening mechanism that results in steadied late activity remained obscure. Because

induced synthesis of IκBε is delayed, this suggests that IκBε may mediate an anti-phase negative feedback that provides effective dampening of IκBα-mediated oscillations. Indeed, simulations of signaling modules lacking IκBε revealed oscillations in nuclear NF-κB that persist with a higher amplitude than those including IκBε and representing wild type cells (Figure 3.4D). In contrast, simulations of cells lacking IκBβ do not show such aberrant oscillations, while systems lacking both IκBε and IκBβ do.

These predictions were tested experimentally using nuclear extracts prepared from TNF treated MEFs harboring genetic deficiencies for IκBε and/or IκBβ. NF-κB DNA binding activity was measured by Electrophoretic Mobility Shift Assay (EMSA, Figure 3.4E) and nuclear localization of the NF-κB protein RelA by Western Blot (Figure 3.5). In both assays, all four cell types exhibit fast induction of nuclear NF-κB in response to TNF stimulation by 15 and 30 min, a transient trough at 60 – 75 minutes and subsequent recovery at 90-120 min. However a second trough at 135-150 min was most pronounced in *iκbε*$^{-/-}$ and *iκbε*$^{-/-}$*β*$^{-/-}$ cells, as was a third trough at around 225 min. These studies suggest that negative feedback provided by IκBε in anti-phase to that of IκBα is the primary mechanism that dampens the propensity for oscillations in NF-κB activity.

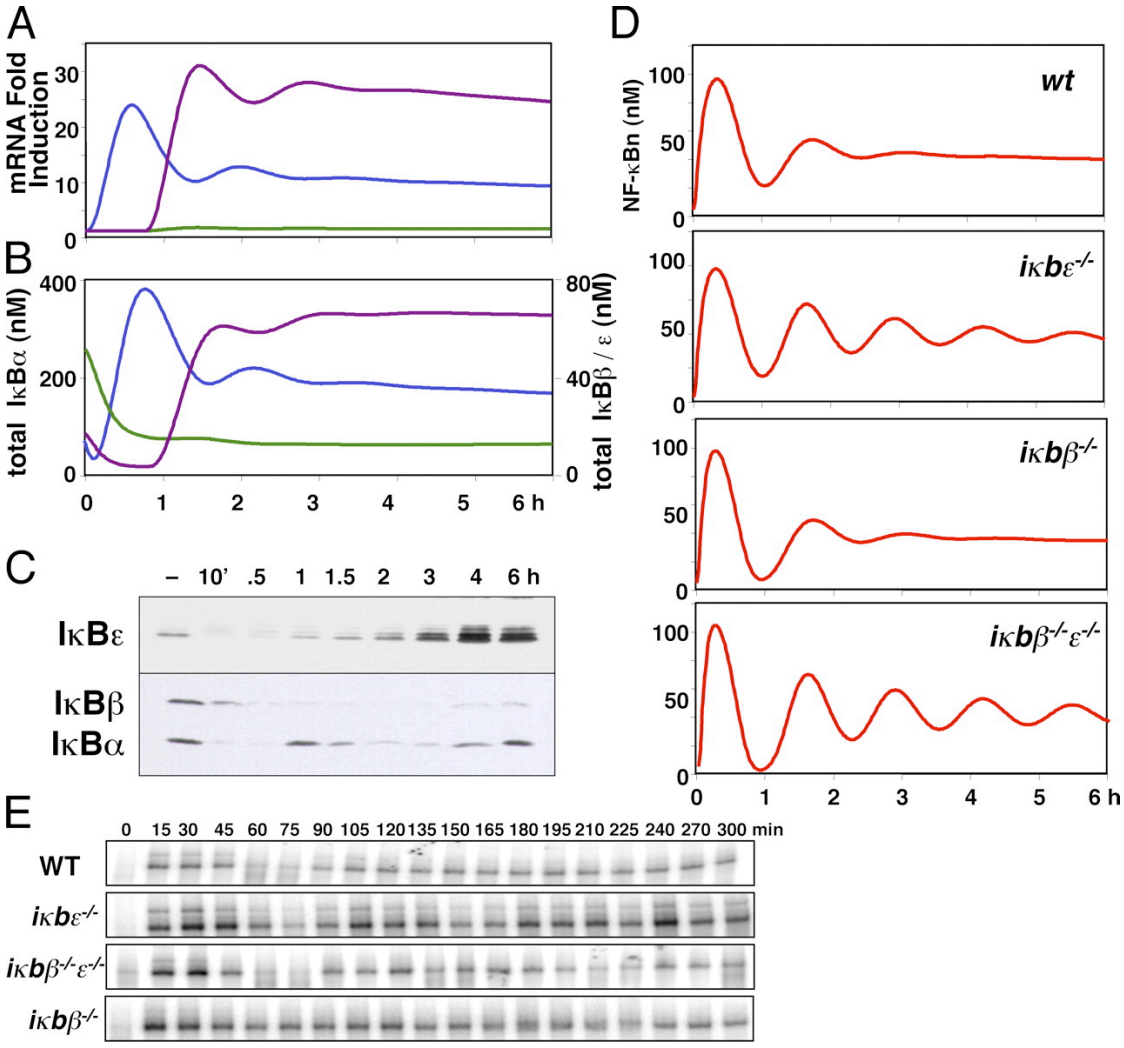

Figure 3.4 Computational modeling of IκB mRNA and protein levels reveals a role for IκBε in regulating the dynamics of NF-κB activity in response stimulation

(A) The results of computational simulations of the fold induction of mRNA synthesis and (B) of the protein levels for IκBα (blue), IκBβ (green), and IκBε (purple) in wild-type cells in response to persistent stimulation with TNF.
(C) Western blots of IκB proteins in wild-type cells in response to persistent stimulation with TNF.
(D) The results of computational simulations and (E) EMSAs of nuclear NF-κB activity in wild type, *iκBε*$^{-/-}$, *iκbβ*$^{-/-}$, and *iκbβ*$^{-/-}$*ε*$^{-/-}$ cells in response to persistent TNF stimulation.

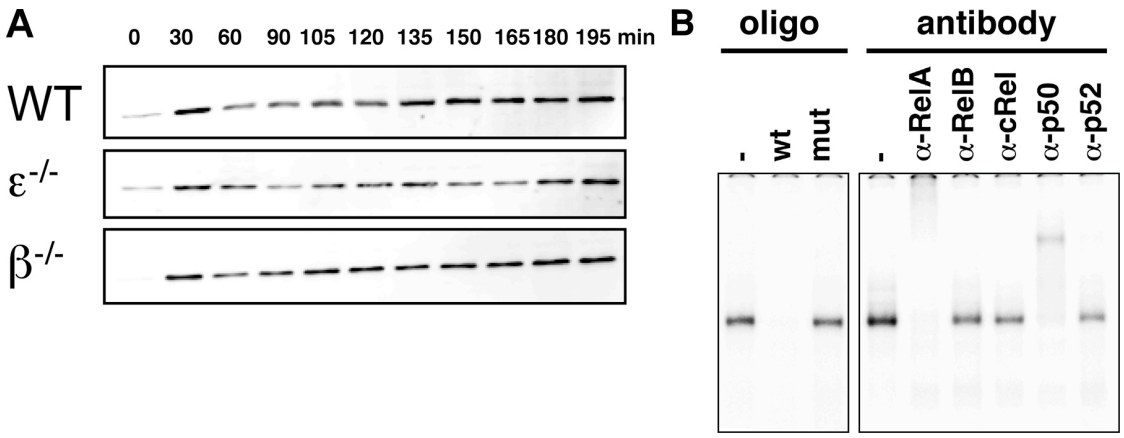

Figure 3.5 Western blots for RelA of nuclear extracts prepared from TNF-stimulated cells and EMSA super-shift analysis

(A) Western Blot of NF-κB activity, using α-RelA antibody (SC-372; Santa Cruz Biotechnology, Inc.), in nuclear extracts prepared at the indicated time points from wild-type, *iκbε*$^{-/-}$, and iκbβ$^{-/-}$cells chronically stimulated with TNF.
(B) EMSA of nuclear extracts prepared from TNF stimulated MEF cells harvested at 30 min post-stimulation. Competition studies were performed with double-stranded wild type and mutant oligonucleotides. Super-shift studies were performed with antibodies for each NF-κB family member as described previously in Hoffmann et al. (2003).

The IκBα and IκBε dual negative feedback circuit is optimally tuned to dampen oscillatory NF-κB activity

The regulatory motif consisting of two anti-phase negative feedback systems may be present in other signaling pathways to control the dynamics of signal transduction and variations in the relative strength of the two systems may provide for altered response dynamics to the same stimulus. More recently, in collaboration with Diane Longo (Institute for Nonlinear Science, UCSD), the dual negative feedback signaling architecture was analyzed to determine its signal processing characteristics (Longo *et al*, in preparation).

Diane constructed an analytically tractable mathematical model that describes the dual IκBα and IκBε negative feedback circuit as a smaller, coarse-grained network (Chapter 1) consisting of a driver (NEMO/IKK2, *K*), a transcriptional activator (NF-κB, *x*), two negative feedback regulators (IκBα and IκBε, *y* and *z*), and inhibitor:activator complexes (IκBα:NF-κB and IκBε:NF-κB, *xy* and *xz*)(Figure 3.6A). Unlike the ODE-based model described earlier that contains 72 reactions, this coarse-grained model consists of only 14 reactions. Importantly, the reactions governing IκB negative feedback (synthesis, nuclear import, association with nuclear NF-κB, and export of the complex) are combined into single compound mathematical expressions. An explicit time delay (τ) is utilized to replace the delay that would have occurred had the individual reactions been modeled sequentially. A parameter, *m*, is included within the IκBε negative feedback expression as a means of tuning the strength of IκBε feedback relative to that of IκBα (where $m = 0$ removes IκBε feedback and $m = 1$ sets IκBε feedback equal to that of IκBα).

This new mathematical model was analyzed to determine the effect of varying the time delay for IκBε feedback (τ) and the strength of IκBε feedback relative to IκBα (m) on the amplitude of NF-κB activity oscillations (Figure 3.6B). For each pair of parameter values, a 6 h simulation of NF-κB activity was calculated and a maximal peak-to-trough difference computed. The full pair wise simulations results for this metric are shown as a color heat map in which severe oscillations are represented in red and fully dampened oscillations in blue. These results show that there is a region of parameter space in which NF-κB activity consists of dampened oscillations.

To validate this finding, I performed experimental studies using wild type MEF that were chronically stimulated with a high dose (10 ng/mL) of TNF cytokine. Using RPA to measure IκBα and IκBε mRNA syntheses, I found that there is a delay of 37 min between the points at which IκBα and IκBε reach half-maximal induction (Figure 3.6C). Using Western blot to measure IκBα and IκBε protein, and converting these results to molecule numbers via standard curves of recombinant protein (C. Lynch and S. Basak, Chapter 6), I determined that the peak abundance of IκBε protein is approximately 1/5 that of IκBα (Figure 3.6D). The experimental results reside within a region of the model parameter space in which dampened oscillations are observed (Figure 3.6B), suggesting that IκBε kinetics are well tuned for dampening IκBα-mediated NF-κB oscillatory activity.

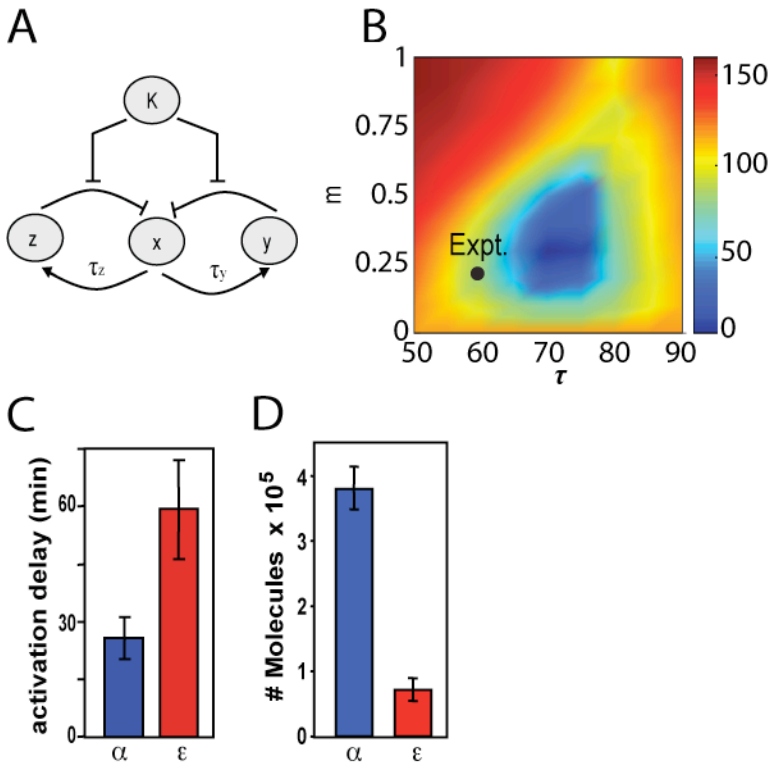

Figure 3.6 IκBε negative feedback is tuned to dampen oscillatory NF-κB activity

(A) Schematic of an analytical model containing two negative feedback mechanisms. The model contains NEMO/IKK2 (K), NF-κB (x), IκBα (y), and IκBε (z). IκB negative feedback is represented by a compound reaction that encompasses NF-κB-induced transcription, translation, nuclear import, association with free nuclear NF-κB, and export of the IκB:NF-κB complex to the cytoplasm. The terms τ_y and τ_z represent the time delay (min) for the IκBα and IκBε compound reactions, respectively.

(B) Optimization of the parameters of the IκBε feedback loop *m* and τ_z towards maximizing dampening of the NF-κB oscillations. Oscillatory amplitude (peak – trough NF-κB activity at 6 hr post stimulation) is represented as a heatmap. The term *m* represents the relative feedback strength of IκBε versus IκBα where $m = 1$ is equal strength and $m = 0$ is an IκBε deficient system. The black dot indicates the experimentally measured parameter values for τ_z (59 min) and for *m* (0.2)

(C) Experimental measurements of IκBα and IκBε synthesis delays determined from repeated (n = 10) RPA measurements of wild type MEFs stimulated with 10 ng/mL TNF.

(D) Experimental measurements by Western blot using recombinant IκB protein standard of maximal/peak IκBα and IκBε protein levels in MEFs stimulated with 10 ng/mL TNF.

IκBε mediates post-induction repression of NF-κB activity and inflammatory gene expression

The full computational model was used to identify conditions in which NF-κB-responsive IκBε expression would mediate negative feedback on stimulus-induced NF-κB activity and found the most significant role for IκBε in systems with reduced IκBα. To model such conditions we used computational simulations to study the temporal profile of nuclear NF-κB in response to 15 min stimulation in systems lacking IκBα, IκBε, or both (Figure 3.7A). Systems containing all three IκBs show rapid nuclear localization of NF-κB followed by removal from the nucleus within 1 h, as previously shown (Hoffmann *et al*, 2002). However, in systems lacking IκBα, we predicted effective down regulation of NF-κB activity in the third hour and beyond. In this context, IκBε deficiency results in prolonged NF-κB activity, while in systems containing high IκBα expression it does not have an effect.

IκBα-deficient MEFs were used as a model for cell types that have reduced IκBα expression. These showed NF-κB activity to about 3 h in response to 15 min transient TNF stimulation, after which it was dramatically attenuated (Figure 3.7B). In contrast, cells deficient in both IκBα and IκBε showed a pronounced delay in attenuation with NF-κB still present in the nucleus even at 6 h. Wild-type and IκBε-deficient cells are nearly indistinguishable and have strong NF-κB accumulation at 30 min and attenuation within 1 h. Taken together, these data strongly suggest that IκBε is responsible for the removal of NF-κB from the nucleus at late time points allowing for dynamic functional interplay with the faster acting feedback of IκBα.

Temporal control of NF-κB localization by IκBα was shown to control NF-κB responsive gene expression not only quantitatively (Nelson *et al*, 2004), but also qualitatively (Hoffmann *et al*, 2002). To study the effects of IκBε negative feedback on NF-κB-dependent gene expression, the transcription of five NF-κB responsive genes was monitored by RPA after transient TNF stimulation in wild-type, $i\kappa b\alpha^{-/-}$, and $i\kappa b\alpha^{-/-}i\kappa b\varepsilon^{-/-}$cells. The genes encoding TNF, G-CSF, and LIF are inducibly expressed in fibroblasts upon TNF stimulation, but mRNA levels return to baseline within 3 h in wild-type cells. In IκBα-deficient cells, these genes are attenuated within 4 h (Figure 3.7C). In this context, the loss of IκBε negative feedback results in a further delay in attenuation and quantitative deregulation of TNF, G-CSF, and LIF expression. Interestingly, the loss of both IκBα and IκBε negative feedback has a dramatic qualitative effect for GM-CSF and MIP-2. While these genes are not induced in wild type or IκBα-deficient cells, both are strongly responsive to NF-κB activation when both IκBα and IκBε negative feedbacks are absent. The data presented here demonstrate that IκBε-dependent negative feedback regulates the termination of NF-κB-responsive gene expression in both a quantitative (in the case of TNF, G-CSF, ad LIF) and qualitative (in the case of GM-CSF, and MIP-2) manner.

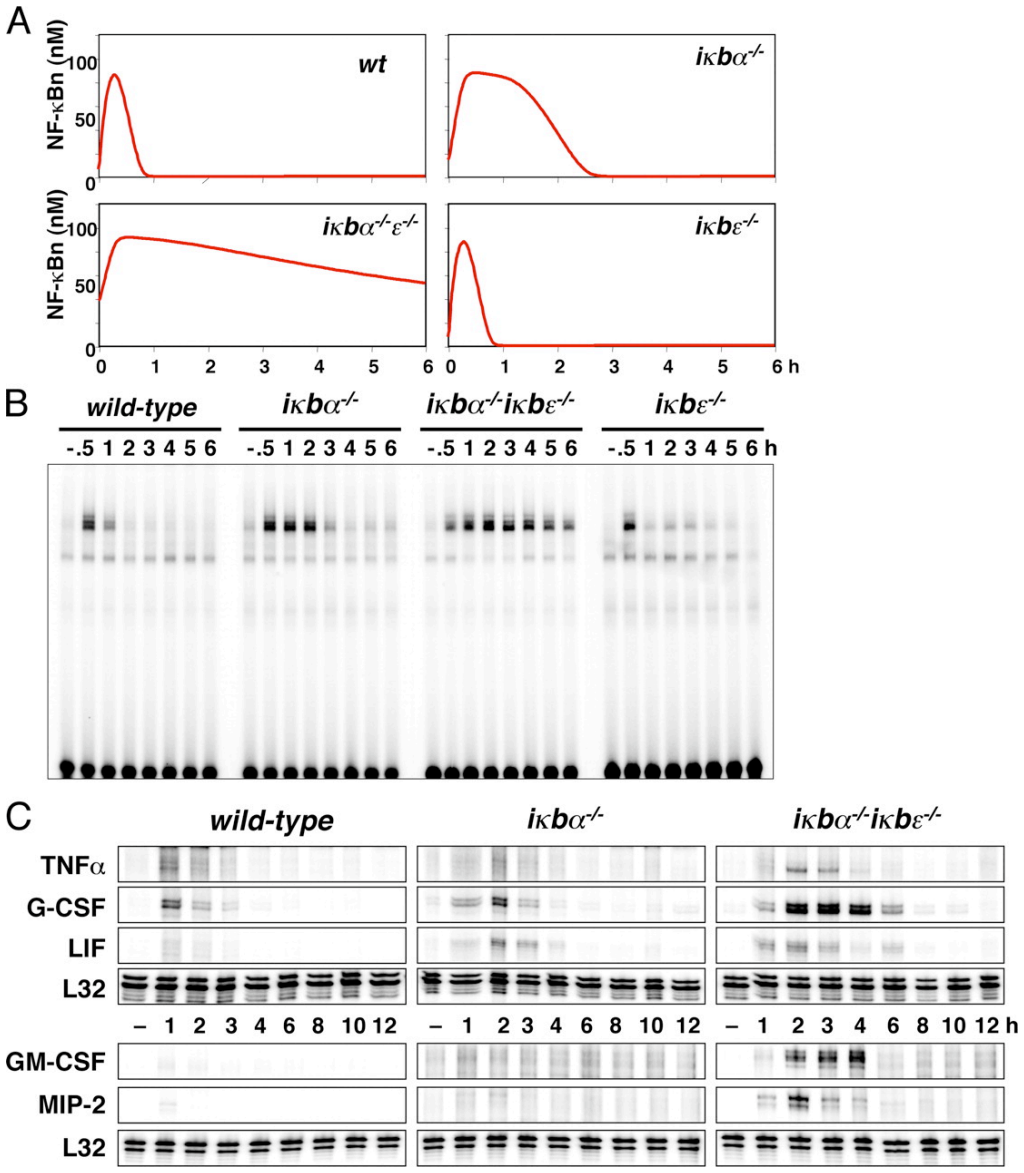

Figure 3.7 IκBε mediates post-induction repression of NF-κB activity and inflammatory gene expression

(A) Nuclear NF-κB activity as predicted by computational modeling following 15 min of TNF stimulation.
(B) EMSA of nuclear NF-κB activity in extracts prepared at the indicated time points from wild-type, *iκbα*$^{-/-}$, *iκbα*$^{-/-}$iκbε$^{-/-}$, and iκbε$^{-/-}$cells transiently stimulated for 15 min with 1ng/mL TNF.
(C) RPA reveals the mRNA levels over an extended time course of indicated NF-κB responsive genes in wild-type, *iκbα*$^{-/-}$, and *iκbα*$^{-/-}$*iκbε*$^{-/-}$ cells that were transiently stimulated for 45 min with TNF.

DISCUSSION

The functional interplay between the anti-phase IκBα and IκBε negative feedback responses may explain differences in NF-κB-dependent gene expression profiles seen in various cell types. In MEFs, IκBε-mediated negative feedback appears to be secondary to that provided by IκBα in response to transient inflammatory stimuli and it is therefore assumed that IκBα controls the bulk of the NF-κB-responsive gene expression (Ghosh *et al*, 1998). However, the ratio of the abundance of IκBε in relation to IκBα is cell type-specific (Doerre *et al*, 2005; Emmerich *et al*, 2003; Memet *et al*, 1999; Spiecker *et al*, 2000), suggesting that IκBε may play a predominant role in NF-κB-responsive gene expression in particular cell types. Indeed, *in vivo* studies have shown that a deficiency of functional IκBε has physiological consequences (Doerre *et al*, 2005; Emmerich *et al*, 2003; Memet *et al*, 1999; Spiecker *et al*, 2000) and thus emphasize the notion that no IκB isoform functions on its own. In order to understand regulation of NF-κB activity in different cell types and in response to diverse stimuli, the interplay of all IκB isoforms within the IKK-IκB-NF-κB signaling module must be considered.

This study aimed to quantitatively characterize the temporal expression profiles of the three IκB isoforms and to examine their functional consequences on NF-κB regulation. Earlier studies showed inducible IκBε expression (Simeonidis *et al*, 1997; Whiteside *et al*, 1997) while this study demonstrates that induction of IκBε is NF-κB-dependent and functions to attenuate NF-κB activity and terminate NF-κB-responsive gene expression. Based on these three criteria, IκBε mediates *bona fide*

functional negative feedback regulation on NF-κB activity. Importantly the delay in the inducible expression of IκBε with respect to that of IκBα creates a two negative feedback regulatory module that critically controls the dynamics of NF-κB activity. A similar model has been proposed for two NF-κB inducing signaling pathways emanating from the TLR4 receptor (Covert *et al*, 2005). In contrast to the two interacting negative feedback mechanisms described here, this model depicts the coupling of two positive oscillatory signals in an anti-phase relationship that produces stable NF-κB activity in response to LPS stimulation in wild type cells. As the temporal control of NF-κB activity determines NF-κB-responsive gene expression (Hoffmann *et al*, 2002; Nelson *et al*, 2004; Werner *et al*, 2005), the interaction of anti-phase regulation by IκBα and IκBε may contribute to the regulation of stimulus-specific and cell type-specific gene expression programs by modulating the dynamics of this transcription factor.

MATERIALS AND METHODS

Experimental Studies:

Cell culture and experiments were performed as described in the Materials and Methods (Chapter 2). Antibodies were generously provided by Santa Cruz Biotechnology (IκBα: sc-371, IκBβ: sc-945, RelA: sc-109, RelB: sc-226, cRel: sc-70, p50: sc-114, p52: sc-298). An antigen-purified polyclonal moue antiserum raised against recombinant full-length mouse protein was used for IκBε (generated previously by Alexander Hoffmann).

Computational Studies:

Description of the Computational Model

The model is comprised of 24 molecular species and 72 reactions that link IKK activity (the *input*) to NF-κB nuclear localization (the *output*) as depicted graphically in Figure 1.3. The species of the model are denoted in Table 3.1 and the reactions and parameters are listed in Table 3.2.

Computational Simulations

The ODEs were solved numerically using MATLAB version R2006a (The MathWorks, Inc.) with subroutine *ode15s*, a variable order, multi-step solver. Prior to stimulation, the system was allowed to equilibrate from starting conditions to a steady state, defined as showing no concentration changes greater than 1% over a period of 4000 minutes. Stimulus-induced perturbation from the equilibrium state was accomplished by increasing the cellular abundance of IKK (second value listed for IKK in Table 3.1).

Table 3.1 Model v1.2 Species and Initial Concentrations

The model contains 24 species that represent the molecular species (mRNA and proteins) within the signaling module. Each species is given an initial concentration that is used as an input to the equilibrium (steady state) simulation. Species are localized to the cytoplasm or the nucleus. The initial concentration of IKK is 0.001 μM and this is retained amongst free IKK and IKK-containing complexes. At the beginning of the stimulation phase, IKK is increased to 0.8 μM and subject to a degradation reaction (Table 3.2). The initial concentration of NF-κB is set to 0.125 μM and is retained amongst free NF-κB and NF-κB-containing complexes during all phases of the simulation.

	mRNA, Proteins and Protein Complexes	**Model Species**	**Initial μM**	**Location**
1	IKK	IKK	0.001, 0.8 *	Cytoplasm
2	NF-κB	NFkB	0.125	Cytoplasm
3	NF-κB	NFkBn	0	Nucleus
4	IκBα	IkBa	0	Cytoplasm
5	IκBα	IkBan	0	Nucleus
6	IκBβ	IkBb	0	Cytoplasm
7	IκBβ	IkBbn	0	Nucleus
8	IκBε	IkBe	0	Cytoplasm
9	IκBε	IkBen	0	Nucleus
10	IκBα mRNA	IkBat	0	Cytoplasm
11	IκBβ mRNA	IkBbt	0	Cytoplasm
12	IκBε mRNA	IkBet	0	Cytoplasm
13	IKK-IκBα	IKKIkBa	0	Cytoplasm
14	IKK-IκBβ	IKKIkBb	0	Cytoplasm
15	IKK-IκBε	IKKIkBe	0	Cytoplasm
16	IκBα-NF-κB	IkBaNFkB	0	Cytoplasm
17	IκBα-NF-κB	IkBaNFkBn	0	Nucleus
18	IκBβ-NF-κB	IkBbNFkB	0	Cytoplasm
19	IκBβ-NF-κB	IkBbNFkBn	0	Nucleus
20	IκBε-NF-κB	IkBeNFkB	0	Cytoplasm
21	IκBε-NF-κB	IkbeNFkBn	0	Nucleus
22	IKK-IκBα-NF-κB	IKKIkBaNFkB	0	Cytoplasm
23	IKK-IκBβ-NF-κB	IKKIkBbNFkB	0	Cytoplasm
24	IKK-IκBε-NF-κB	IKKIkBeNFkB	0	Cytoplasm

Table 3.2 Model v1.2 Reactions and Rate Constants

The model contains 72 reactions. Each reaction has a kinetic rate constant and is localized to either the cytoplasm (cyt) or nuclear (nuc) cellular compartments. The reactant or product 'null' represents a source (in the case of constitutive RNA synthesis) or a sink (in the case of RNA or protein degradation).

The transcription of IκBs is governed by multiple parameters and follows the form:

$$\frac{\mathbf{dmRNA}}{\mathbf{dt}} = \mathbf{k1 + k2^{*}\ NF\text{-}\kappa Bn^{H} - k3}$$

Where *k1* is the constitutive transcription rate, *k2* is the inducible transcription rate, *H* is the Hill Coefficient, and *k3* is the constitutive mRNA degradation rate.

IκBα	IκBβ	IκBε	Units	Description and Notes
1.1848e-4	4.272e-5	4.572e-6	min^{-1}	**Constitutive transcription** null => mRNA mRNA synthesis parameters were derived from mRNA and protein expression profiles measured by RPA and Western Blots in wild type and NF-κB-deficient cells
1.386	0.01	0.18	μM^{-2} min^{-1}	**Inducible transcription** null => mRNA *refer to Constitutive Transcription*
0	45	45	min^{-1}	**Inducible transcription delay** Component of the inducible transcription reaction that delays synthesis until this time point has been reached. Zero in equilibrium phase. Delays were measured via RPA.
2	2	2	-	**Hill Coefficient** Component of the inducible transcription reaction that imparts cooperativity of NF-κB DNA binding and transactivation.
0.0336	0.0168	0.0118	min^{-1}	**mRNA degradation** mRNA => null (Hoffmann *et al*, 2002)
0.2448	0.2448	0.2448	min^{-1}	**Translation** mRNA => mRNA + IκB (Hoffmann *et al*, 2002)
0.018	0.018	0.018	min^{-1}	**Free IκB Nuclear Import** IκB => IκBn (Hoffmann *et al*, 2002)
0.012	0.012	0.012	min^{-1}	**Free IκB Nuclear Export** IκBn => IκB (Hoffmann *et al*, 2002)

Table 3.2 Model v1.2 Reactions and Rate Constants, Continued.

0.828	0.414	0.414	min^{-1}	**IκB:NF-κB Nuclear Export** IκB:NF-κBn => IκB:NF-κB (Hoffmann *et al*, 2002)
IκB independent, 5.4			min^{-1}	**NF-κB Nuclear Import** NF-κB => NF-κBn (Hoffmann *et al*, 2002)
IκB independent, 0.0048			min^{-1}	**NF-κB Nuclear Export** NF-κBn => NF-κB (Hoffmann *et al*, 2002)
30	30	30	μM^{-1} min^{-1}	**IκB:NF-κB Association (cyt, nuc)** IκB + NF-κB => IκB:NF-κB (Hoffmann *et al*, 2002)
6e-5	6e-5	6e-5	min^{-1}	**IκB:NF-κB Dissociation (cyt, nuc)** IκB:NF-κB => IκB + NF-κB (Hoffmann *et al*, 2002)
1.35	0.36	0.54	μM^{-1} min^{-1}	**IκB:IKK Association** IκB + IKK => IκB:IKK (Hoffmann *et al*, 2002)
0.075	0.105	0.105	min^{-1}	**IκB:IKK Dissociation** IκB:IKK => IκB:IKK (Hoffmann *et al*, 2002)
11.1	2.88	4.2	μM^{-1} min^{-1}	**IκB:NF-κB + IKK Association** IκB:NF-κB +IKK =>IκB:NF-κB:IKK (Hoffmann *et al*, 2002)
0.075	0.105	0.105	min^{-1}	**IκB:NF-κB + IKK Dissociation** IκB:NF-κB:IKK =>IκB:NF-κB+IKK (Hoffmann *et al*, 2002)
30	30	30	μM^{-1} min^{-1}	**IκB:IKK + NF-κB Association** IκB:IKK +NF-κB =>IκB:NF-κB:IKK (Hoffmann *et al*, 2002)
6e-5	6e-5	6e-5	μM^{-1} min^{-1}	**IκB:IKK + NF-κB Dissociation** IκB:IKK:NF-κB =>IκB:IKK +NF-κB (Hoffmann *et al*, 2002)
0.12	0.18	0.18	min^{-1}	**Free IκB degradation (cyt, nuc)** IκB => null (Hoffmann *et al*, 2002)
6e-5	6e-5	6e-5	min^{-1}	**Bound IκB degradation (cyt, nuc)** IκB:NF-κB => null + NF-κB (Hoffmann *et al*, 2002)
1.8e-3	1.8e-3	1.8e-3	min^{-1}	**IKK-mediated free IκB degradation** IκB:IKK => null + IKK (Hoffmann *et al*, 2002)
0.36	0.12	0.18	min^{-1}	**IKK-mediated bound IκB degradation** IκB:NF-κB:IKK => NF-κB + IKK (Hoffmann *et al*, 2002)
IκB independent, Phase 1 (Equilibrium) : 0.0 Phase 2 (Stimulation) : 7.2e-3 Phase 3 (after TNF pulse) : 1.0			min^{-1}	**Free IKK degradation** IKK => null IKK is given an exponential decay that is different for each phase of the simulation, as denoted. (Hoffmann *et al*, 2002)

ACKNOWLEDGEMENTS

Text and figures are adapted from a *JCB* research report for which I am the primary author (Kearns *et al*, 2006). Soumen Basak, Shannon L. Werner, and Christine S. Huang provided help with some of the experiments. Soumen provided laboratory training and performed the EMSA shown in panel B of Figure 3.5, Shannon and I jointly performed the RPA shown in panel C of Figure 3.7, and Christine performed the EMSA shown in panel B of Figure 3.7. Professor Alexander Hoffmann is the corresponding author.

Figure 3.6 and its accompanying text are derived from research that is in preparation for submission (Longo *et al*, in preparation) for which I am a co-author. Diane Longo constructed the mathematical model and performed the simulations (Figure 3.6A and B). I performed the experiments (Figure 3.6C and D). Professors Alexander Hoffmann, Jeff Hasty, and Lev Tsimring (corresponding) are also co-authors.

Chapter 4

IκBα and A20 negative regulators have distinct roles in determining TNF-induced NF-κB activity

ABSTRACT

TNF-induced NF-κB activity shows complex temporal regulation whose different phases lead to distinct gene expression programs. Combining experimental studies and mathematical modeling, we identify two temporal amplification steps – one determined by the obligate negative feedback regulator IκBα – that define the duration of the first phase of NF-κB activity. The second phase is defined by A20, whose inducible expression provides for a rheostat function by which other inflammatory stimuli can regulate TNF responses. Our results delineate the non-redundant functions implied by the knockout phenotypes of IκBα and A20, and identify the latter as a signaling crosstalk mediator controlling inflammatory and developmental responses.

INTRODUCTION

Tumor Necrosis Factor (TNF) is a potent cytokine and critical regulator of apoptosis, inflammation and immunity (Wallach *et al*, 1999) *via* control of the transcription factor Nuclear Factor kappaB (NF-κB). In response to injury or infection, TNF is secreted in bursts by tissue-resident macrophages, and due to a short half-life (Beutler *et al*, 1985) is sensed by responsive cells as transient, or pulse, stimulation. Termination of the resulting NF-κB activity is critical to preventing aberrant inflammatory gene expression, and its misregulation has been implicated in pathologies including cancer, heart disease and Crohn's disease (Aggarwal *et al*, 2002; Kaufman and Choi, 1999; Monaco and Paleolog, 2004).

Several attenuators of the TNF-NF-κB axis have been described, including the rapidly and highly inducible IκBα and A20 genes (Scott *et al*, 1993; Song *et al*, 1996). IκBα attenuates NF-κB nuclear localization and DNA-binding (Scott *et al*, 1993), and A20 inhibits signaling upstream of IKK by interfering with the K63-linked ubiquitin chains on RIP1 that are required for activation of the TNFR associated signaling complex (Wertz *et al*, 2004)(Boldin and Baltimore, unpublished results). Based on their NF-κB-dependent, inducible expression, IκBα and A20 are commonly thought of as negative feedback regulators in the TNF-NF-κB signaling pathway. However, whether inducible expression is required for their function (i.e. as obligate negative feedback regulators) remains to be tested. Abolishing both constitutive and inducible expression by genetic deletion in mice results in lethality, perinatally in the case of IκBα (Beg *et al*, 1995; Klement *et al*, 1996) or within a few weeks of age in the case

of A20 (Lee *et al*, 2000). This suggests that even though IκBα and A20 act in the same signaling axis, they apparently have non-redundant (i.e. differential or specific) functions. Indeed, mutations in the IκBα gene are linked to Hodgkins lymphoma (Cabannes *et al*, 1999; Krappmann *et al*, 1999), whereas A20 has been shown to control the severity of atherosclerosis (Wolfrum *et al*, 2007), the responsiveness to commensual bacteria (Hitotsumatsu *et al*, 2008; Turer *et al*, 2008) and of T-cells (Stilo *et al*, 2008), as well as the development of regulatory T cells and anti-tumor responses (Song *et al*, 2008).

Negative feedback regulators not only terminate cellular responses, they also modulate the dynamics of cellular signaling (Kholodenko, 2006; Stelling *et al*, 2004). In the case of TNF signaling, the temporal profile of NF-κB activity is complex: a first phase NF-κB activity is associated with the expression of a large number of genes that mediate non-specific inflammatory and stress responses (such as cytokines, anti-apoptotic regulators and heat shock proteins), whereas longer lasting NF-κB activity elicits the expression of chemokines (e.g. MCP3, MCP5 and RANTES) and tissue proteases (e.g. MMP3, 9, 10, 12, 13) required for an effective adaptive immune response (Hoffmann *et al*, 2003; Hoffmann *et al*, 2002; Saccani *et al*, 2001; Tian *et al*, 2005; Werner *et al*, 2005).

To examine how temporal control of NF-κB is encoded in response to TNF stimulation, we identified functional signaling modules (Hartwell *et al*, 1999) within the inflammatory network: first, I constructed a mathematical model for the TNFR-IKK signaling module that recapitulates the biochemical events triggered by TNFR engagement, and then integrated it with the IκB-NF-κB module to yield a

mathematical description of the TNF-NF-κB signaling axis. Using the combined model in conjunction with experiments performed by my collaborators in the laboratory (Shannon L. Werner, Victoria Zadorozhnaya, Candace Lynch, and Ellen O'Dea), we reveal distinct roles of IκBα and A20 in encoding NF-κB temporal control.

RESULTS

A mathematical model was constructed and parameterized that recapitulates TNF signaling to NF-κB. The model is comprised of 33 species and 98 reactions (Table 4.2, Table 4.3) and consists of a newly constructed model for the TNFR-IKK signaling module (Figure 4.1, blue box) combined with the model for the IκB-NF-κB signaling module (Figure 4.1, yellow box) that is based on previously published work (Hoffmann *et al*, 2002; Kearns *et al*, 2006; O'Dea *et al*, 2007; Werner *et al*, 2005). Our model of the TNFR-IKK signaling module includes the TNF-induced receptor trimerization step (Banner *et al*, 1993; Grell *et al*, 1998), receptor internalization (Watanabe *et al*, 1988), recruitment and activation of the TRAF2, TRADD, RIP (TTR) complex to TNFR1 to form active Complex 1 (C1*) *via* K63 ubiquitination of RIP (Schneider-Brachert *et al*, 2004), and activation of the TAK1/TAB2/TAB3 kinase complex (TAK) (Wang *et al*, 2001). IKK is activated *via* phosphorylation of activation loop serines (Mercurio *et al*, 1997) and inactivated *via* an activity-dependent mechanism (Delhase *et al*, 1999). The combined model of the TNFR-IKK and IκB-NF-κB modules (Figure 4.2) also includes the reactions that control NF-κB-dependent synthesis of A20, which directly counteracts C1 activation by deubiquitinating RIP (Wertz *et al*, 2004).

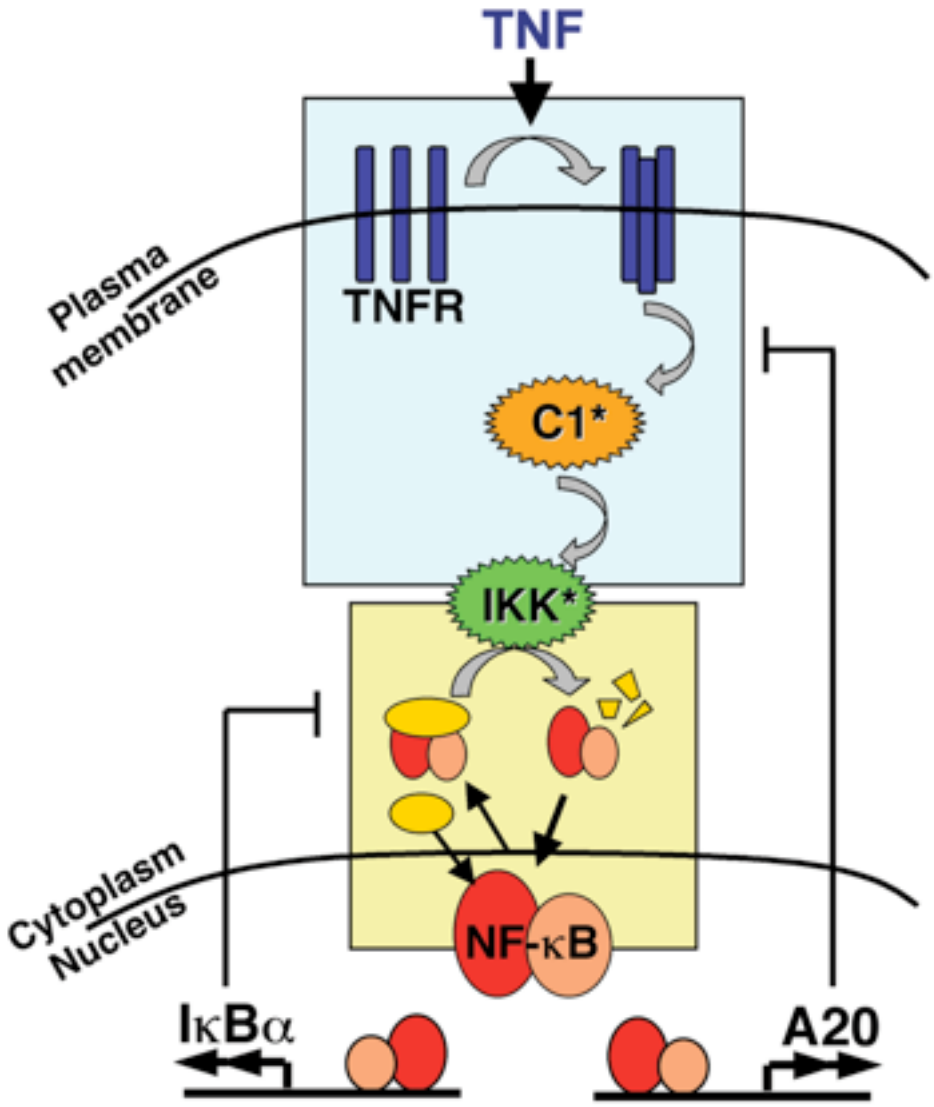

Figure 4.1 A mathematical model of TNFR signaling to NF-κB

Schematic depicting TNF signaling from TNFR to IKK, which function as the input to the NF-κB signaling module. The two most rapidly NF-κB-inducible attenuators, IκBα and A20, are shown. TNF cytokine induces trimerization of TNFR monomers which then associate with intracellular cofactors to form active Complex 1 (C1*). Signaling from C1* activates IKK.

Rate constants (parameters) for the TNFR-IKK module were derived either from the literature or our own experimental data For example, parameter values for A20 mRNA/protein synthesis and half-life were derived from experimentally determined mRNA and protein expression profiles. Other rate constants were derived *via* parameter fitting techniques and ascribed values within ranges that satisfied a set of experimentally determined constraints (Table 4.1, Figure 4.14). The constraints were expressed in quantitative terms that enabled the direct interpretation within the model of simulations results. This allowed for high-throughput screening of parameter values to ascertain the ranges of values for each parameter that satisfy all constraints (Figure 4.15).

Simulation of chronic TNF stimulation results in curves for the concentrations over time of "free" TNF protein, of IKK and NF-κB activities (Figure 4.4, left) that were validated against experimental measurements of similarly treated MEF (Figure 4.4, right). *In vitro* kinase activity measurements of immunoprecipitated IKK complexes confirmed that peak activation occurs at 10 min followed by a rapid attenuation to a plateau that is just a few fold above baseline. Similarly, TNF-induced IκBα protein degradation and rapid resynthesis is accurately reproduced in the model simulation, as is the induction of A20 protein synthesis. The model correctly describes the experimentally measured NF-κB activity profile, which peaks at 30 min, followed by post-induction repression at 90 min, and a subsequent plateau of late activity.

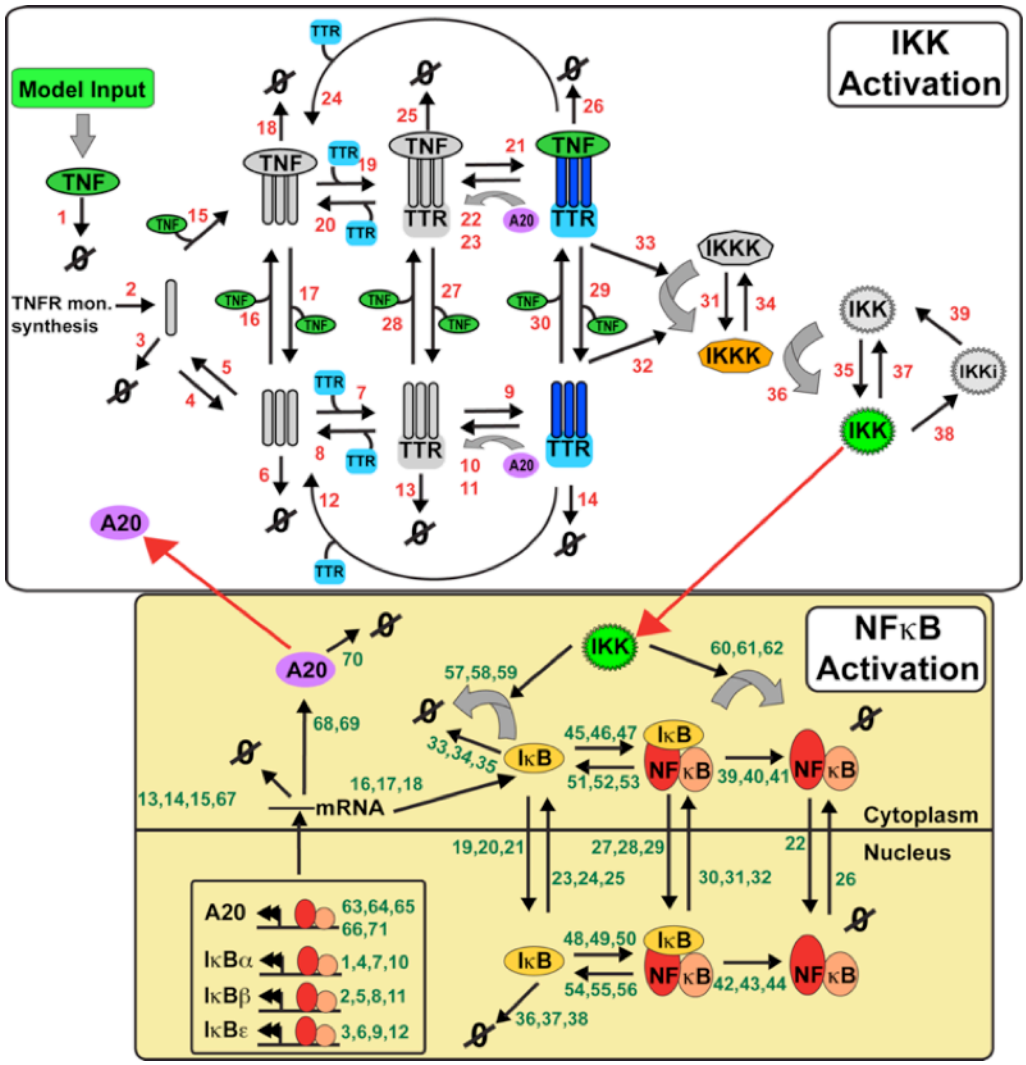

Figure 4.2 Reaction map of the combined IKK and NF-κB activation modules

The model is comprised of two connected signaling modules that govern IKK and NF-κB activation. The input to the model is a concentration of TNF ligand. The model contains 33 species listed in tabular (Table 4.2) and graphical forms (Figure 4.3). Numbers adjacent to reaction arrows denote individual model rate constants and are listed in Table 4.3.

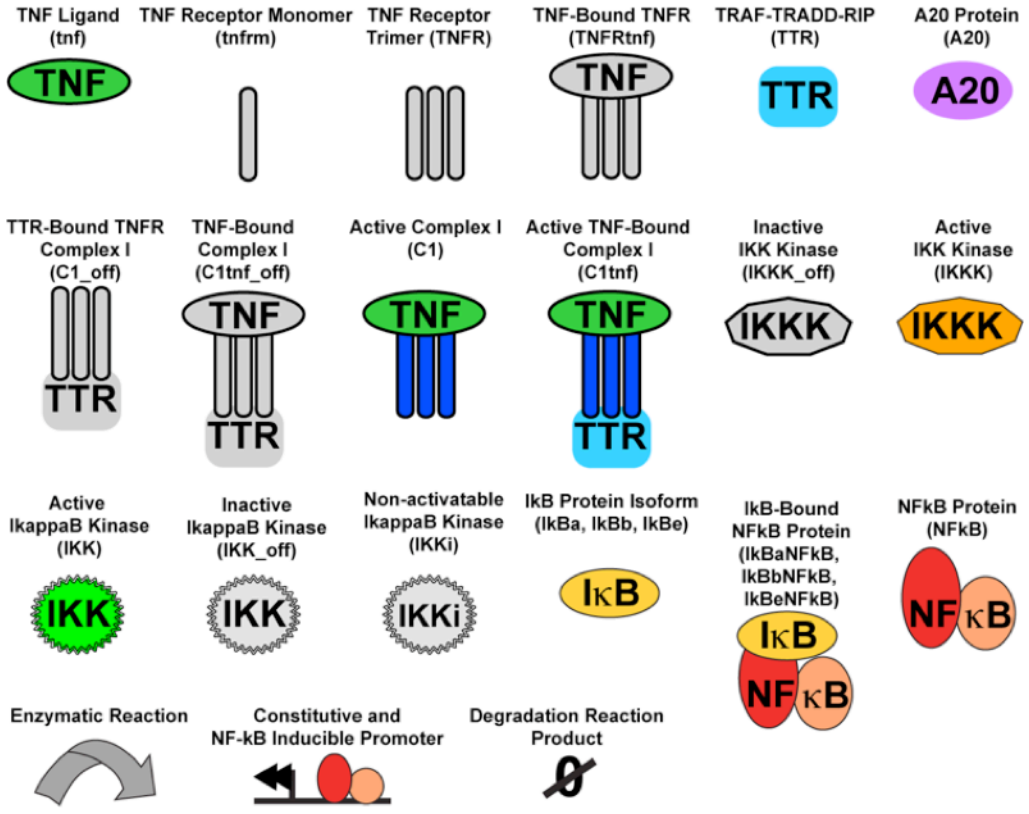

Figure 4.3 Graphical legend for TNF-IKK-NF-κB reaction map

This legend connects the symbols used in the reaction map (Figure 4.2) to the textual names used within the computational model (Table 4.2).

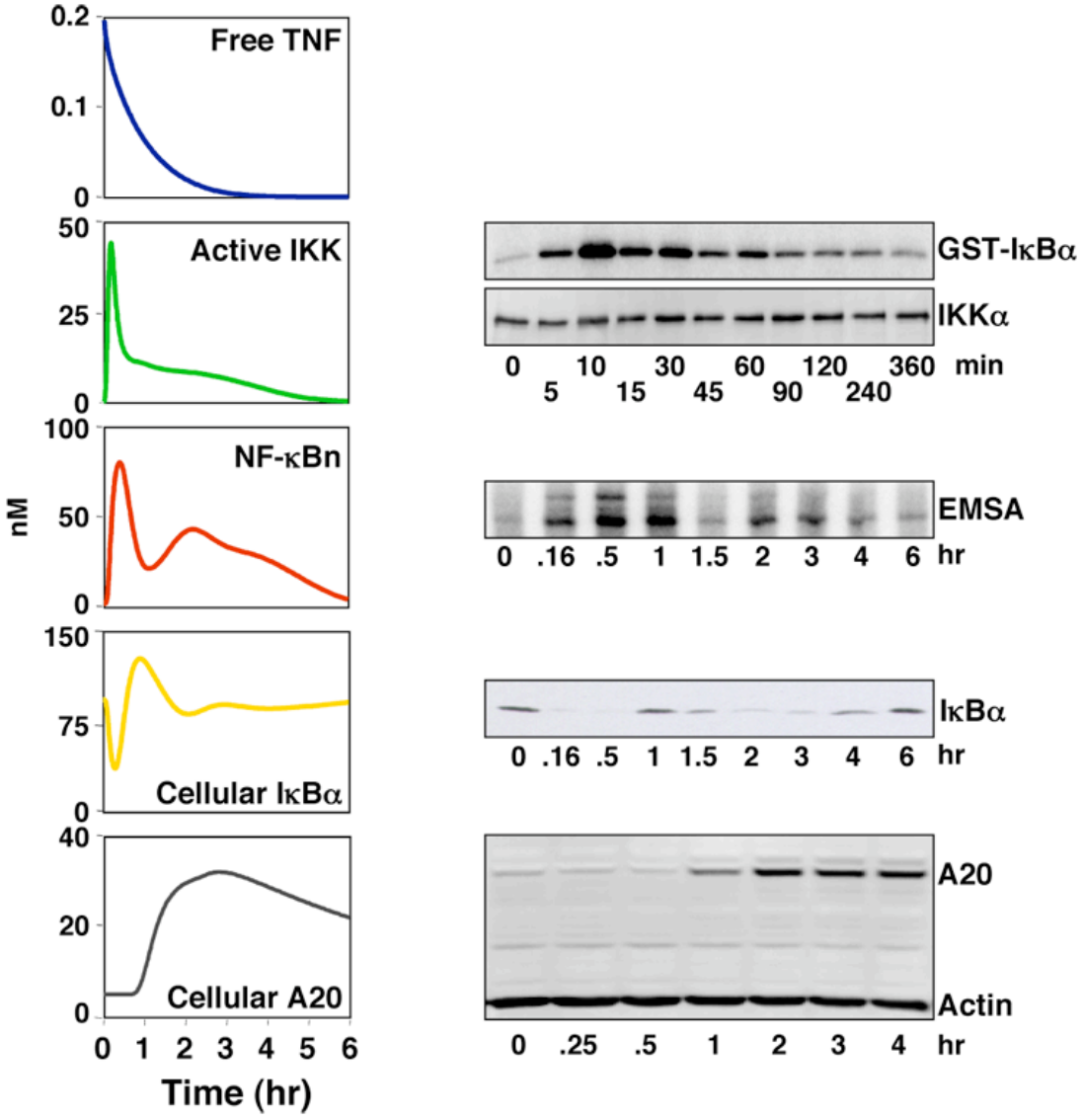

Figure 4.4 Experimental validation of the TNFR-IKK-NF-κB model

(Left) The model was simulated with persistent TNF stimulation (the model was given initial conditions and allowed to reach a steady state followed by the an addition of 1 ng/mL TNF at the 0 h time point) and the levels of key signaling molecules were plotted over a 6 h time course.

(Right) Experimental results from cells similarly treated with 1ng/mL persistent TNF. IKK kinase activity was measured by *in vitro* kinase assay. NF-κB nuclear localization was measured by EMSA. IκBα and A20 total cellular abundance was measured by Western Blot.

Given that TNF secretion by macrophages occurs in transient bursts, we first examined signaling to NF-κB by very short pulses of TNF. In simulations, we found that both IKK and NF-κB activity profiles are strikingly similar no matter how long the TNF pulses are: a 1 min TNF pulse was predicted to provide the same degree of activation as a 15-minute pulse (Figure 4.5A). We addressed this prediction experimentally. Treating cells with TNF pulses of 1, 2, 5, and 15 min, we found that the temporal profile of IKK and nuclear NF-κB activities did not change with the duration of the TNF pulse (Figure 4.5B, left and middle). The results suggest that the TNF-NF-κB signaling axis ensures that NF-κB activity lasts at least 45 min to provide for robust stress response gene expression program. Indeed, we found that even a 1 min pulse of TNF stimulation was able to induce inflammatory gene expression (Figure 4.5B, right).

This first invariant phase of NF-κB activity may be described as "hardwired" as it is not only independent of the TNF pulse duration, but also (to a large degree) the TNF concentration (Cheong *et al*, 2006; Werner *et al*, 2005). The hardwired sensitivity of the pathway to transient TNF bursts is due to two temporal amplification steps (Figure 4.5C): the first, within the TNFR-IKK signaling module, is determined by the auto-inhibitory mechanism of the IKK complex that was proposed to involve C-terminal phosphorylation (Delhase *et al*, 1999) and ensures that IKK activity lasts at least 15 min no matter how short the TNF pulse duration; the second, within the IκB-NF-κB signaling module, is a function of the IκBα feedback. This explains, why the first mathematical model of NF-κB activation (Hoffmann *et al*, 2002), which did not include the TNF-IKK module, correctly recapitulated NF-κB responses to transient

TNF stimuli of greater than 15 min, but erroneously predicted reduced NF-κB activation with shorter TNF stimuli.

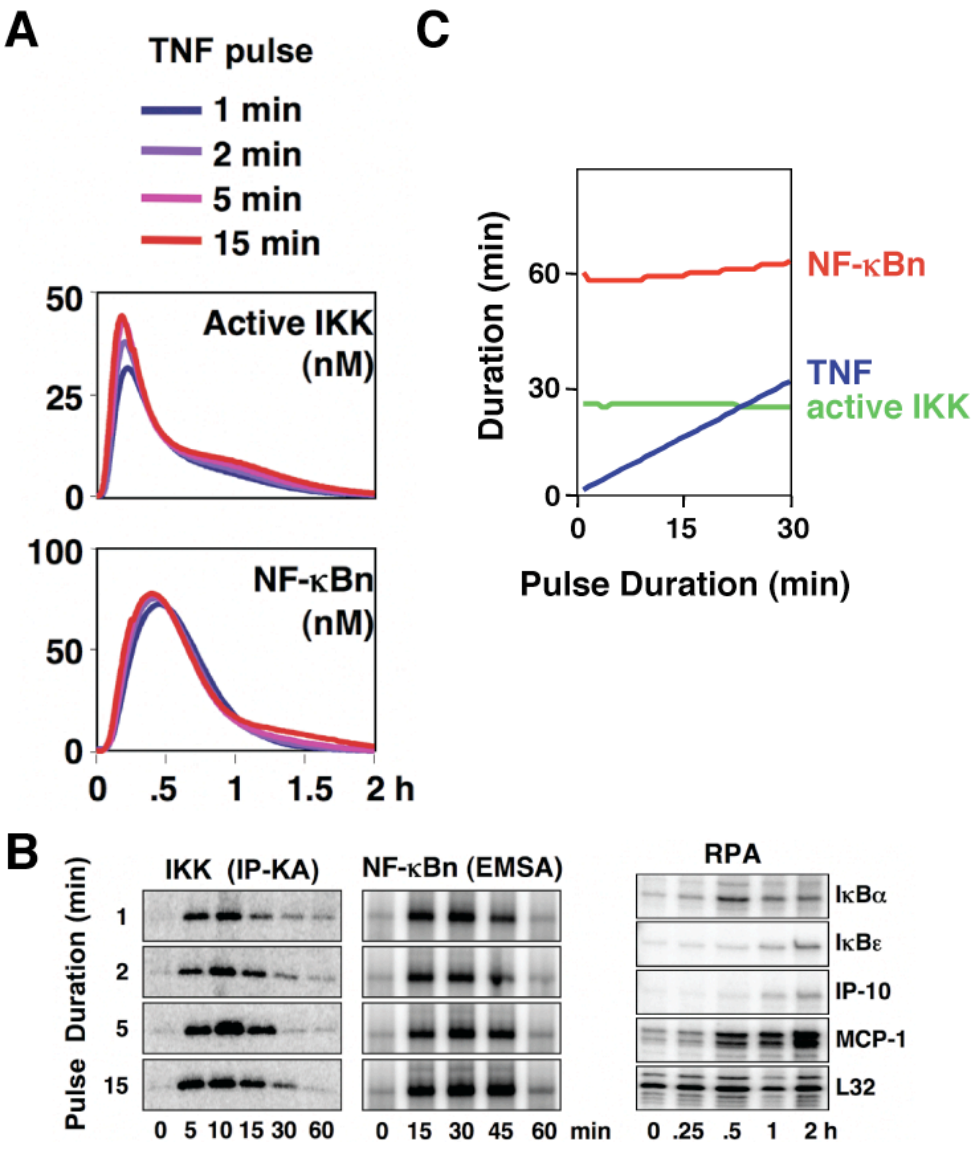

Figure 4.5 The first phase of TNF-induced NF-κB activity is hard-wired

(A) Computational simulations of IKK (top) and NF-κB (bottom) activities in response to 1-, 2-, 5-, or 15-min TNF pulses

(B) IKK and NF-κB activities were experimentally measured in wild-type MEFs in response to 1-, 2-, 5-, or 15-min 1ng/mL TNF pulses via in vitro IP-kinase assay and EMSA, respectively. mRNA expression of 4 NF-κB target genes was measured by RPA in wild-type MEFs in response to a 1-min pulse of 1ng/mL TNF. L32 is shown as a housekeeping control.

(C) The model was simulated with pulses of increasing TNF duration (x-axis) and the resulting durations of IKK and NF-κB activities over a threshold of 20nM were calculated and plotted.

Distinguishing between obligate and non-obligate feedback regulation

Both IκBα and A20 protein expression are rapidly induced in response to TNF, and have been reported to play important roles in regulating NF-κB responses (Beg *et al*, 1995; Klement *et al*, 1996; Lee *et al*, 2000). In our computational simulations (Figure 4.6A), post-induction repression of NF-κB activity occurs at 1 h in wild type cells, but is delayed to 3 h in *iκbα*$^{-/-}$ cells. In *a20*$^{-/-}$ cells, NF-κB activity is sustained and elevated between 3 and 6 h. These simulations conform to experimental results (Hoffmann *et al*, 2002; Werner *et al*, 2005), where only *a20*$^{-/-}$ cells exhibited elevated IKK and NF-κB activity at late (>3 h) time points. One consequence of a greatly enhanced first phase of NF-κB activity in *iκbα*$^{-/-}$ cells is elevated A20 induction which results in complete attenuation of late IKK (Figure 4.6B). This, together with elevated IκBε induction (Kearns *et al*, 2006), diminishes the second phase of NF-κB activity.

We asked whether feedback control by these regulators *via* inducible synthesis is important, or whether constitutive transcription alone could provide proper control of NF-κB activity. Using a parameter sensitivity analysis, we set the inducible IκBα or A20 transcription rates to zero and repeatedly simulated the model while modulating the constitutive transcription rate by 2^x (where $-10 \leq x \leq 10$ and 2^0 is the rate constant for wild type cells). We then plotted the simulation outputs (nuclear NF-κB activity) over time (x-axis) using a color heat map, ranging from blue (0 nM) to red (100 nM) (Figure 4.7), with the constitutive transcription rate modifier on the y-axis.

For IκBα, removing inducible transcription while maintaining the original constitutive transcription parameter value results in NF-κB activity similar to that seen

in *iκbα*$^{-/-}$ cells, where peak activation occurs between 1-2 h, and is attenuated by 3 h (Figure 4.7A, left). Though turning down the parameter had little effect, increasing it impacts NF-κB activation severely. At a 16-fold (2^4) increase, NF-κB activation was limited to 1 h as in wild-type cells; however, the amplitude of this first phase peak is significantly reduced and no late activity is seen. Interestingly, increasing the constitutive IκBα transcription rate by ≥ 2^5 (a level that is similar to the maximal inducible rate) completely abrogates NF-κB activation. We conclude that inducible IκBα synthesis is critical for timely post-induction repression of NF-κB.

In the case of A20, model simulations also predict that removing A20 inducible transcription results in IKK and NF-κB activity resembling that in an *a20*$^{-/-}$ (Figure 4.7A and B, right). Although the temporal profiles of IKK and NF-κB activity are largely invariant to turning down the constitutive A20 transcription rate, increasing it has two effects. First, late NF-κB activity (3-6 h) is dampened as in wild type cells. Second, further increases of A20 expression results in a delay and reduction of the peak of NF-κB activity. In other words, our computational simulations predict that - unlike the case of IκBα - a specific range of the constitutive transcription rate of A20 (4-16-fold higher than that estimated for MEFs) allows for a TNF-induced NF-κB activity profile that is similar to that observed in wild-type cells.

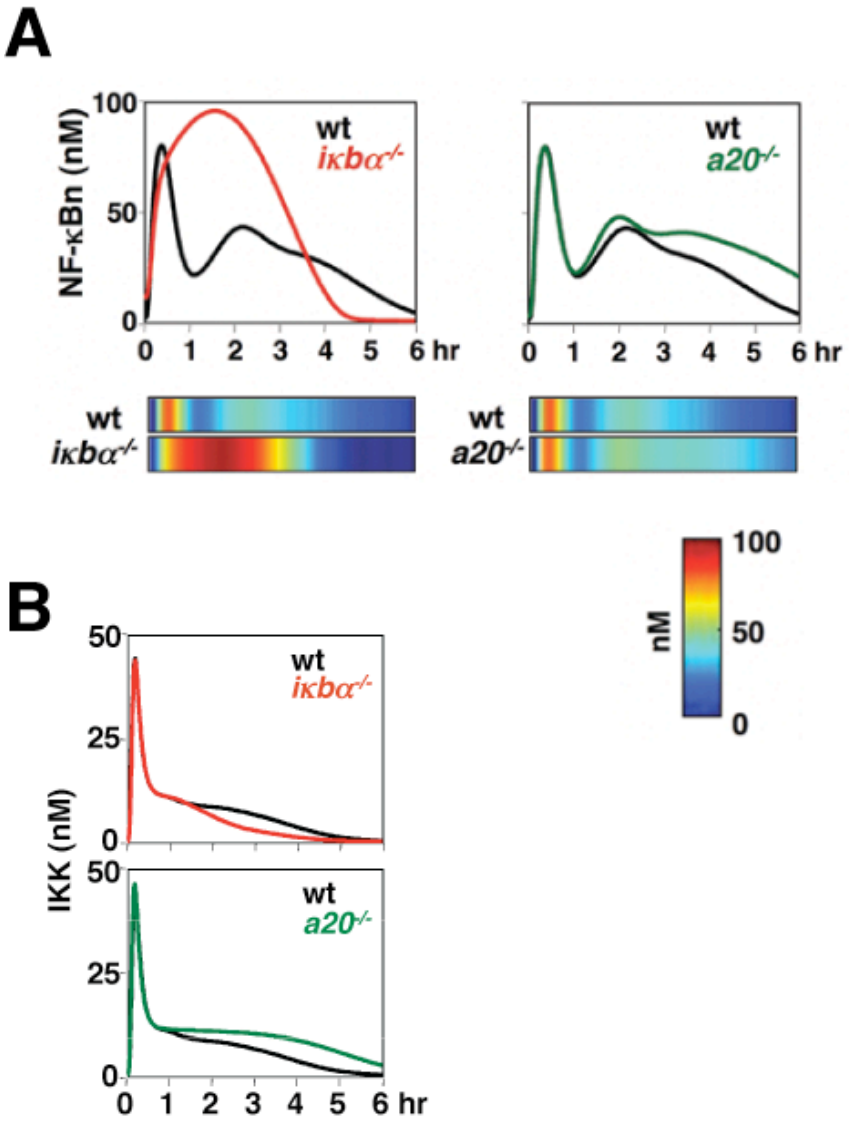

Figure 4.6 IκBα and A20 mediate distinct phases of TNF-induced NF-κB activity

(A) Simulations of nuclear NF-κB activity in wild-type, *iκbα*$^{-/-}$, and *a20*$^{-/-}$ MEFs in response to TNF. The data are presented as graphs (top) and heat maps (bottom) in which the level of NF-κB is color-coded from 0 nM (blue) to 100 nM (red).

(B) IKK activity from simulations as in (A).

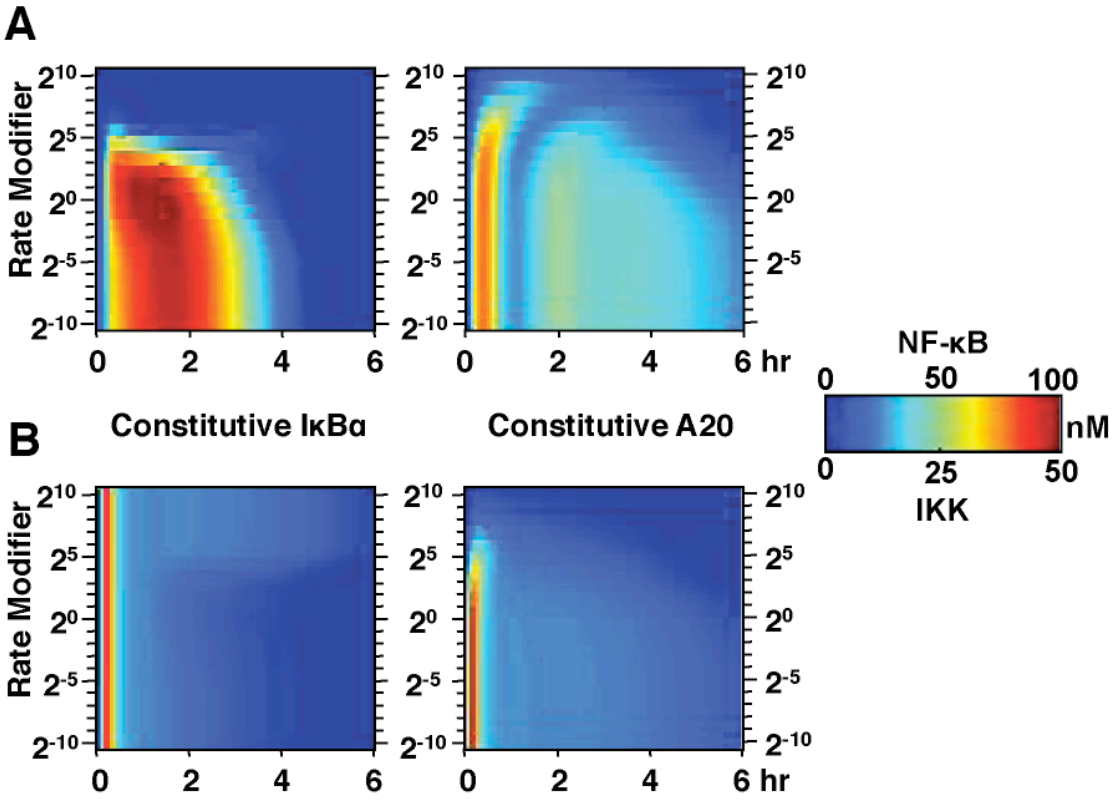

Figure 4.7 Inducible expression is critical for the function of IκBα but not A20

Simulations of nuclear NF-κB (A) and IKK (B) activity in models with altered constitutive transcription rates of IκBα (left) or A20 (right) in the absence of the respective inducible transcription. In each simulation, the constitutive rate was multiplied by one of the 21 modifier values, ranging from 2^{-10}, 2^{-9}, 2^{-8} … 1 … 2^{8}, 2^{9}, 2^{10}. The results were plotted as time (X-axis) vs. the rate modifier (Y-axis) using the same heat map color scheme as in Figure 4.6A.

We tested these predictions experimentally by reconstituting individual knockout cells with IκBα or A20 expressing transgenes containing heterologous promoters. In a cell line that constitutively expresses IκBα (*iκbα*$^{-/-}$.pBABE.IκBα), we did indeed find, as computationally predicted (Figure 4.8A, top), that NF-κB activity induced by a 15 min TNF pulse was equivalent to that seen in *iκbα*$^{-/-}$ (Figure 4.8A, bottom). In contrast, either constitutive or inducible transcription of A20 was able to restore late NF-κB attenuation *in silico* and *in vivo* (Figure 4.8B). Constitutive A20 transcription was modeled 4 fold higher than that of wild type cells, consistent with our experimental work where resting *a20*$^{-/-}$.pBABE.A20 cells contained 3.6 fold more A20 mRNA than wild type cells (data not shown). Overall our analysis makes a strong case for the necessity for feedback control for IκBα, but not for A20. We surmised that there might be additional explanations for the physiological relevance of inducible A20 expression.

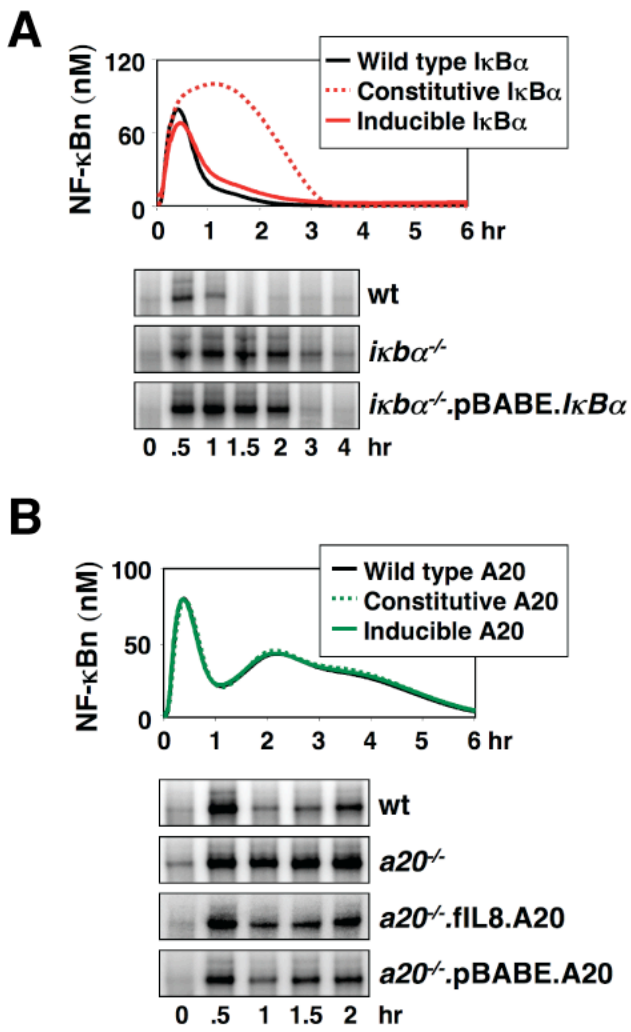

Figure 4.8 Experiments confirm that inducible expression is critical for the function of IκBα but not A20

(A) Simulations of nuclear NF-κB activity in models possessing both constitutive and inducible expression of IκBα (wild type), or each individually. Nuclear NF-κB activity was then measured via EMSA in wild-type cells or in *iκbα*$^{-/-}$ cells reconstituted with a constitutively expressing *iκbα* transgene (pBABE.IκBα.puro) or an empty vector control (pBABE.EV.puro, labeled *iκbα*$^{-/-}$) in response to a 15-min pulse of 1ng/mL TNF.

(B) Simulations predict NF-κB activity in cells chronically stimulated with TNF that have either constitutive or inducible A20 expression, or both (wild type). Nuclear NF-κB activity was measured via EMSA in wild-type cells or in *a20*$^{-/-}$ cells reconstituted with a constitutively expressing *a20* transgene (pBABE.A20.puro), an NF-κB-inducible transgene (fIL8.A20.puro), or an empty vector control (pBABE.EV.puro, labeled *a20*$^{-/-}$) in response to persistent 1 ng/mL TNF stimulation.

Signaling crosstalk mediated by A20

Both IκBα and A20 are highly inducible genes whose expression is activated in response to several NF-κB-inducing inflammatory stimuli (Dixit *et al*, 1990). Interestingly, IL-1 induces A20 expression, but A20, unlike IκBα, does not affect IL-1 signaling (Lee *et al*, 2000). What may be the functional role of IL-1-induced A20? *In vivo*, cells are continuously exposed to a variety of stimuli, and we speculated that cells that are "primed" by IL-1 to increase cellular A20 expression might be less responsive to subsequent TNF stimulations.

We employed the computational model to examine potential A20-dependent crosstalk between IL-1 and TNF. The model was simulated with a 1 h pretreatment of IL-1 stimulation, allowed to "rest" for 1 or 24 h in the absence of stimulus, and then stimulated with a range of TNF concentrations (Figure 4.9A). The maximum value of NF-κB activity following TNF stimulation was plotted for each condition to generate TNF dose response curves (ranging from 10^{-3} to 10^{3} ng/ml) for naïve vs. IL-1 pretreated cells. Simulations in which a 1 h rest is used following IL-1 pretreatment show that NF-κB activity is diminished vs. naïve simulations in a TNF dose dependent manner (Figure 4.9B). NF-κB activity in simulations with IL-1 pretreatment followed by low TNF stimulations (0.1 ng/ml or less) is much more affected than higher doses (1ng/ml or more). Simulations in which a 24 h rest period show no difference between naïve and IL-1 pretreated conditions, suggesting that the effect is temporally transient (Figure 4.9C).

To test whether A20 is involved in the observed IL1-TNF crosstalk, wild type and *a20*$^{-/-}$ model systems were simulated as in Figure 4.9A. The maximal dampening of NF-κB activity with the IL-1 pretreatment regime was observed with a 1 h rest and then a low TNF dose (0.1 ng/mL or less). This effect is not observed in the A20-deficient model system at either the level of IKK or NF-κB activities (Figure 4.10A & B, left). No dampening in the wild type system was observed at high TNF dose (1 ng/mL) or following a 24 h rest and this is unaltered in the *a20*$^{-/-}$ model system (Figure 4.10A & B, right, Figure 4.10C). We tested these predictions experimentally by measuring TNF-induced NF-κB activity in cells exposed to the IL-1 pretreatment regime (Figure 4.10D). For a 0.1 ng/ml TNF treatment, NF-κB activation was severely diminished in wild type cells, but not in *a20*$^{-/-}$ cells. At 1ng/ml of TNF, IL-1 pre-treatment also had a small effect but this was A20-independent, possibly *via* TNFRI ectodomain shedding (Islam *et al*, 2006). Together, these *in silico* and *in vivo* results suggest that A20 mediates cellular memory to inflammatory signaling in a transient (< 24 h) and TNF dose (0.1 ng/mL or less) dependent manner.

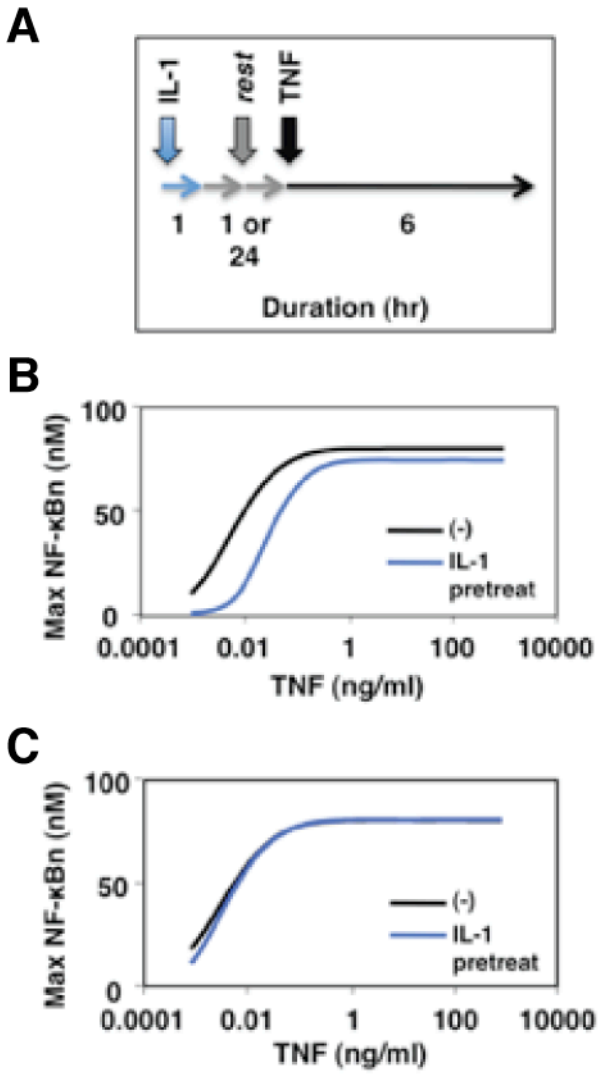

Figure 4.9 IL-1 pre-treatment modulates subsequent TNF signaling

(A) Schematic of IL-1 pretreatment strategy. The model is simulated for 1 h with an experimentally derived numerical input curve representing IL-1 induced IKK activity and is then simulated in the absence of stimulus for 1 or 24 h. Naïve and IL-1 pretreated models are then simulated with a dose of TNF.

(B) Naïve and IL-1 pretreated models (with 1 h rest) are simulated with a range of TNF doses and the maximum NF-κB activities following each stimulation dose are plotted.

(C) The model is simulated as in (B), but with a 24 h rest following IL-1 pretreatment.

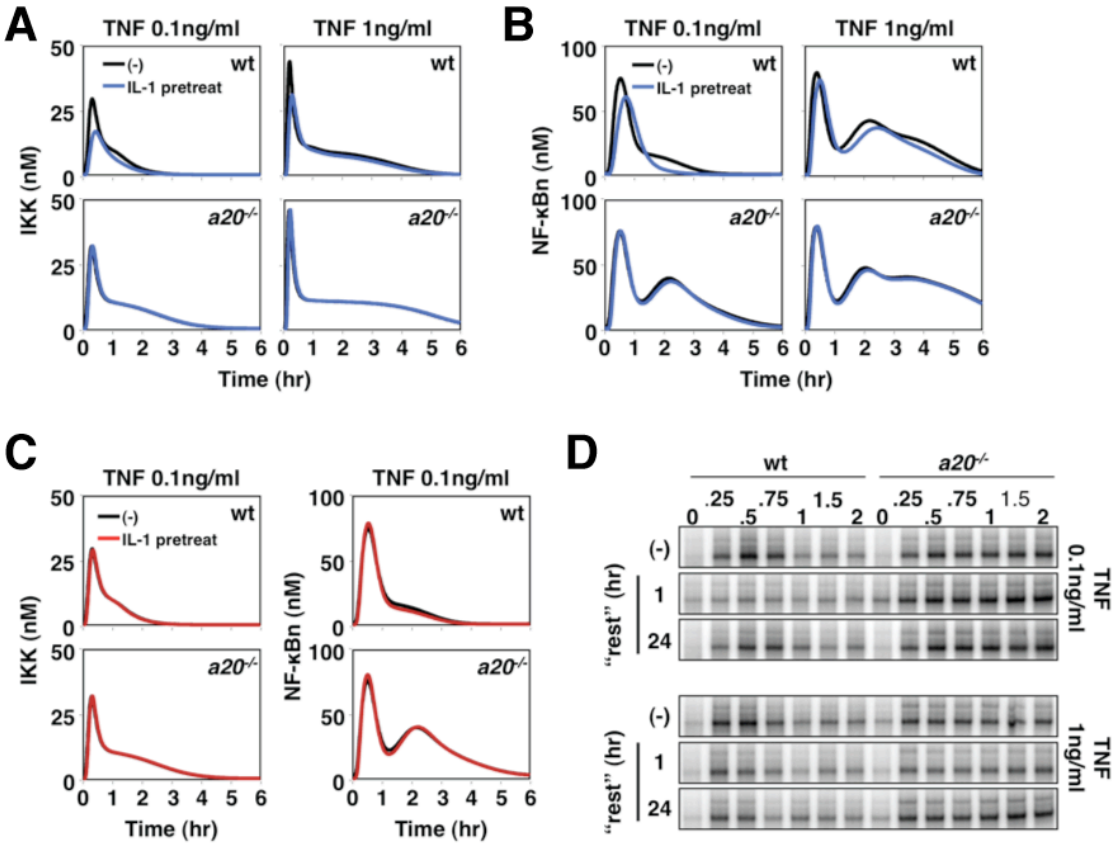

Figure 4.10 The effect of A20 on IL1-TNF crosstalk is transient and TNF dose dependent

(A) IKK activation was simulated in wild type and *a20*$^{-/-}$ cells in response to either 0.1 or 1 ng/mL TNF alone (black), or to a 1 h IL-1 pretreatment followed by 1 h "rest" (no stimulation) and then subsequent TNF challenge (blue).

(B) NF-κB activation was simulated as in (A).

(C) Simulations were repeated as in (A) in wild type and *a20*$^{-/-}$ cells with 0.1 ng/mL TNF but with a 24 h rest period following IL-1 pretreatment.

(D) Nuclear NF-κB activity in response to persistent TNF stimulation (0.1 or 1 ng/mL) was measured by EMSA in wild type and *a20*$^{-/-}$ cells that were naïve (-) or pretreated with IL-1 for 1 h, followed by 1 or 24 h of "rest."

A temporal dose response analysis reveals distinct roles of IκBα and A20

As a paracrine mediator with a short half-life, cellular exposure to TNF is usually transient but of variable duration. Thus, we investigated the roles of IκBα and A20 in mediating NF-κB signal processing in response to TNF stimulations of various durations. Using a three-dimensional plot, we graphed IKK and NF-κB activity (color heat map) over time (x-axis) for TNF pulses of various durations (y-axis) (Figure 4.11). In wild-type cells, even very short TNF pulses provide for almost an hour of NF-κB activity (Figure 4.5, Figure 4.11, top). Longer lasting TNF stimulations do not change the duration of the first phase of NF-κB activity, but allow for a second phase of NF-κB activity of proportionally increasing duration. However, in the absence of IκBα, the first invariant phase of NF-κB activity balloons to 3 h (Figure 4.11, middle). In A20-deficient cells, our model simulations indicate a largely intact first phase of NF-κB but a second phase that is enhanced (Figure 4.11, bottom). Even very short stimuli elicit a second phase that is predicted to last at least 3 h.

Given that A20 protein expression is markedly upregulated only after 1 h following stimulation onset (Figure 4.4), the prediction that A20 plays a role in regulating responses to much shorter pulses of TNF seemed surprising. Single simulations of 5, 15, and 45 min TNF pulses reiterated that A20-deficient cells were predicted to have elevated NF-κB activity at 2 h and longer (Figure 4.12, top). Experimentally, we found this to indeed be the case: an EMSA analysis revealed that NF-κB activity is elevated in *a20*$^{-/-}$ cells during the later phase in response to short TNF pulse stimulations (Figure 4.12, bottom). This effect is correlated with incomplete attenuation of IKK activity in the knockout cells (data not shown).

Overall, our study reveals distinct roles for the two highly inducible negative feedback regulators IκBα and A20 (Figure 4.13, top). Whereas the inducibility of IκBα determines the duration of the first phase of NF-κB activity (Figure 4.13, bottom), A20 determines the temporal dose response of the TNF-NF-κB signaling pathway by controlling primarily the duration of the second phase of NF-κB activity. Interestingly, we found that the concentration, not the rate of synthesis or inducibility of the A20 protein, determines the duration of the second phase (Figure 4.13, bottom). The concentration of A20 protein can be modulated not only by TNF itself but also by multiple inflammatory stimuli (Figure 4.13, top), thus conferring a rheostat function. At high levels of expression in "primed" cells, the A20 rheostat may even dampen the amplitude of the first phase of NF-κB activity (but never the duration), suggesting a role in establishing inflammatory tolerance.

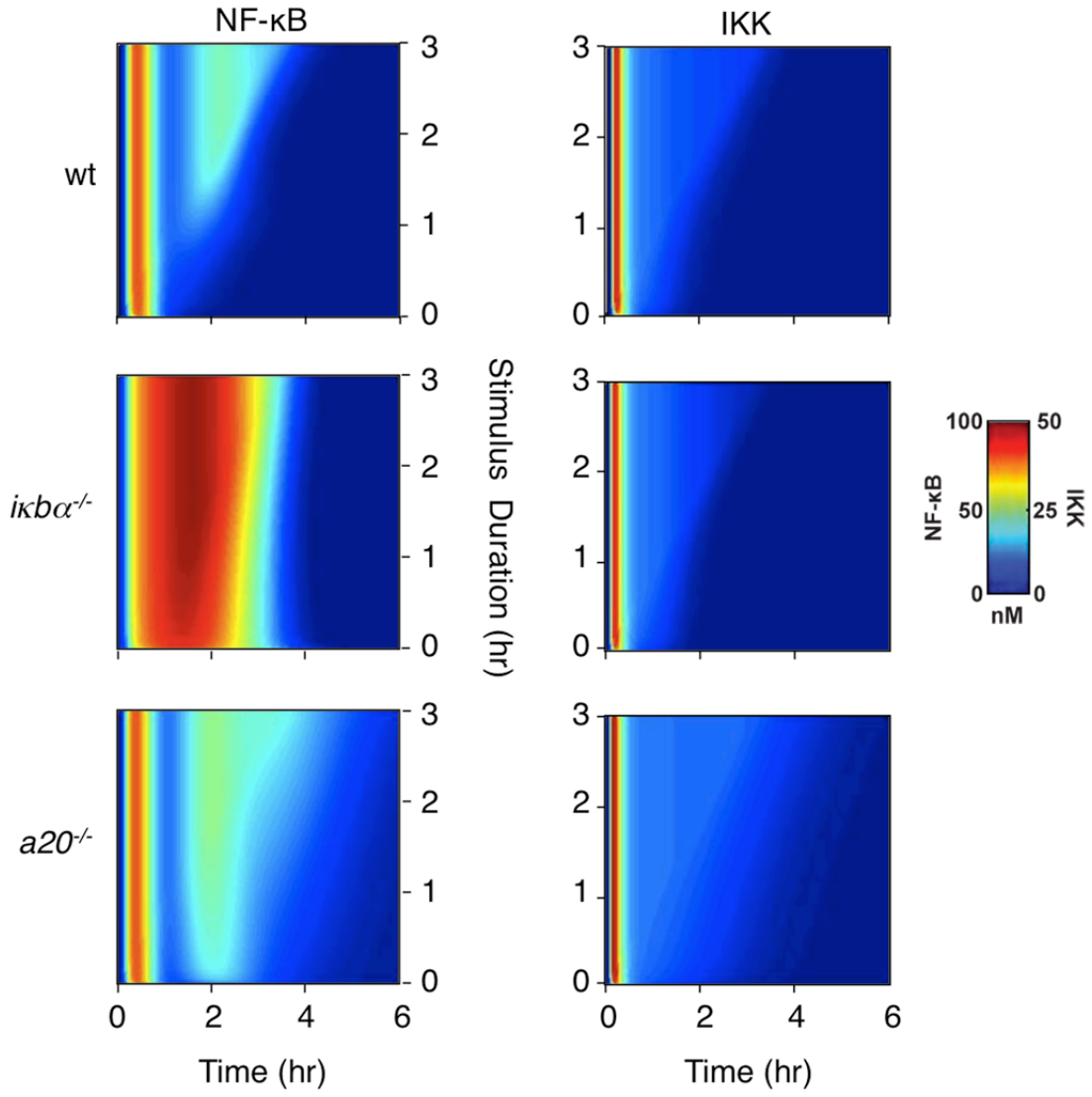

Figure 4.11 Temporal dose response analysis of TNF-induced NF-κB activity

Simulation of NF-κB (left) and IKK (right) activities in wild-type, *iκbα*$^{-/-}$, and *a20*$^{-/-}$ cells in response to TNF pulses ranging from 1 min to 180 min in 1-min increments. The results were graphed over time (hours), with the pulse duration (hours) on the Y-axis. The heat maps are color-coded as in Figure 4.7.

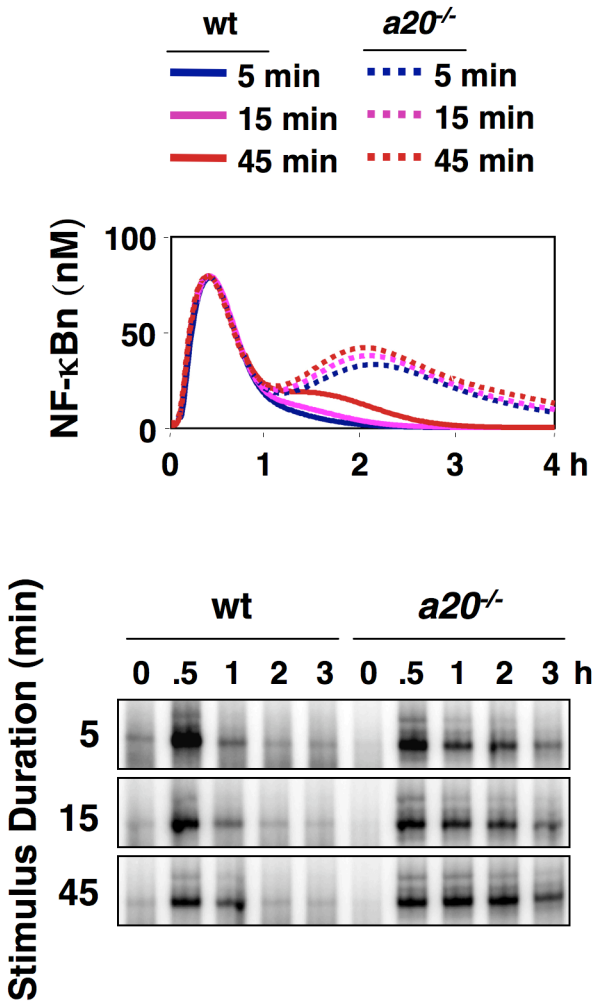

Figure 4.12 Experiments confirm that A20 limits late NF-κB activity

NF-κB activity profiles were simulated in response to 5-, 15-, or 45-min TNF pulses in wild-type and *a20*$^{-/-}$ cells (top), and were then measured experimentally via EMSA (bottom).

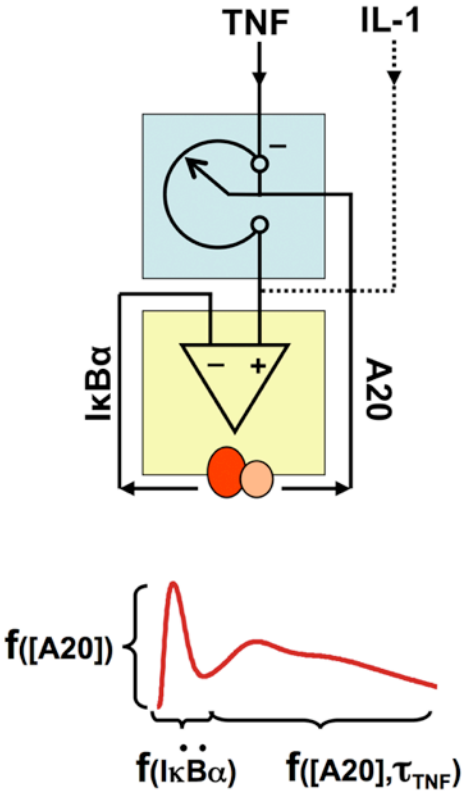

Figure 4.13 Schematic of how IκBα and A20 encode NF-κB dynamics in the TNF signaling pathway

Whereas dynamic feedback (yellow box) is critical to IκBα's function, inducible expression of A20 confers a tunable rheostat (blue box) function. Via this rheostat function, A20 mediates signaling cross-talk, for example, from prior cellular exposure to IL-1. (Below) TNF produces a typically biphasic NF-κB activity that is encoded by the differential functions of A20 and IκBα. The duration of the first phase is a function of the inducibility (change in synthesis rate, or second-order derivative, denoted by "¨") of IκBα, but is not a function of the TNF stimulus duration or concentration. The duration of the second phase is a function of the concentration of the A20 protein at that time. High concentrations of A20 protein during the early phase (as a result of prior NF-κB activity) may also affect the amplitude of the first phase, but not its duration.

DISCUSSION

As the molecular connectivity within signaling networks has increasingly become a focus of biomedical research, a surprising number of inducible negative regulators have been identified – these are usually categorized as negative feedback regulators. However, remarkably few have been examined to determine what functional roles their inducible expression may play; indeed, little is known about whether inducible expression can allow for distinct functional roles within a signaling network. Our analysis demonstrates distinct functions for IκBα and A20, whose expression is driven by similarly inducible promoters. In the case of IκBα, negative feedback is required for its function; that is to say that no value of constitutive IκBα expression will provide the degree of NF-κB activation and post-induction repression that NF-κB-responsive expression of IκBα allows for. In contrast, in the case of A20, a range of constitutive expression rates provides for the functionality observed in wild type cells. Hence we distinguish between an obligate (IκBα) and a non-obligate (A20) feedback regulator. Indeed, the A20 regulatory mechanism may not fit a narrower definition of a negative feedback regulator.

Instead, the inducibility of A20 expression functions to tune a rheostat that controls cellular signaling responsiveness. This is demonstrated most clearly by the fact that that A20 mediates signaling crosstalk between inflammatory stimuli when they are administered sequentially. However, A20's rheostat function is not limited to crosstalk between IL-1 and TNF, as its promoter is inducible by all NF-κB inducing stimuli tested so far. It provides short-term cellular memory by transiently

"tolerizing" (i.e. reducing the sensitivity of) the TNF signaling pathway. Whereas the dynamics of IκB inducibility but not the actual protein concentration critically define NF-κB activity, the A20 protein concentration determines signaling, regardless of whether that protein level was the result of inducible or constitutive expression, This distinction between the negative regulators may explain how subtle misregulation of A20 protein levels have been implicated in a range of physiological and pathological processes, including atherosclerosis (Wolfrum *et al*, 2007), T-cell responsiveness (Stilo *et al*, 2008), the homeostasis of signaling by pathogen-sensing receptors (Turer *et al*, 2008) and of commensual bacteria (Hitotsumatsu *et al*, 2008), and suppression of autoreactive immune responses (Song *et al*, 2008).

What might be the molecular basis for the differential functionality? There are differences in network connectivity (model topology) and rate constants (parameter values) that may be relevant to consider. Although both IκBα and A20 are rapidly and highly inducible at the level of mRNA transcripts (which show a similarly short half-life), producing the larger A20 protein takes more time. More importantly, a significantly longer protein half-life allows not only allows for a gradual build-up of the protein, but also confers a memory function that we revealed in crosstalk or priming experiments. Whereas the obligate negative feedback regulator IκBα functions as a stochiometric binder of the NF-κB activator, the non-obligate feedback attenuator A20 reaches back many more reactions into the pathway making its effect more temporally diffuse at the NF-κB level. In addition, A20 possesses enzymatic function, which further slows its total functional effect. These conclusions are insensitive to the alterations parameter values within the ranges set by experimental

constraints (Figure 4.16). In fact, model topology aspects mirror prior theoretical considerations pertaining to metabolic networks (Dibrov *et al*, 1982), but we suggest that theoretical modeling work may prove useful in distinguishing between different categories of negative feedback regulators in signaling. In addition, our combined computational and experimental strategy may be applied to other signaling systems to characterize the functional diversity of negative feedback regulators.

The TNF induced NF-κB dynamics are not only critically encoded by IκBα and A20, but also by an IKK auto-repression mechanism. It provides powerful negative feedback on a faster scale than possible by mechanisms involving *de novo* gene expression, but it requires further molecular characterization. Indeed, recent work suggests that the association of the essential IKK scaffold subunit NEMO with catalytic subunits IKK1 and IKK2 is regulated *via* phosphorylation (Hayden and Ghosh, 2008). Though our model recapitulates the observed temporal IKK activity profile, it does not describe the actual regulatory mechanism. Similarly the mechanism by which K63-linked ubiquitin chains activate IKK, the involvement of A20 in their removal (Boldin and Baltimore, unpublished results), and whether and how TAK1/Tab2/3 is involved in IKK control remains to be characterized in more detail. New mechanistic insights should lead to a revision of our mathematical model, in turn enabling their role in NF-κB dynamics to be investigated. The iterative strategy of combined experimental and modeling work promises to result in amply validated and sufficiently detailed models that they may function as a stand-alone discovery tools.

MATERIALS AND METHODS

Laboratory Experiments

Immortalized MEFs were cultured and analyzed (EMSA, RPA, and Western Blot) as described previously (*Methods*, Chapter 2). *a20*$^{-/-}$ MEFs were reconstituted with retroviral vectors pBABE.A20.puro (created by cloning a human A20 ORF into pBABE-puro) and fIL8.A20.puro (generated by inserting an inducible A20 ORF under the control of the IL-1 promoter followed by a Puro^{R} expression module into a FUGW vector). IκBα-/- MEFs were reconstituted with pBABE.IκBα.puro or empty vector controls, and were a kind gift from Erika Mathes (UCSD). A20 antibody was obtained from Imgenex (IMG-161). IKK activity was measured via immunoprecipitation kinase assay (Werner *et al*, 2005).

Computational Modeling

Description of the Computational Model

The model is comprised of two connected modules (Figure 4.2). The first receives a dose of TNF ligand as an *input* and computes the activation of IKK as an *output*. The second module is based on a previous model (Werner *et al*, 2005) and uses the active IKK as an *input* and computes the activation of free nuclear NF-κB as an *output*. The complete new model contains 33 species (components) and 98 reactions governed by 110 parameters and describes the biochemical reactions involved in signal processing between TNF engagement of the TNF Receptors and nuclear NF-κB localization. The species of the model are depicted graphically in Figure 4.3 and listed in Table 4.2. The reactions and parameters are listed in Table 4.3.

Computational Simulations

The ODEs were solved numerically using MATLAB version R2008a (The MathWorks, Inc.) with subroutine *ode15s*, a variable order, multi-step solver. Prior to stimulation, the system was allowed to equilibrate from starting conditions to a steady state, defined as showing no concentration changes greater than 1% over a period of 4000 minutes. Stimulus-induced perturbation from the equilibrium state was accomplished by introducing an extracellular concentration of TNF ligand or by direct modulation of IKK activity via a numerical input curve representing IL-1β stimulation (as in Werner et al., 2005). During an IL-1β stimulation, the reactions governing IKK cycling between IKK (on), IKK (off) and IKK (inactive) were disabled. As such, co-treatment of IL-1β and TNF is not possible in this version of the model.

The model was simulated with multiple doses of TNF. We calculated that a 1ng/mL dose of TNF used in cell culture experiments was equivalent to 1.96e-4 uM in the model (the molecular weight of the TNF trimer is 45 kDa). Other concentrations were simulated in the model via multipliers of this number: ie: 0.1ng/mL is equivalent to 1.96e-5 uM.

The IL-1β numerical input curve was generated based upon IKK Kinase Assay measurements of IKK activity at time points following a 15 min pulse of IL-1β stimulation (Table 4.4). A full curve was generated from these measurements in MATLAB using the built-in interpolation libraries with the Piecewise Cubic Hermite Interpolating Polynomial (PCHIP) method.

Parameter Fitting and Sensitivity Analysis

Most model parameter values were derived from the literature or measured / tightly constrained by biochemical or biophysical techniques. The values of remaining model parameters were selected such that the output of the model recapitulated observed results. This process is commonly referred to as parameter fitting and is essential when constructing a model representing a large reaction network.

Experiments yielded steady state and stimulation time course data that function to constrain the parameter fitting. The constraints were defined with broad ranges so as to minimize the possibility of arbitrarily biasing the results and were expected to be met in response to pulse or chronic stimulation with 1ng/mL TNF (Table 4.1, Figure 4.14).

Examining the values listed in Table 4.3, we identified 15 parameters or groups of related parameters in each of the two signaling modules that were fit (Figure 4.15A, B). We then determined for each of these parameters what ranges of their values would satisfy the established list of constraints. To do this, the model was simulated repeatedly with rate multipliers between 1/100 and 100x for each parameter. We calculated the highest and lowest multiplier values that when run in the model still satisfy all constraints (Figure 4.15C, D).

We found that the majority of these parameters can be given values within a 2-5 fold range. This finding shows that the network allows for some degree of flexibility in parameter values while maintaining its function.

Four parameters can be given values over several orders of magnitude. These include the rates of inducible IκBβ expression, TNF-independent TNFR trimerization, constitutive IKKK activation, and constitutive IKK activation. These findings are not surprising as all four of these processes are kinetically ‘slow’ and the latter three are counteracted by fast reverse reactions.

Table 4.1 Model v4.0 Constraints

Fifteen constraints, based upon experimental measurements, were developed that capture the important characteristics of basal (steady state) and TNF-induced signaling responses.

	Description	**Source**
C1	Basal NF-κB activity is less than 5% of the total NF-κB	EMSA
C2	Basal free IkB protein is less than 25% of total IκB	(O'Dea *et al*, 2007)
C3	Basal total cellular protein of IκBα > IκBβ > IκBε	(O'Dea *et al*, 2007)
C4	15' TNF Pulse: NF-κB activity is > 50nM within 45 min	(Cheong *et al*, 2006)
C5	15' TNF Pulse: NF-κB activity is < 10nM by 90 min	(Cheong *et al*, 2006)
C6	TNF Chronic: NF-κB activity is > 50nM within 45 min	(Cheong *et al*, 2006)
C7	TNF Chronic: NF-κB activity is > 20nM at 240 min	(Cheong *et al*, 2006)
C8	TNF Chronic: IκBα mRNA induction fold is 5 to 100 fold	This study and (Kearns *et al*, 2006)
C9	TNF Chronic: IκBβ mRNA induction is 1 to 10 fold	(Kearns *et al*, 2006)
C10	TNF Chronic: IκBε mRNA induction is 5 to 100 fold	(Kearns *et al*, 2006)
C11	TNF Chronic: A20 mRNA induction is 5 to 100 fold	This study
C12	TNF Chronic: IKK activity peaks between 5 and 15 min	(Werner *et al*, 2005)
C13	TNF Chronic: peak IKK activity is above 33% of the total IKK	(Werner *et al*, 2005)
C14	Basal IKK activity is below 2% of the total IKK pool	(Werner *et al*, 2005)
C15	TNF Chronic: IKK activity (>75min) is < 1/3 of the peak value	(Werner *et al*, 2005)

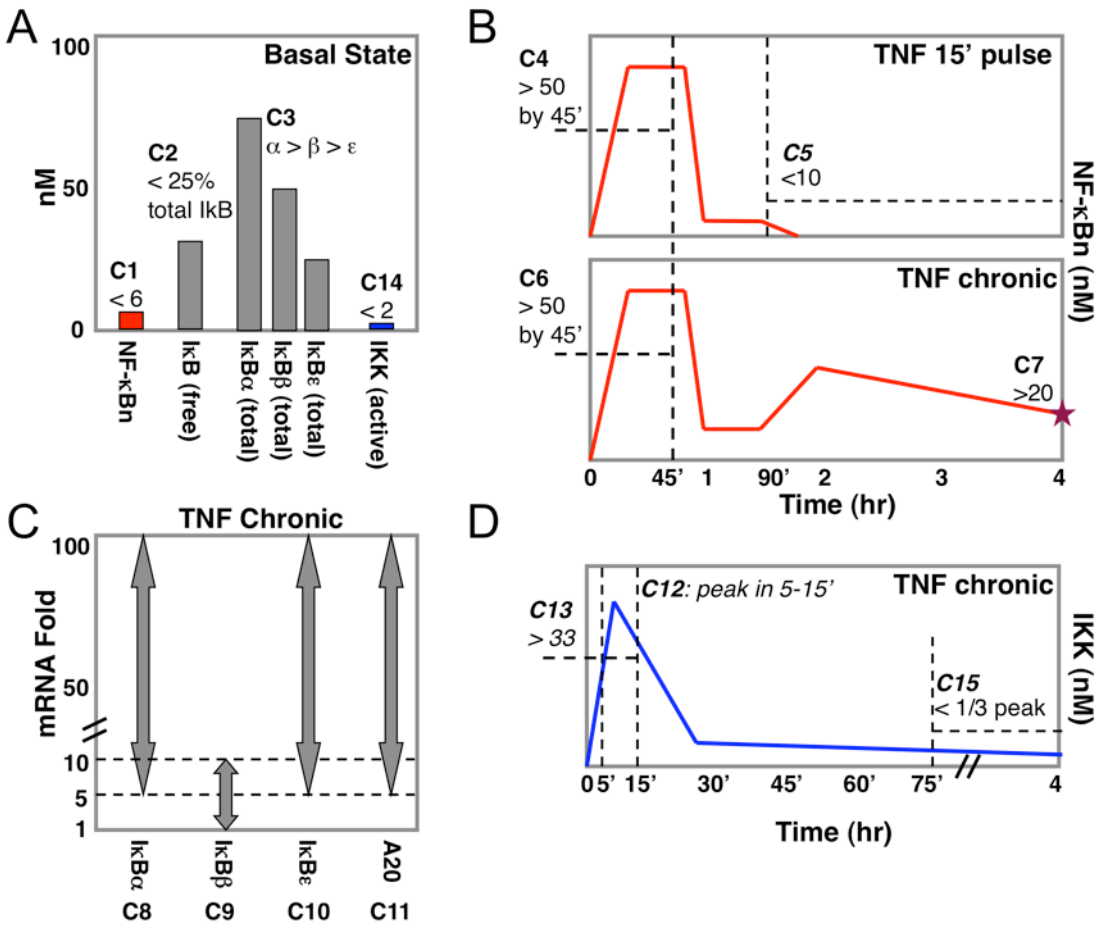

Figure 4.14 Diagrams of constraints used to constrain the model

(A) Maximum basal concentration of specific species
(B) Characteristics of NF-κB activity curves in response to 15 min 1ng/mL TNF pulse or TNF chronic stimulation
(C) Allowable ranges for IκB and A20 mRNA induction folds in response to 1 ng/mL TNF chronic stimulation
(D) Characteristics of the IKK activity curve in response to 1 ng/mL TNF chronic stimulation.

A

NF-κB Activation Module

#	Parameter	Function
1	1	IκBα const. txn
2	2	IκBβ const. txn
3	3	IκBε const. txn
4	4	IκBα inducible txn
5	5	IκBβ inducible txn
6	6	IκBε inducible txn
7	16	IκBα translation
8	17	IκBβ translation
9	18	IκBε translation
10	57,60	IKK-IκBα Deg.
11	58,61	IKK-IκBβ Deg.
12	59,62	IKK-IκBε Deg.
13	63	A20 const. txn
14	64	A20 inducible txn
15	68	A20 translation

B

IKK Activation Module

#	Parameter	Function
1	4	TNFR trimerization
2	5	TNFR dissociation
3	7,19	TTR recruitment
4	8,12,20,24	TTR dissociation
5	9,21	ComplexI activation
6	10,22	ComplexI inactivation
7	11,23	A20 Complex1 inactivation
8	31	Const. IKKK activation
9	32,33	C1-mediated IKKK activation
10	34	Const. IKKK inactivation
11	35	Const. IKK activation
12	36	IKKK-mediated IKK activation
13	37	Const. IKK inactivation
14	38	IKK to IKKi conversion
15	39	IKKi to IKKoff conversion

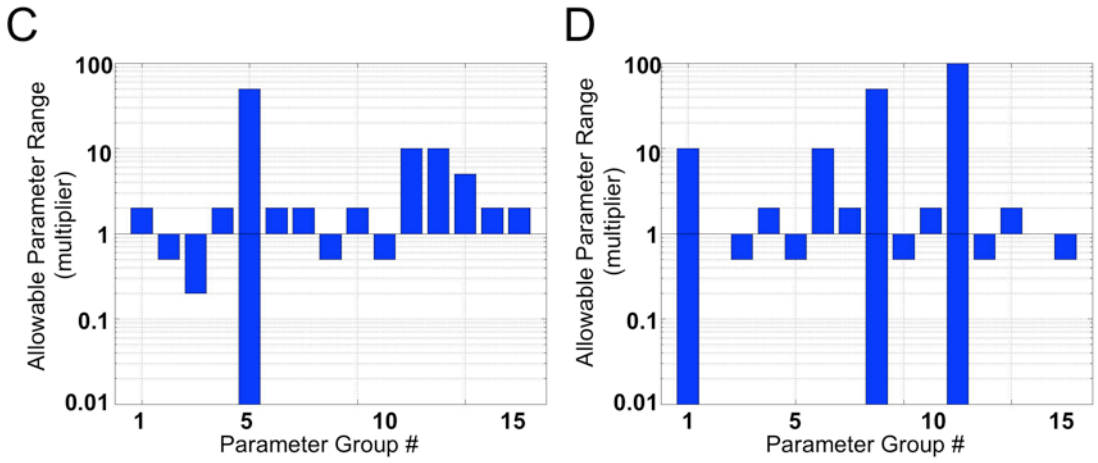

Figure 4.15 Determining the range of parameter values that satisfy all constraints

(A and B) There are 15 parameters or sets of related parameters in each signaling module that required parameter fitting to select their values

(C and D) For each of these, the model was simulated repeatedly with that rate value(s) multiplied by 0.01, 0.02, 0.025, 0.1, 0.2, 0.5, 1, 2, 5, 10, 25, 50, and 100x. Following each simulation, the model was compared against the list of 13 established constraints. Plotted are the maximum and minimum multipliers for each rate constant group that still satisfies all constraints. The absence of a bar, such as with Groups 2 and 14 in the IKK module, means that this group only meets all constraints with the 1x value.

Testing the robustness of conclusions

To determine whether the predictions of the model hold true over these ranges of parameter values that were defined by the experimental constraints, all model simulations relevant for the conclusions were repeated with the ranges of allowable values (Figure 4.16). We identified 4 primary conclusions in our study:

(1) *IκBα controls the duration of the first phase of NF-κB activity in response to a pulse of TNF stimulation.* NF-κB activity should last ~1 h in wild-type cells and be prolonged to ~3 h in IκBα-deficient cells (Figure 4.16A).

(2) *A20 controls the amplitude of the second phase of NF-κB activity in response to chronic TNF stimulation* (Figure 4.16B compare top and middle).

(3) *Constitutive transcription of A20 is sufficient for A20's function in controlling late phase of NF-κB activity.* NF-κB-mediated inducible synthesis is not required for this behavior and can be replaced with elevated constitutive transcription (~4x) (Figure 4.16B bottom).

(4) *Pretreatment with IL-1β followed by treatment with TNF will result in lowered NF-κB activity in wild-type but not in A20-deficient cells*, and this effect is relived by 24 h (Figure 4.16C)

We found that the model retains these conclusions when simulated with the parameter value ranges, with only small fluctuations observed. The exception is the rate constant governing constitutive Complex I deactivation (IKK Module Parameter Group #6), the same function performed by A20. This confirms that A20 represents a tunable Complex I deactivation mechanism. Together, this analysis leads us to believe that the model predictions are not impacted by the choice of parameter values.

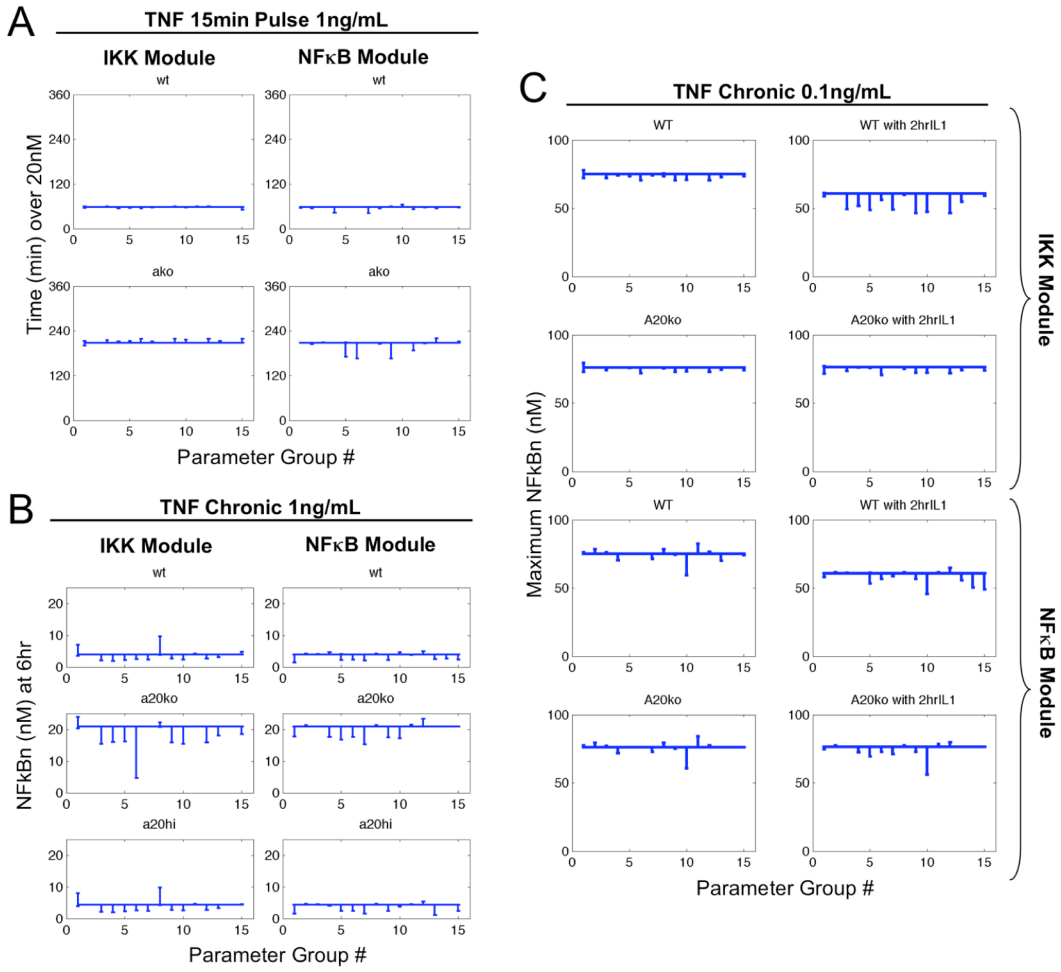

Figure 4.16 The model predictions are robust to the parameter range

The plots show how a metric that encapsulates each conclusion is affected by simulating the model with the calculated maximum and minimum values for each of the 15 parameters fit in the NF-κB and IKK activation modules. The horizontal line denotes a model with all parameters at 1x values. Error bars denote the deviation from 1x when using the range for each parameter.
(A) Wild-type and A20-/- model systems were stimulated with a 15 min TNF pulse and the duration of the NF-κB activity over a 20nM threshold was calculated.
(B) Wild-type, A20-/-, and A20 4x constitutive expressing (no inducible expression) systems were chronically stimulated with TNF and the value of NF-κB activity at 6hrs was calculated.
(C) Naïve and IL-1β pretreated wild-type and A20-/- systems were chronically stimulated with TNF and the maximum (peak) value of NF-κB activity in the first hour was calculated.

Table 4.2 Model v4.0 Species and Initial Concentrations

The model contains 33 species that represent the molecular species (mRNA and proteins) within the signaling module. Each species is given an initial concentration that is used as an input to the equilibrium (steady state) simulation. Species are localized to the cytoplasm (cyt), nucleus (nuc), extracellular space (ext), or the cell membrane (mem). The initial concentrations of IKK, TAK1, and NF-κB are retained amongst their various forms/complexes during all phases of the simulation. TNF is the model input and is added at the beginning of the stimulation phase of the simulation.

	mRNA, Proteins and Protein Complexes	**Model Species**	**Initial μM**	**Loc.**
1	IκBα	IkBa	0	Cyt
2	IκBα	IkBan	0	Nuc
3	IκBα-NF-κB	IkBaNFkB	0	Cyt
4	IκBα-NF-κB	IkBaNFkBn	0	Nuc
5	IκBα mRNA	IkBat	0	Cyt
6	IκBβ	IkBb	0	Cyt
7	IκBβ	IkBbn	0	Nuc
8	IκBβ-NF-κB	IkBbNFkB	0	Cyt
9	IκBβ-NF-κB	IkBbNFkBn	0	Nuc
10	IκBβ mRNA	IkBbt	0	Cyt
11	IκBε	IkBe	0	Cyt
12	IκBε	IkBen	0	Nuc
13	IκBε-NF-κB	IkBeNFkB	0	Cyt
14	IκBε-NF-κB	IkBeNFkBn	0	Nuc
15	IκBε mRNA	IkBet	0	Cyt
16	A20	A20	0	Cyt
17	A20 mRNA	A20t	0	Cyt
18	NF-κB	NFkB	0	Cyt
19	NF-κB	NFkBn	0.125	Nuc
20	TNF	tnf	0	Ext
21	TNF Receptor Monomer	tnfrm	0	Mem
22	TNF Receptor Trimer	TNFR	0	Mem
23	TNF-Bound TNF Receptor Trimer	TNFRtnf	0	Mem
24	TNFR Complex I (active)	C1	0	Mem
25	TNFR Complex I (inactive)	C1_off	0	Mem
26	TNF-Bound TNFR Complex I (active)	C1tnf	0	Mem
27	TNF-Bound TNFR Complex I (inactive)	C1_tnf_off	0	Mem
28	TRAF-TRADD-RIP	TTR	8.3e-4	Cyt
29	TAK1 (active)	IKKK	0	Cyt
30	TAK1 (inactive)	IKKK_off	0.1	Cyt
31	IKK (active)	IKK	0	Cyt
32	IKK (inactive)	IKK_off	0.1	Cyt
33	IKK (auto-inactivated)	IKK_i	0	Cyt

Table 4.3 Model v4.0 Reactions and Rate Constants

The model contains NF-κB and an IKK activation modules which have 70 and 39 reactions. respectively. Each reaction has a kinetic rate constant and is localized to the cytoplasm (cyt), nucleus (nuc), extracellular space (ext), or the cell membrane (mem). The reactant or product 'null' represents a source (in the case of constitutive RNA synthesis) or a sink (in the case of RNA or protein degradation).

NF-κB Activation Module					
IκB mRNA and Protein Synthesis Reactions					
#	**Reaction**	**Parameter Value**	**Category**	**Loc**	**Source of Parameter Value**
1	null => IkBat (constitutive)	7 E-5 min^{-1}	RNA Synth.	-	Parameter value chosen to fit mRNA and protein expression profiles as measured by RNase Protection (RPA) and Western Blot assays.
2	null => IkBbt (constitutive)	1 E-5 min^{-1}	RNA Synth.	-	*Refer to #1.*
3	null => IkBet (constitutive)	1 E-6 min^{-1}	RNA Synth.	-	*Refer to #1.*
4 **7** **10**	null => IkBat (induced by NFkBn)	8 μM^{-2} min^{-1} Hill Coeff.: 3 Delay: 0 min	RNA Synth.	-	(Kearns *et al*, 2006) (Werner *et al*, 2005) (Kearns *et al*, 2006) and unpublished results
5 **8** **11**	null => IkBbt (induced by NFkBn)	0.02 $\mu M^{-2} min^{-1}$ Hill Coeff.: 3 Delay: 37 min	RNA Synth.	-	(Kearns *et al*, 2006) (Werner *et al*, 2005) (Kearns *et al*, 2006) and unpublished results
6 **9** **12**	null => IkBet (induced by NFkBn)	0.3 $\mu M^{-2} min^{-1}$ Hill Coeff.: 3 Delay: 37 min	RNA Synth.	-	(Kearns *et al*, 2006) (Werner *et al*, 2005) (Kearns *et al*, 2006) and unpublished results
13	IkBat => null	0.035 min^{-1}	RNA Deg.	Cyt	mRNA half-life measurements using actinomycin-D treatment of cells and RPA. (unpublished results)
14	IkBbt => null	3 E-3 min^{-1}	RNA Deg.	Cyt	*Refer to #7.*
15	IkBet => null	4 E-3 min^{-1}	RNA Deg.	Cyt	*Refer to #7.*
16	IkBat => IkBa + IkBat	0.25 min^{-1}	Prot. Synth.	Cyt	(Hoffmann *et al*, 2002)
17	IkBbt => IkBb + IkBbt	0.25 min^{-1}	Prot. Synth.	Cyt	(Hoffmann *et al*, 2002)
18	Ikbet => IkBe + IkBet	0.25 min^{-1}	Prot. Synth.	Cyt	(Hoffmann *et al*, 2002)

Table 4.3 Model v4.0 Reactions and Rate Constants, Continued.

IκB and NFκB Cellular Localization Reactions					
19	IkBa => IkBan	0.09 min^{-1}	Import	-	(Werner *et al*, 2005)
20	IkBb => IkBbn	0.009 min^{-1}	Import	-	(Werner *et al*, 2005)
21	IkBe => IkBen	0.045 min^{-1}	Import	-	(Werner *et al*, 2005)
22	NFkB => NFkBn	5.4 min^{-1}	Import	-	(Werner *et al*, 2005)
23	IkBan => IkBa	0.012 min^{-1}	Export	-	(Werner *et al*, 2005)
24	IkBbn => IkBb	0.012 min^{-1}	Export	-	(Werner *et al*, 2005)
25	IkBen => IkBe	0.012 min^{-1}	Export	-	(Werner *et al*, 2005)
26	NFkBn => NFkB	0.0048 min^{-1}	Export	-	(Werner *et al*, 2005)
27	IkBaNFkB => IkBaNFkBn	0.276 min^{-1}	Import	-	(Werner *et al*, 2005)
28	IkBbNFkB => IkBbNFkBn	0.0276 min^{-1}	Import	-	(Werner *et al*, 2005)
29	IkBeNFkB => IkBeNFkBn	0.138 min^{-1}	Import	-	(Werner *et al*, 2005)
30	IkBaNFkBn => IkBaNFkB	0.828 min^{-1}	Export	-	(Werner *et al*, 2005)
31	IkBbNFkBn => IkBbNFkB	0.414 min^{-1}	Export	-	(Werner *et al*, 2005)
32	IkBeNFkBn => IkBeNFkB	0.414 min^{-1}	Export	-	(Werner *et al*, 2005)
IκB Protein Degradation Reactions					
33	IkBa =>	0.12 min^{-1}	Prot. Deg.	Cyt	(O'Dea *et al*, 2007)
34	IkBb =>	0.18 min^{-1}	Prot. Deg.	Cyt	(O'Dea *et al*, 2007)
35	IkBe =>	0.18 min^{-1}	Prot. Deg.	Cyt	(O'Dea *et al*, 2007)
36	IkBan =>	0.12 min^{-1}	Prot. Deg.	Cyt	(O'Dea *et al*, 2007)
37	IkBbn =>	0.18 min^{-1}	Prot. Deg.	Nuc	(O'Dea *et al*, 2007)
38	IkBen =>	0.18 min^{-1}	Prot. Deg.	Nuc	(O'Dea *et al*, 2007)
39	IkBaNFkB => NFkB	6E-5 min^{-1}	Prot. Deg.	Cyt	(O'Dea *et al*, 2007)
40	IkBbNFkB => NFkB	6E-5 min^{-1}	Prot. Deg.	Cyt	(O'Dea *et al*, 2007)
41	IkBeNFkB => NFkB	6E-5 min^{-1}	Prot. Deg.	Cyt	(O'Dea *et al*, 2007)
42	IkBaNFkBn => NFkBn	6E-5 min^{-1}	Prot. Deg.	Nuc	(O'Dea *et al*, 2007)
43	IkBbNFkBn => NFkBn	6E-5 min^{-1}	Prot. Deg.	Nuc	(O'Dea *et al*, 2007)
44	IkBeNFkBn => NFkBn	6E-5 min^{-1}	Prot. Deg.	Nuc	(O'Dea *et al*, 2007)
IκB:NFκB Association and Dissociation Reactions					
45	IkBa+NFkB=> IkBaNFkB	30 μM^{-1} min^{-1}	Association	Cyt	(Hoffmann *et al*, 2002)
46	IkBb+NFkB=> IkBbNFkB	30 μM^{-1} min^{-1}	Association	Cyt	(Hoffmann *et al*, 2002)
47	IkBe+NFkB => IkBeNFkB	30 μM^{-1} min^{-1}	Association	Cyt	(Hoffmann *et al*, 2002)
48	IkBan + NFkBn => IkBaNFkBn	30 μM^{-1} min^{-1}	Association	Nuc	(Hoffmann *et al*, 2002)
49	IkBbn + NFkBn => IkBbNFkBn	30 μM^{-1} min^{-1}	Association	Nuc	(Hoffmann *et al*, 2002)
50	IkBen + NFkBn => IkBeNFkBn	30 μM^{-1} min^{-1}	Association	Nuc	(Hoffmann *et al*, 2002)
51	IkBaNFkB => IkBa + NFkB	6E-5 min^{-1}	Dssn.	Cyt	(Hoffmann *et al*, 2002)
52	IkBbNFkB => IkBb + NFkB	6E-5 min^{-1}	Dssn.	Cyt	(Hoffmann *et al*, 2002)
53	IkBeNFkB => IkBe + NFkB	6E-5 min^{-1}	Dssn.	Cyt	(Hoffmann *et al*, 2002)
54	IkBaNFkBn => IkBan + NFkBn	6E-5 min^{-1}	Dssn.	Nuc	(Hoffmann *et al*, 2002)
55	IkBbNFkBn => IkBbn + NFkBn	6E-5 min^{-1}	Dssn.	Nuc	(Hoffmann *et al*, 2002)
56	IkBeNFkBn => IkBen + NFkBn	6E-5 min^{-1}	Dssn..	Nuc	(Hoffmann *et al*, 2002)

Table 4.3 Model v4.0 Reactions and Rate Constants, Continued.

IKK-mediated IκB Degradation Reactions					
57	IkBa => null	0.36 min^{-1}	Prot. Deg.	Cyt	(Mathes et al, 2008)
58	IkBb => null	0.12 min^{-1}	Prot. Deg.	Cyt	(Mathes et al, 2008)
59	IkBe => null	0.18 min^{-1}	Prot. Deg.	Cyt	(Mathes et al, 2008)
60	IkBaNFkB => NFkB	0.36 min^{-1}	Prot. Deg.	Cyt	(Hoffmann *et al*, 2002)
61	IkBbNFkB => NFkB	0.12 min^{-1}	Prot. Deg.	Cyt	(Hoffmann *et al*, 2002)
62	IkBeNFkB => NFkB	0.18 min^{-1}	Prot. Deg.	Cyt	(Hoffmann *et al*, 2002)
A20 mRNA and Protein Synthesis and Degradation Reactions					
63	null => A20t (constitutive)	2 E-6 min^{-1}	RNA Synth.	-	*Refer to #1.*
64 **65** **66** **71**	null => A20t (induced by NFkBn)	0.4 $\mu M^{-2}min^{-1}$ Hill Coeff.: 3.0 Delay: 0 min Off: 120 min	RNA Synth.	-	- *Refer to #1.* - *Refer to #1.* - *Refer to #1.* - A20 inducible transcription, as measured by RPA, appears to halt abruptly 2 h into TNF stimulation.
67	A20t => null	0.035 min^{-1}	RNA Deg.	Cyt	*Refer to #1.*
68 **69**	null => A20	0.25 min^{-1} Delay: 30 min	Prot. Synth.	Cyt	- Assumed to be equal to IkB translation rates. - Delay was added to account for time between A20 mRNA expression as measured by RPA and A20 protein expression as measured by Western Blot.
70	A20 => null	0.0029 min^{-1}	Prot. Deg.	Cyt	Western Blot.

Table 4.3 Model v4.0 Reactions and Rate Constants, Continued.

IKK Activation Module					
TNF-Independent Complex I Activity Reactions					
2	null => tnfrm	2 E-7 min^{-1}	Prot. Synth.	mem	Parameter value fit to recapitulate the measured steady-state amount of TNF receptor (Watanabe et al. 1988)
3	tnfrm => null	0.0058 min^{-1}	Prot. Deg.	mem	Measured in (Watanabe et al. 1988)
4	3 tnfrm => TNFR	1 E-5 $\mu M^{-1}min^{-1}$	Association	mem	Parameter value fit to account for minimal TNF receptor aggregation in the absence of ligand as observed in numerous published studies.
5	TNFR => 3 tnfrm	0.1 min^{-1}	Dssn.	mem	*Refer to #4.*
6	TNFR => null (internalization)	0.0017 min^{-1}	Prot. Deg.	mem	Based upon results published in (Watanabe *et al*, 1988) showing that the temporal profile of TNF receptor following TNF stimulation.
7	TNFR + TTR => C1_off	100 $\mu M^{-1}min^{-1}$	Association	mem	Recruitment of TRAF2, TRADD, and RIP adaptors (TTR) to TNFR is required (but not sufficient) for signaling by the TNFR-containing signaling complex (C1). Little biophysical data is available for this reaction; recruitment appears to be simultaneous (Schneider-Brachert *et al*, 2004). The parameter value represents a compound mechanistic rate constant. It was fit to enable quick activation of downstream IKK activity within the first minutes of stimulation and repression upon removal of TNF ligand in pulse stimulations.

Table 4.3 Model v4.0 Reactions and Rate Constants, Continued.

8	C1_off => TNFR + TTR	0.75 min^{-1}	Dssn.	mem	*Refer to #7.*
9	C1_off => C1	30 min^{-1}	Activation	mem	The molecular complex containing TNFR, TRAF2, TRADD and RIP undergoes an activation step that involves K63-ubiqutination of RIP. Little biophysical data is available for this step, but parameter fitting was constrained by the fast activation profile of IKK.
10	C1 => C1_off	2.0 min^{-1}	Deactivation	mem	*Refer to #9.*
11	C1 => C1_off (A20 mediated)	1000 $\mu M^{-1}min^{-1}$	Deactivation	mem	A20 is known to repress the activity of Complex I. It is a protease of K63-linked ubiquitin chains that deubiquitinates RIP (Wertz *et al*, 2004). Little biophysical data is available for this step, but parameter fitting was constrained by the IKK activity profiles measured in *wild type* and *a20*$^{-/-}$ cells.
12	C1 => TNFR + TTR	0.75 min^{-1}	Dssn.	mem	*Assumed to be equal to #8.*
13	C1_off => null (internalization)	0.0017 min^{-1}	Prot. deg.	mem	*Assumed to be equal to #6.*
14	C1 => null (internalization)	0.0017 min^{-1}	Prot. deg.	mem	*Assumed to be equal to #6.*
TNF-Dependent Complex I Activity Reactions					
1	tnf => null	0.0154 min^{-1}	Prot. deg.	Ext	The half-life of recombinant TNF ligand in cell culture medium was measured by its manufacturer, Roche Diagnostics, to be 45-minutes.
15	tnf + 3 tnfrm => TNFRtnf	1100 $\mu M^{-1}min^{-1}$	Association	mem	Measured in (Grell *et al*, 1998).
16	tnf + TNFR => TNFRtnf	1100 $\mu M^{-1}min^{-1}$	Association	mem	*Assumed to be equal to #15.*
17	TNFRtnf => TNFR + tnf	0.021 min^{-1}	Dssn.	mem	Measured in (Grell *et al*, 1998).

Table 4.3 Model v4.0 Reactions and Rate Constants, Continued.

18	TNFRtnf => null (internalization	0.0017 min^{-1}	Prot. Deg.	mem	*Assumed to be equal to #6.*
19	TNFRtnf + TTR => C1tnf_off	100 $\mu M^{-1}min^{-1}$	Association	mem	*Assumed to be equal to #7.* TNF binding to the extra-cellular domain of TNFR monomers speeds up trimerization and stabilizes the trimer, but recruitment of the TTR complex to trimerized TNF receptor are assumed to proceed with the same kinetics regardless of the presence of TNF ligand.
20	C1tnf_off => TNFRtnf + TTR	0.75 min^{-1}	Dssn.	mem	*Refer to #19. Assumed to be equal to #8.*
21	C1tnf_off => C1tnf	30 min^{-1}	Activation	mem	*Refer to #19. Assumed to be equal to #9.*
22	C1tnf => C1tnf_off	2.0 min^{-1}	Deactivation	mem	*Refer to #19. Assumed to be equal to #10.*
23	C1tnf => C1tnf_off (A20 mediated)	1000 $\mu M^{-1}min^{-1}$	Deactivation	mem	*Refer to #19. Assumed to be equal to #11.*
24	C1tnf => TNFRtnf + TTR	0.75 min^{-1}	Dissociation	mem	*Refer to #19. Assumed to be equal to #8.*
25	C1tnf_off => null (internalization)	0.0017 min^{-1}	Prot. deg.	mem	*Refer to #19. Assumed to be equal to #6.*
26	C1tnf => null (internalization)	0.0017 min^{-1}	Prot. deg.	mem	Refer to #19. Assumed to be equal to #6.
27	C1tnf_off => C1_off + tnf	0.021 min^{-1}	Dssn.	mem	*Assumed to be equal to #17.*
28	C1_off + tnf=> C1tnf_off	1100 $\mu M^{-1}min^{-1}$	Association	mem	*Assumed to be equal to #15.*
29	C1tnf => C1 + tnf	0.021 min^{-1}	Dssn.	mem	*Assumed to be equal to #17.*
30	C1 + tnf => C1tnf	1100 $\mu M^{-1}min^{-1}$	Dssn.	mem	*Assumed to be equal to #15.*
IKKK (TAB1/2-TAK1 complex) Activity Reactions					
31	IKKK_off => IKKK (constitutive)	5 E-7 min^{-1}	Activation	Cyt	Parameter value fit to account for low IKK activity in the absence of ligand as measured by IKK Kinase Assay (O'Dea *et al*, 2007).
32	IKKK_off => IKKK (C1 mediated)	500 $\mu M^{-1}min^{-1}$	Activation	Cyt	*Refer to #7.*
33	IKKK_off => IKKK (C1tnf mediated)	500 $\mu M^{-1}min^{-1}$	Activation	Cyt	*Refer to #19. Assumed to be equal to #32.*

Table 4.3 Model v4.0 Reactions and Rate Constants, Continued.

34	IKKK => IKKK_off (constitutive)	0.25 min^{-1}	Deactivation	Cyt	The constitutive inactivation rate of this complex was fit to ensure low basal activity and efficient repression following TNF pulse stimulation.
IKK Activity Reactions					
35	IKK_off => IKK	5 E-5 min^{-1}	Activation	Cyt	*Refer to #31*
36	IKK_off => IKK (IKKK mediated)	520 $\mu M^{-1}min^{-1}$	Activation	Cyt	*Refer to #7.*
37	IKK => IKK_off	0.02 min^{-1}	Deactivation	Cyt	*Refer to #34.*
38	IKK => IKK_i (self-inactivation)	0.15 min^{-1}	Deactivation	Cyt	IKK is thought to down-regulate its own activity via auto-phosphorylation of C-terminal serine residues (Delhase *et al*, 1999). This mechanism was not shown to cause IKK protein degradation and is distinct from inactivating IKK *via* constitutive phosphatase activity (*Refer to* #94). The parameter was fit to temporal profiles of IKK activity in response to TNF stimulation (Werner *et al*, 2005).
39	IKK_i => IKK_off	0.02 min^{-1}	Deactivation	Cyt	C-terminally phosphorylated IKK is assumed to be subject to constitutive phosphatase activity. *Refer to #38.*
x	IL1_IKK Activity	Numerical Curve	-	-	Stimulation by IL1 is enabled through a numerical input curve (as first used in (Werner *et al*, 2005)) that specifies time-dependent activation kinetics of a pool of IL1-responsive IKK.

Table 4.4 Model v4.0 IL-1β-Induced Numerical IKK Activity Profile

IKK activity is defined by a numerical curve that correlates percent IKK activity (between 0 and 100%) with time. This curves is based upon measurements performed in MEF cells via *in vitro* kinase assay, as in (Werner *et al*, 2005).

15' IL-1β pulse activity	**%**	1	60	100	65	50	36	21	16	10	1	1
	Time (min)	0	5	10	15	20	25	30	45	50	60	120

ACKNOWLEDGEMENTS

This chapter is adapted from a 2008 *Genes & Development* research article for which I share co-primary authorship with Shannon L. Werner (Werner *et al*, 2008). This work was a truly collaborative effort. Shannon L. Werner and Victoria Zadorozhnaya performed the bulk of the experiments and were aided by Candace Lynch and Ellen L O'Dea. Mark P. Boldin (Caltech) and professors Averil Ma (UCSF) and David Baltimore (Caltech) provided experimental reagents and insightful discussions. I constructed the computational model and performed the simulations. Professor Alexander Hoffmann is the corresponding author.

Chapter 5

The kinetics of p100/IκBδ negative feedback allow for both signaling crosstalk and differential regulation of inflammatory responses

ABSTRACT

Inflammatory and developmental stimuli activate NF-κB via two distinct signaling pathways—one driven by NEMO/IKK2 and the other by NIK/IKK1 kinase complexes, respectively. Negative feedback mediated by IκBα and IκBε have been shown to be critically important for the regulation of inflammatory-induced NF-κB activity. Here, we describe that a third IκB negative feedback mechanism, p100/IκBδ, regulates developmental NF-κB activity. The stable kinetics of p100/IκBδ expression are found to constitute a cellular memory that enables pathway crosstalk in which a pre-challenge with inflammatory stimulus primes cells for elevated NF-κB activity in response to subsequent developmental stimulus. Further, we explore the role of IκBδ negative feedback in mediating inflammatory NF-κB activity, in which the NEMO/IKK2 kinase complex does not induce its degradation. I developed a computational phenotyping analysis tool that enabled us to contrast the functions of IκBα and IκBδ in inflammatory signaling and found that differences in their kinetics conferred specificities to cytokine or pathogen-derived cellular stimuli, respectively.

INTRODUCTION

The two preceding chapters have explored the roles of negative feedback in regulating the dynamics of NF-κB activity in response to inflammatory stimuli (TNF, IL-1β) that signal via a complex of NEMO and IKK2-containing dimer. This signaling axis is generally termed as the "canonical" or "classical" NF-κB pathway and is proximally regulated by the IκBα, -β, and -ε isoforms and distally regulated by other NF-κB-responsive regulators, such as A20 deubiquitinase, that act upstream of the NEMO/IKK2 complex (Hoffmann *et al*, 2006a; Werner *et al*, 2008).

In contrast, developmental stimuli such as CD40L, LTαβ, and BAFF activate NF-κB through a second signaling axis, termed as the "non-canonical" or "alternative" NF-κB pathway, that signals via a complex of NIK serine/threonine protein kinase and IKK1 homodimer (Ramakrishnan *et al*, 2004; Senftleben *et al*, 2001). This mode of activation is independent of IκBα, -β, and -ε degradation, as is required for canonical signaling, but does involve proteolysis of p100 NF-κB monomer (Dejardin *et al*, 2002; Jiang *et al*, 2003). IκB proteins share a conserved domain consisting of 6 sequential ankyrin repeat motifs that is required for association with NF-κB dimers (Ghosh *et al*, 1998). The p52 and p50 NF-κB monomers are initially expressed as the precursor proteins p100/*nfkb2* and p105/*nfkb1*, respectively, that contain both the NF-κB Rel-homology domain as well as the IκB 6 ankyrin repeat domain. Activation of NIK/IKK1 complex drives processing of p100 precursor to p52 that acts to release RelA/NF-κB and RelB/NF-κB dimers (Dejardin *et al*, 2002; Jiang *et al*, 2003).

In this chapter, I discuss how computational modeling has been utilized in two published studies to explore the function of p100 in regulating both developmental and inflammatory NF-κB signaling (Basak *et al*, 2007; Shih *et al*, 2009)(Figure 5.1). S. Basak *et al* initially confirmed with experiments that MEF treated with a monoclonal antibody that binds and activates LTβR show nuclear accumulation of RelA/NF-κB and RelB/NF-κB dimers that is independent of both NEMO/IKK2 activity and IκBα, -β, and -ε degradation but dependent upon NIK and IKK1. Further, they found that the precursor p100 protein, and not its processed p52 form, is required for noncanonical signaling but is dispensable for TNF-induced canonical signaling. Importantly, they characterized an asynchronous p100 homodimer, in which one ankyrin repeat domain self-inhibits the dimer while the other remains exposed, that is associated with latent NF-κB dimers and is degraded upon LTβR stimulation. As p100/*nfkb2* is, like IκBα/*nfkbia* and IκBε/*nfkbie*, an NF-κB target gene, they termed the asynchronous p100 homodimer as a *bona fide* IκB protein, IκBδ.

The experimental discovery of IκBδ as a negative feedback regulator led us to question how its kinetic properties affect the dynamics of NF-κB signaling. Using an integrated experimental and computational modeling approach, we address the role of IκBδ negative feedback in two contexts. First, how does IκBδ regulate developmental NF-κB signaling? Second, does IκBδ have a role in regulating inflammatory signaling and, if so, how is it different from that of the predominant IκBα negative feedback?

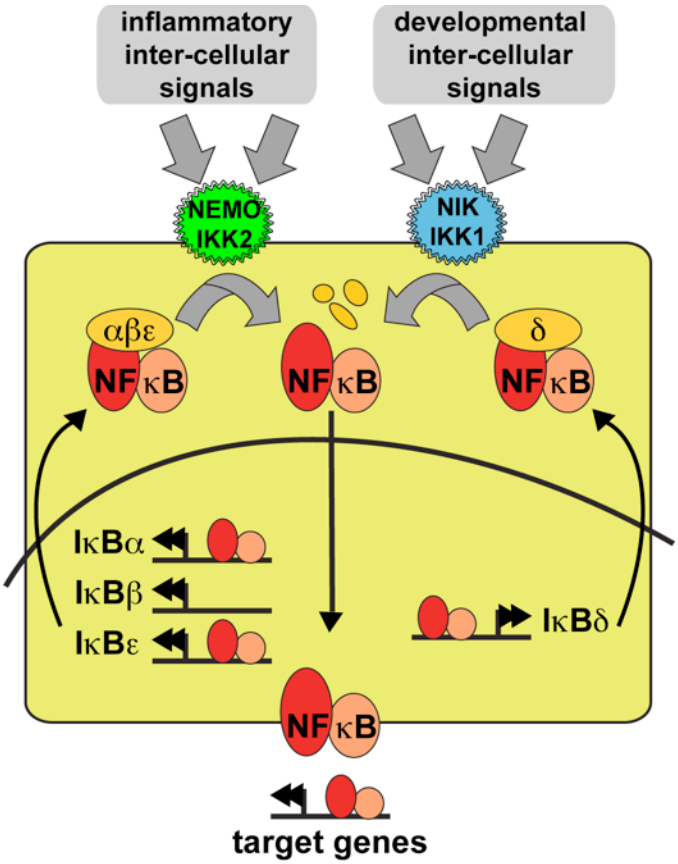

Figure 5.1 Inflammatory and developmental stimuli activate NF-κB

IKK signaling complexes act as central hubs for the diverse set of stimuli and cellular stresses that activate NF-κB. The NEMO/IKK2 complex is responsive to inflammatory signals and activates NF-κB via phosphorylation-dependent degradation of canonical IκB proteins. The NIK/IKK1 complex is responsive to developmental signals and activates NF-κB via phosphoryltation-dependent degradation and processing of noncanonical p100/IκBδ protein.

RESULTS

Construction of a computational model that integrates inflammatory and developmental NF-κB signaling

To investigate how the dynamics of IκBδ regulation affect NF-κB activation in response to noncanonical signaling, we described the synthesis, degradation, and molecular interactions of IκBδ with ODEs and included them in a computational model that already recapitulated TNF and LPS signaling (Werner *et al*, 2005). The resulting model (version 3.0) includes 98 biochemical reactions (Figure 5.2), which were parameterized based on published measurements, out own measurements, and fitting procedures (Table 5.2). The resulting *in silico* model of the NF-κB signaling module predicts RelA/NF-κB activity in response to either canonical or noncanonical stimuli, as well as the abundances of the 32 model components (Table 5.1).

Simulations of LPS and TNF pulse stimulations show the dynamics of NF-κB activities and cellular canonical IκB levels (Figure 5.3, left and center) that match previous measurements (Werner *et al*, 2005). Unlike the canonical IκB proteins, IκBδ is not degraded in response to NEMO/IKK2-mediated inflammatory signals (Figure 5.3, bottom row). In contrast, NIK/IKK1-mediated LTβR signaling results in IκBδ degradation while the canonical IκB proteins are unaffected (Figure 5.3, right). Importantly, the model recapitulates the experimental measurements of slow induction by LTβR stimulation of nuclear RelA/NF-κB activity that reaches a maximum at 5-15 hr (Basak *et al*, 2007, Supplementary Figure 1B).

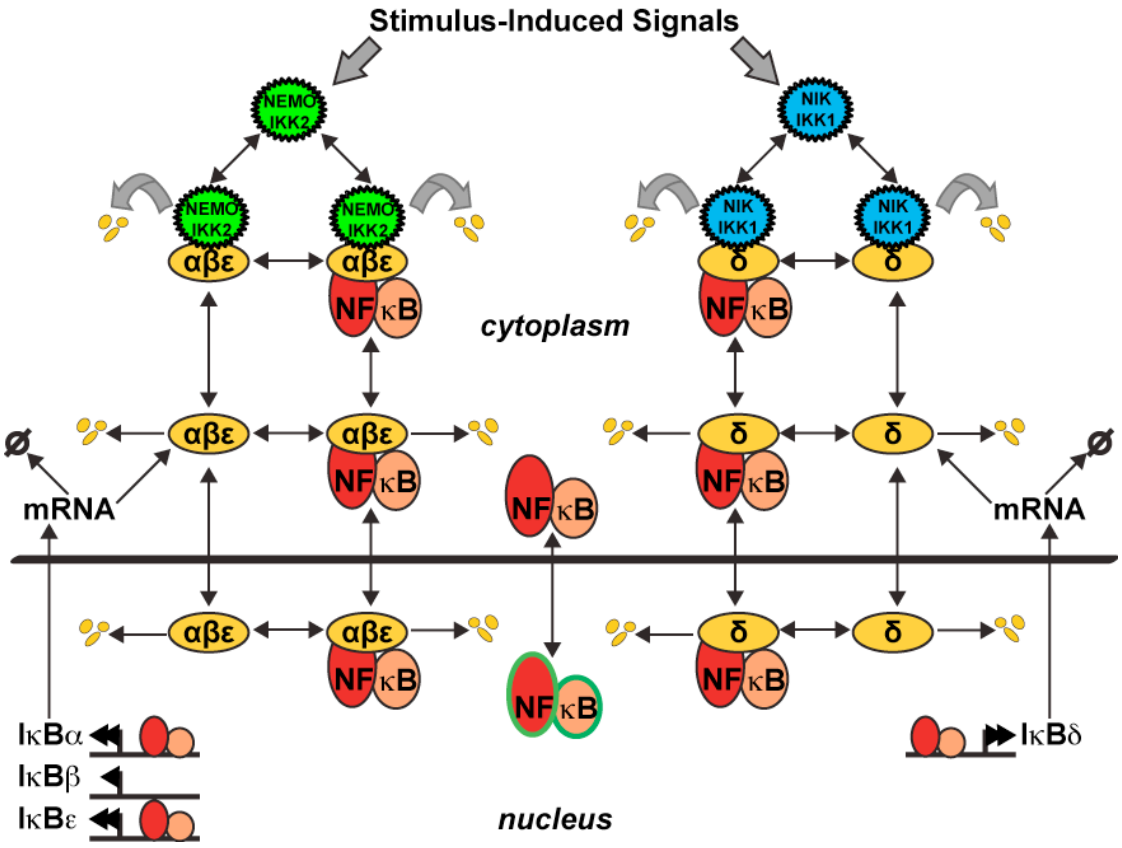

Figure 5.2 Reaction map of an inflammatory/developmental NF-κB signaling module

Schematic diagram of the components and reactions that are described within versions 3.0 and 3.1 of the NF-κB computational model. Distinct reactions exist for each IκB isoform (α, β, ε, δ) and are controlled by isoform-specific reaction rate constants. Reactions control synthesis and degradation of the IκBs, association and dissociation of IκBs, NF-κB, and IKK complexes, and cellular localization. NF-κB is a product or reactant in multiple reactions and, for clarity, is included once in the middle of the diagram. The temporal profiles of NIK/IKK1 and NEMO/IKK2 activity are used as the model inputs. Free NF-κB in the nucleus, denoted with a green outline, is used as the model output.

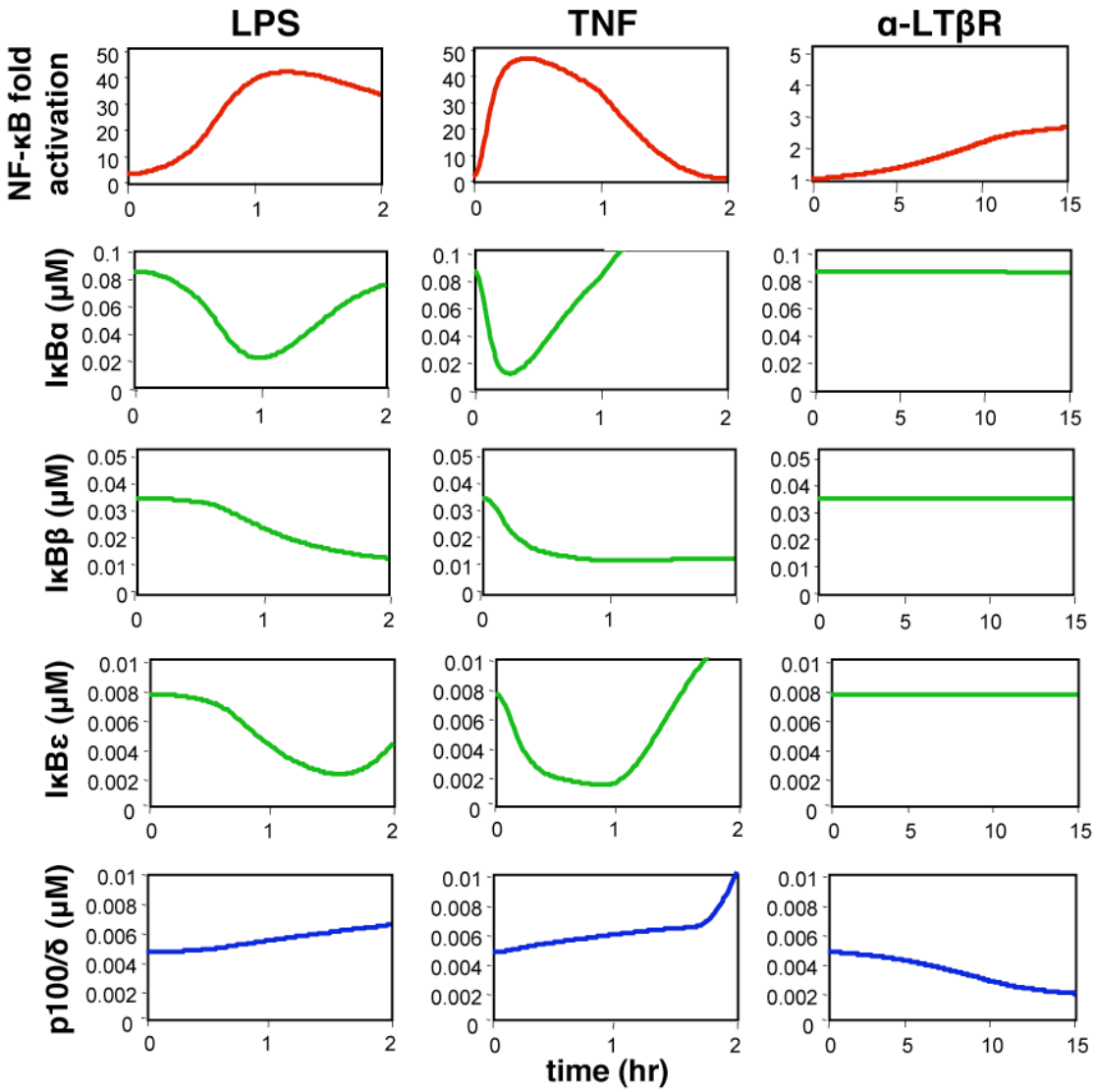

Figure 5.3 A single NF-κB signaling module mediates NF-κB activation in response to inflammatory and developmental signals

Computational simulations of the dynamic regulation of nuclear RelA:p50 NF-κB activity (top panels, red), total cellular protein levels of canonical IκB proteins (middle panels, green), and noncanonical IκB protein p100 (bottom panels, blue). Simulations are shown for the IKK2-inducing stimuli TNF and LPS and the IKK1-inducing developmental signals mediated by LTβR.

Crosstalk between inflammatory and developmental NF-κB signaling

We used computational simulations so explore the feedback regulation and the dynamics of p100/IκBδ protein levels in a variety of stimulation regimes. Remarkably, we found that a 1hr pulse of TNF stimulation resulted in an elevation of p100/IκBδ protein of about 4-fold that persisted for more than 20 hr (Figure 5.4A, top). In contrast, the sum of all canonical IκB proteins revealed the expected transient trough and rapid recovery. The model therefore predicts that "priming" of cells with a pulse of TNF stimulation can shift the balance of latent NF-κB associated with canonical or noncanonical IκB proteins (Figure 5.4A, bottom). We examined this prediction experimentally. Immunoblotting of total cellular IκB protein confirmed that the p100/IκBδ protein is induced by 1 hr TNF pulse stimulation, while the levels of canonical IκB proteins were not discernibly different (Figure 5.4B).

This shift in the IκB homeostasis may have functional consequences. Computational simulations in naïve and TNF-primed cells led to the prediction that primed cells may respond with a stronger NF-κB activation profile (Figure 5.5A). Indeed, this prediction is confirmed under identical experimental conditions by EMSA (Figure 5.5B). This finding is remarkable because in this stimulation regimen canonical signaling has long ceased when cells are exposed to agonist antibody, and it thus not only constitutes an example of signaling crosstalk but also of cellular memory.

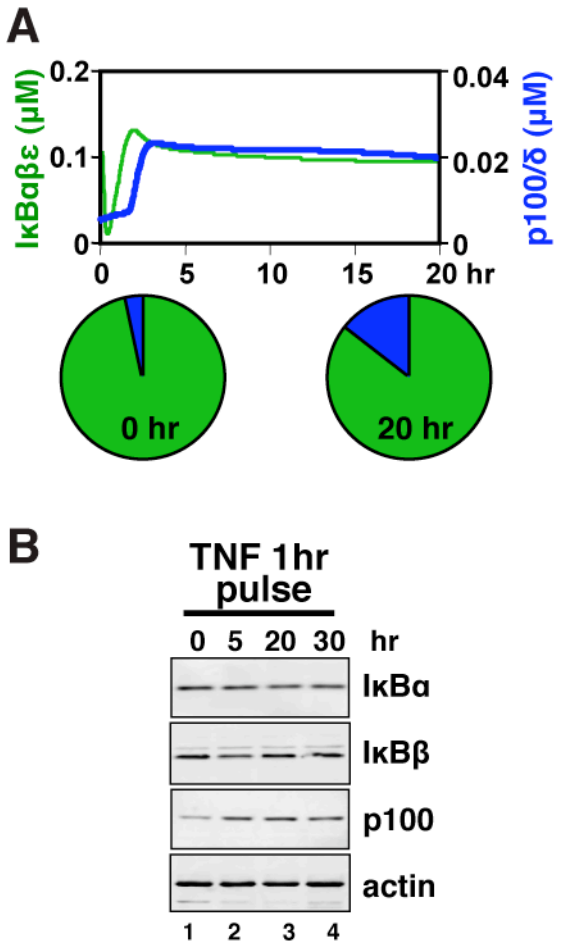

Figure 5.4 Inflammatory TNF stimulation modulates the distribution of canonical vs. noncanonical IκBs

(A) Cellular levels of canonical (IκBα, IκBβ, IκBε; green) and noncanonical (p100/IκBδ) IκB proteins over a 20 hr time course as predicted by computational simulations of cells stimulated with a 1 hr pulse of TNF. The pie charts indicate the proportion of NF-κB bound to canonical IκBs (green) vs. the noncanonical IκB (blue) in resting (left) vs. TNF-primed (right) cells.

(B) Immunoblots for canonical IκBα and IκBβ and noncanonical p100/IκBδ protein of whole-cell lysates prepared at the indicated times from wild type MEF that were transiently stimulated with 1ng/mL TNF for 1 hr.

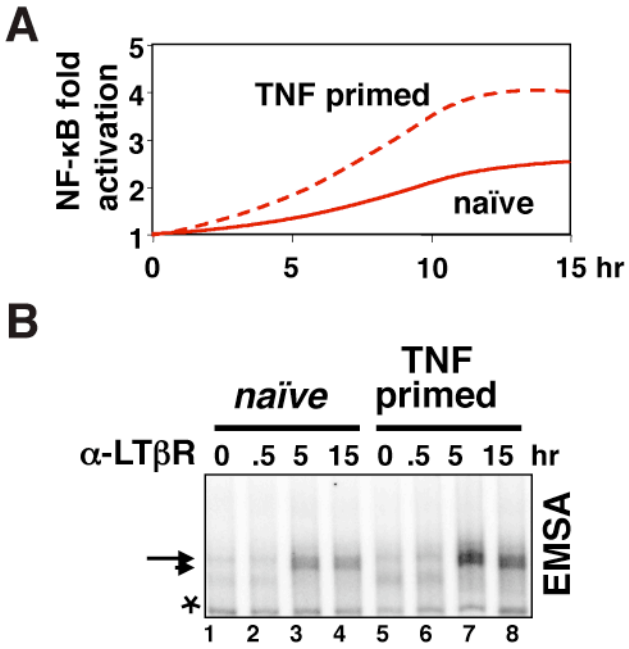

Figure 5.5 p100/IκBδ mediates crosstalk between inflammatory and developmental signals

(A) Computational stimulations of NF-κB activity induced by LTβR stimulation of naïve or TNF-primed cells.

(B) Experimental analysis of LTβR signaling in naïve or TNF-primed cells. Cells were harvested at indicated time points after LTβR stimulation and nuclear extracts were tested for RelA:p50 DNA binding activity by EMSA.

Genetic perturbations of IκB homeostasis

The homeostasis of canonical and noncanonical IκB proteins may not only be subject to physiological stimuli, but altered homeostasis due to genetic aberrations may be the underlying cause for pathological misregulation of stimulus-specific NF-κB activity. To examine this possibility and further test the validity of our model, we used computational simulations to predict the relative amounts of p100/IκBδ protein in a panel of cells deficient for one or more canonical IκB proteins. For example, cells deficient in IκBα were predicted to have 2-fold more p100/IκBδ protein than wild type cells (Figure 5.6A). Similarly, doubly-deficient and triply-deficient cells are predicted to show further increases in p100/IκBδ except for IκBβ/IκBε-deficient cells, in which p100/IκBδ levels were predicted to be near wild type. Immunoblotting for p100 with extracts derived from these different cell lines confirmed this prediction (Figure 5.6B); in particular, we observed no significant increases in p100 levels in IκBβ/IκBε-deficient cells while immunoblot signals were elevated in other knockouts as predicted.

Altered balances in the canonical and noncanonical IκB proteins may be expected to lead to alterations in the LTβR responsiveness. Computational simulations indeed predicted that NF-κB responses to agonist receptor would be highest in IκB triple-knockout and IκBα/IκBε-deficient cells, intermediate in IκBα- and IκBα/IκBβ-deficient cells, and relatively low in wild type and IκBβ/IκBε-deficient cells (Figure 5.6C). The results from experimental analysis using EMSA of nuclear extracts prepared from LTβR-stimulated cells of each respective genotype were in overall agreement with these simulations (Figure 5.6D).

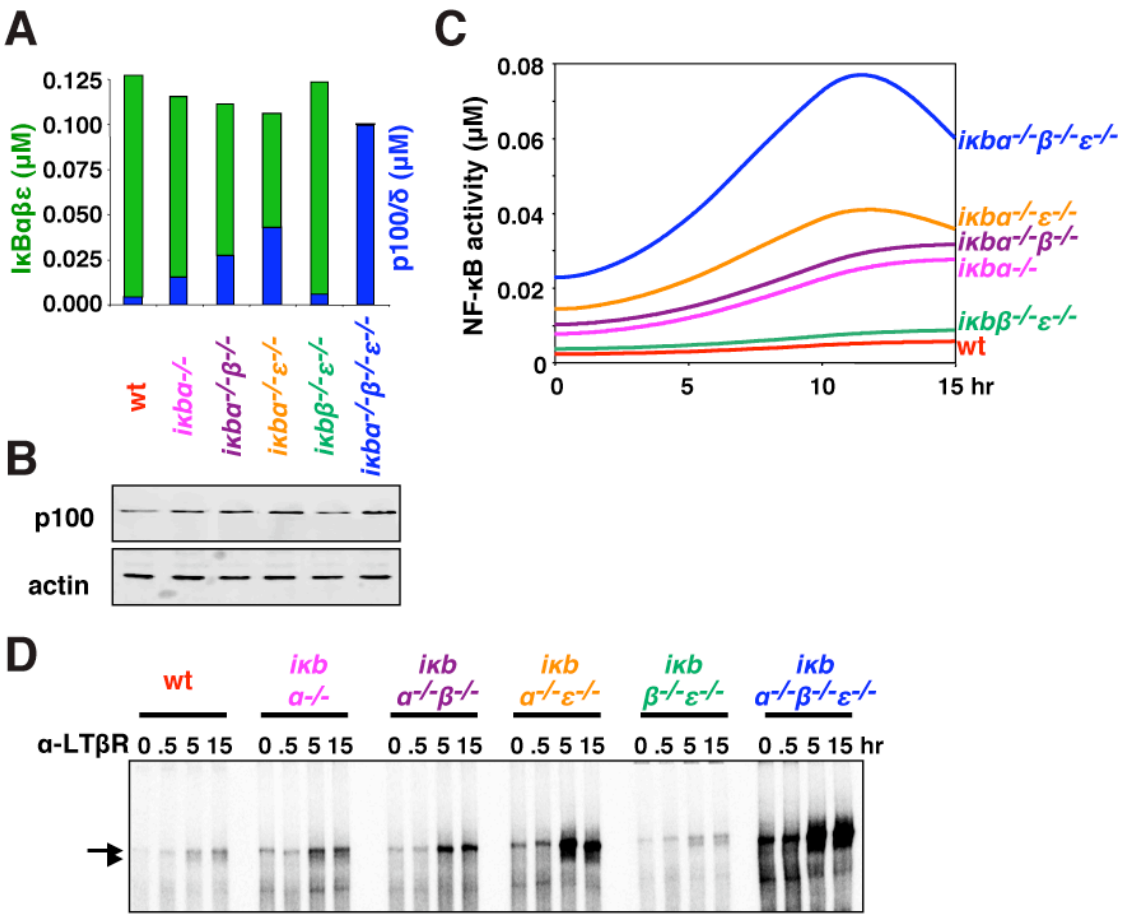

Figure 5.6 Misregulation of canonical and noncanonical IκB homeostasis alters stimulus-specific NF-κB activity

(A) Cellular proteins levels of canonical (IκBα, IκBβ, IκBε; green) and noncanonical (p100/IκBδ; blue) IκB proteins in unstimulated cells of the indicated genotype as predicted by computational simulations.
(B) Quantitative immunoblot for p100 of lysates prepared from equivalent number of wild type or mutant MEF of the indicated genotype.
(C) Computational simulations of nuclear NF-κB activity induced by LTβR stimulation of the indicated genotype
(D) EMSA for NF-κB binding activity of nuclear extracts prepared from LTβR-stimulated cells of the indicated genotype. Wild type or mutant MEF that lack one or more IκB isoforms were simulated with LTβR for the indicated times.

Computational phenotyping of IκBα and IκBδ negative feedback regulators

Having demonstrated that inducible synthesis of asynchronous p100 homodimer, IκBδ, constitutes a fourth *bona fide* IκB activity and is required for developmental signaling via NIK/IKK1 complex, we sought to determine its role in regulating inflammatory signaling downstream of the canonical NEMO/IKK2 complex. To do so, we first refined the 4-IκB computational model described earlier (v3.0) by changing rate constant values to reflect new experimental findings. Specifically, mRNA and protein half-lives were more accurately measured and showed that IκBδ is significantly more stable than IκBα (data not shown). While IκBα has a 20 min mRNA half-life and 6 min free/unbound protein half-life, p100/IκBδ has 360 min and 480 min half-lives, respectively.

To explore NF-κB regulation in response to diverse canonical IKK dynamics, we generated a library of canonical IKK curves using an algorithm that controls the amplitudes and durations of several activity phases (Figure 5.7). The resulting 1044 unique curves were used as inputs for repeated simulations of NF-κB activation in wild type, IκBδ-, and IκBα-deficient models (Figure 5.8A). By calculating the difference in NF-κB activities generated by wild type and mutant modules for a given IKK input profile, we assessed the functional importance of each IκB.

At a first glance, the simulation data indicated IκBδ does have a role in inflammatory signaling and that IKK curves for which IκBδ-mediated feedback is functionally important do not generally require regulation by IκBα. Sorting these simulation results in order of increasing sensitivity to IκBδ revealed that IκBδ- and IκBα-mediated feedback are important for attenuating NF-κB activity in response to

different types of canonical IKK profiles (Figure 5.8B). Plotting the 2 groups of IKK curves showed that IκBδ-deficient systems causes misregulation of NF-κB in response to prolonged canonical IKK stimuli, whereas IκBα-deficiency causes misregulation in response to transient stimuli (Figure 5.8C). Thus, the computational analysis suggested that the relative importance of different negative feedback regulators is determined by the temporal profiles of IKK activity and, specifically, that IκBδ may be important in providing negative feedback on NF-κB in response to stimuli that elicit sustained canonical IKK activity.

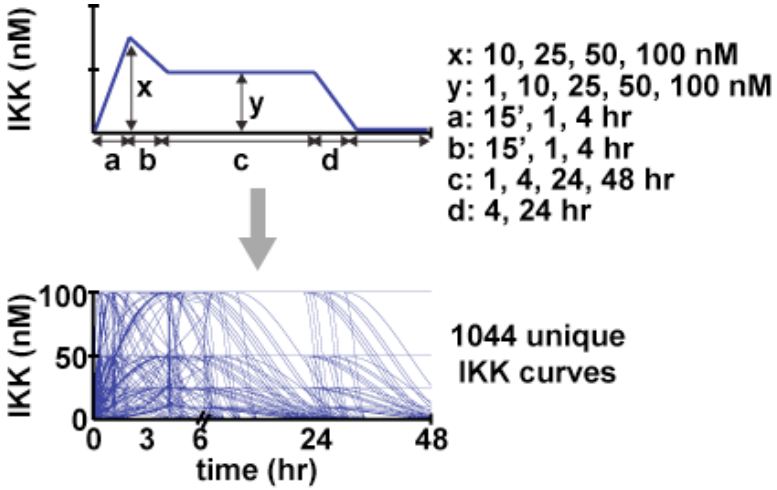

Figure 5.7 Algorithm to develop a library of theoretical NEMO/IKK2 input curves

A library of 48 hr NEMO/IKK2 input curves was generated by an algorithm that incorporates, combinatorially, six variables (top). Two variables, *x* and *y*, control the amplitude of a first and second peak of IKK activity, respectively. The remaining four variables control the duration of these two phases— *a* the rise time from the basal state to the first peak, *b* the fall/rise time from the first peak to the second peak, *c* the duration of the second peak, and *d* the fall time from the second peak back to basal activity (1 nM). Combinations that were shorter than 48 hr in duration were increased by appending basal activity out to 48 hr. This algorithm generates 1044 unique 48 hr NEMO/IKK2 input curves (bottom).

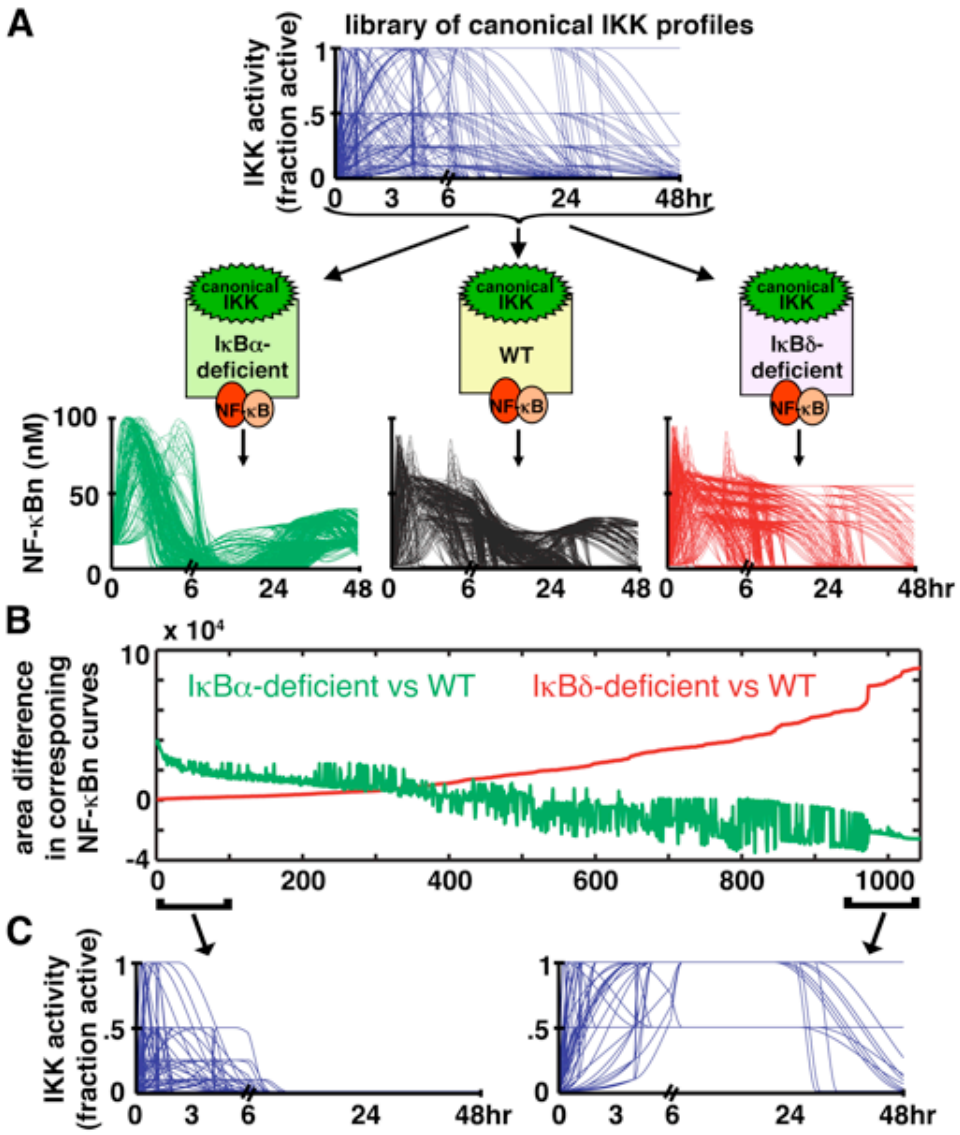

Figure 5.8 Phenotyping negative feedback regulators within signaling dynamics

(A) The library of 1044 hypothetical NEMO/IKK2 input curves (top) was fed into wild type, IκBα-, or IκBδ-deficient computational models (middle) to calculate the corresponding 1044 NF-κB outputs for each model (bottom).

(B) A plot of the quantitated phenotype for each IKK input curve in IκBα- or IκBδ-deficient cells, as predicted by simulations. Differences of NF-κB between wild type and knockout cells ("the phenotype") were calculated for each simulation and plotted after sorting the 1044 simulations for increasing NF-κB phenotypes in IκBδ-deficient models.

(C) Time course plots of the IKK input curves that gave rise to the least or maximum IκBδ phenotype, as defined by the bottom and top 10% of the curves found in (B).

IκBα attenuates NF-κB activation triggered by cytokines, but not pathogens

TNF and LPS have been shown to activate canonical IKK activity with different dynamics within a 2 h time course (Werner *et al*, 2005). In extended time course experiments, we found that TNF stimulation triggered a transient canonical IKK activity that decreased after 1 h and reached the basal level before 24 hr (Figure 5.9A). In contrast, LPS stimulation led to delayed canonical IKK activation that peaked at 1 h and was sustained at ~40% of the peak activity even at the 48 h time point.

Based on the computational phenotyping methodology, we predicted that IκBδ-deficient cells would be more defective in controlling the LPS- than TNF-induced NF-κB activity profiles. To test the model predictions, wild type and IκBδ-deficient cells were stimulated with TNF and LPS for 24 h. As predicted, TNF-induced NF-κB activation was similar in wild type and IκBδ-deficient cells whereas in response to LPS, prolonged NF-κB activation was observed in IκBδ-deficient cells (Figure 5.9B). These results indicate that IκBδ dampens NF-κB activity stimulus-specifically such that a sustained canonical IKK activity is more susceptible to its feedback mechanism.

What is the molecular basis for IκBδ feedback's specificity for LPS/TLR-mediated signals? Using chimeric IκBα/IκBδ mutants *in silico*, we found that neither IκBδ's binding affinities for NF-κB (chimera C1) nor its shuttling rate constants (chimera C2) were sufficient to dampen pathogen-induced NF-κB activity. However, mRNA and protein synthesis and degradation rate constants of IκBδ are critical in conjunction with its unresponsiveness to canonical IKK signals: When controlling the

expression of an IκBα protein, which is responsive to canonical IKK degradative signals, chimeras with IκBδ synthesis and degradation rates provide some dampening (chimeras C3 and C4); in the context of a canonical IKK-unresponsive IκBδ-protein, IκBα synthesis and degradation rates are predicted to dramatically over-attenuate, not allowing fro any late NF-κB activity (chimera C5). These analyses suggest that the combination of IκBδ's unresponsiveness to the degradation signaling of canonical IKK and relatively low synthesis and degradation rates allows for a slow build-up of IκBδ inhibitory activity even in the context of long-lasting canonical IKK activity; these are the critical determinants of the stimulus-specific function of IκBδ-mediated feedback to persistent signaling.

Our combined computational and experimental studies suggest different roles for IκBα and IκBδ. We propose that IκBα-mediated negative feedback regulates NF-κB primarily in response to inflammatory cytokines such as TNF and IL-1β, which produce transient canonical IKK activities. In contrast, long-lasting canonical IKK activities that render IκBδ functionally important are hallmarks of pathogen signaling via Toll-like receptors (Werner *et al*, 2005)(Figure 5.10).

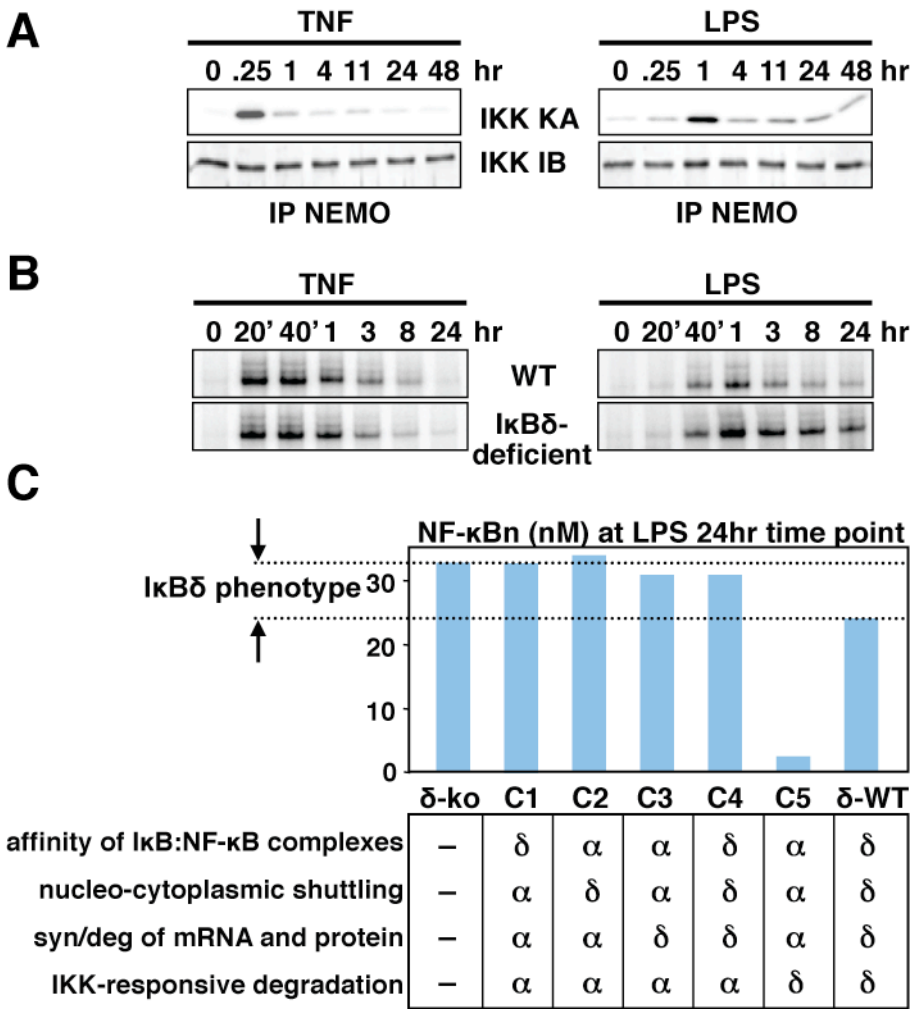

Figure 5.9 IκBα and IκBδ mediate NF-κB attenuation stimulus-specifically

(A) IKK kinase activity assays (IKK KA) from MEF chronically stimulated with TNF (1 ng/mL) or LPS (100 ng/mL). NEMO-associated kinase complex immunoprecipitated from extracts prepared at the indicated times, and used for a kinase assay with GST-IκBα (1-54) as a substrate. Equal loading was confirmed by immunoblotting against IKK1 (IKK IB).

(B) NF-κB DNA binding activities measured by EMSA in wild type and IκBδ-deficient MEF stimulated as in (A).

(C) Computational analyses of *in silico* chimeras reveal the relative importance of kinetic rate constants for IκBδ-mediated attenuation of LPS signaling. Chimeric mutants were made by swapping rate constants of IκBα to those of IκBδ as indicated. NF-κB activities induced by 24 hr LPS stimulation were plotted for each chimera.

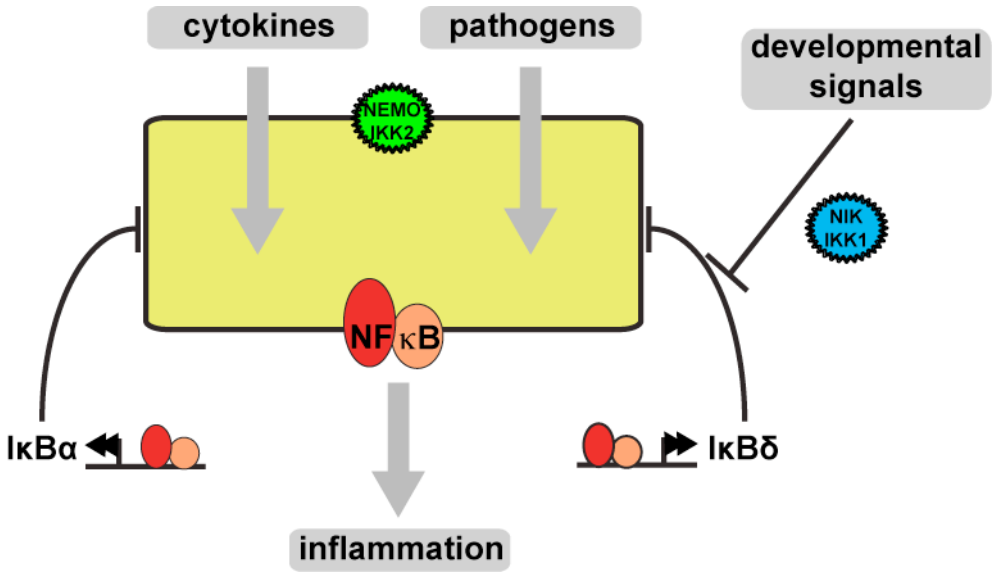

Figure 5.10 IκBα and IκBδ mediate responses to specific stimuli

The quick kinetics of IκBα are tuned to regulate NF-κB activity in response to acute inflammatory stimuli (cytokines) while the slow/stable kinetics of IκBδ impart specificity for regulating chronic inflammatory signaling (pathogens). Developmental signaling via NIK/IKK1 may modulate pathogenic responses via inducible degradation of IκBδ.

DISCUSSION

Asynchronous p100 homodimer was found experimentally to constitute the fourth described IκB activity, IκBδ. The function of IκBδ to regulate NF-κB signaling dynamics was further examined via an experimentally validated computational modeling methodology. In two related studies, IκBδ was shown to be critically important for noncanonical signaling induced by developmental stimuli and for persistent canonical signaling most often associated with pathogen-induced responses.

Inflammatory and developmental NF-κB signaling was thought to be spatially insulated by way of two IKK complexes, NEMO/IKK2 and NIK/IKK1, with specific activities for NF-κB inhibitors (Hoffmann *et al*, 2006a). Our studies suggest that such insulation does not exist and that IκBδ, the putative target for NIK/IKK1 activity, in fact imparts specific regulatory control in both canonical and noncanonical NF-κB pathways.

First, IκBδ was found to be essential for activation of NF-κB in response to developmental LTβR stimulation. Second, IκBδ was found to constitute a form of cellular memory to previous NF-κB activation, as inducible expression from the *nfkb2* gene produces p100 protein which homodimerizes to form the kinetically stable IκBδ activity. "Priming" of cells with a transient TNF inflammatory stimulation perturbs the distribution of canonical- (IκBα, IκBβ, IκBε) vs. noncanonical- (IκBδ) bound NF-κB such that the fraction of NIK/IKK1-responsive NF-κB increases 4-fold over a 24 h period. This further led to the conclusion that the amplitude of the NF-κB activity was directly proportional to the fraction of the latent NF-κB dimer sequestered by IκBδ in

the cytoplasm in a NIK/IKK1-responsive poised state. Simulations of genetic knockouts deficient in one or more canonical IκB proteins revealed that the homeostatic abundance of IκBδ-bound NF-κB increases in these systems and that this leads to aberrant inflammatory-type NF-κB activity in response to subsequent developmental challenge with LTβR.

Second, IκBδ was found to regulate NF-κB activity in response to inflammatory canonical signaling in which it is not degraded by the NEMO/IKK2 complex. We developed a computational phenotyping tool that enabled the direct comparison of the roles of IκBα and IκBδ negative feedback. By abstracting the canonical pathway into a library of hypothetical IKK profiles, we explored the signal processing space comprehensively, unbiased by the limitations of currently known stimuli. Mapping our insights back to actual Toll-like receptor and cytokine receptor-mediated signals, we were able to experimentally examine the computational predictions. IκBα and IκBδ were found to have contrasting functions that derived form differences in the kinetic rate constants governing their NF-κB-inducible synthesis, half-life, and canonical IKK-inducible degradation. Our combined computational and experimental studies revealed that these characteristics are important in the context of stimulus-specific control of canonical IKK activities: pathogen-derived substances (i.e. LPS) are only slowly metabolized and activate canonical IKK for extended durations (Werner *et al*, 2005) which allows signal-unresponsive IκBδ to accumulate. In contrast, high inducibility of IκBα allows it to react swiftly to transient (i.e. cytokine) stimuli but its similarly swift degradation kinetics hinders its ability to regulate long-lasting (i.e. pathogen) signaling (Figure 5.10).

MATERIALS AND METHODS

Experimental Studies:

Experimental assays were performed by my collaborators (S. Basak and V. Shih). Immortalized MEFs were prepared and cultured as previously described (*Materials and Methods*, Chapter 2). Western Blot and EMSA are described in *Methods* Chapter 2 and *in vitro* kinase assay in (Werner *et al*, 2005). The cell lines used were: wild-type (Hoffmann *et al*, 2002), *iκbα*$^{-/-}$ (Hoffmann *et al*, 2002), *iκbα*$^{-/-}$ *iκbε*$^{-/-}$ (Hoffmann *et al*, 2002), *iκbα*$^{-/-}$*iκbβ*$^{-/-}$ (Hoffmann *et al*, 2002), *iκbβ*$^{-/-}$*iκbε*$^{-/-}$ (Hoffmann *et al*, 2002), *iκbα*$^{-/-}$*iκbβ*$^{-/-}$*iκbε*$^{-/-}$ (O'Dea *et al*, 2007), and p100/*nfkb2*$^{-/-}$ *(Hoffmann et al, 2003)*. IκBα (sc-371), IκBβ (sc-946), and actin (sc-1615) antibodies were provided by Santa Cruz Biotechnology. p100 C-terminal antisera was a generous gift from Nancy Rice (NIH). The cellular stimuli used were: recombinant murine TNF (Roche), LPS (Sigma, B5:055), and agonstic LTβR monoclonal antibody raised in AF.H6 hamster (generous gift from Jeff Browning, Biogen Inc.).

Computational Studies:

Description of the Computational Model

Two related models were constructed based upon the v2.1 modeling framework described in (Werner *et al*, 2005). Model v3.0 was constructed to discern the role of IκBδ negative feedback on NIK/IKK1 developmental stimulus and its effect on crosstalk from NEMO/IKK2 inflammatory stimulus (Basak *et al*, 2007). It contains *inputs* for both of the IKK signaling complexes (Table 5.4). Model v3.1 was constructed to discern the role of IκBδ negative feedback, in contrast to that of IκBα,

on NEMO/IKK2 inflammatory stimulus alone (Shih *et al*, 2009). It contains an *input* for NEMO/IKK2 (Table 5.5) and does not modulate NIK/IKK1 activity from its basal 1% activity level. Both models share the same set of molecular species and reactions and differ only in the rate constants values and the IKK activity profiles used as inputs. The models are comprised of 32 molecular species and 100 reactions that link NIK/IKK1 and NEMO/IKK2 activities (the *inputs*) to NF-κB nuclear localization (the *output*) as depicted graphically in Figure 4.2. The species of the models are listed in Table 5.1 and the reactions and parameters are listed in Table 5.3 and Table 5.2.

Computational Simulations

The ODEs were solved numerically using MATLAB versions R2006a and R2008a (The MathWorks, Inc.) with subroutine ode15s, a variable order, multi-step solver. Prior to stimulation, the system was allowed to equilibrate from starting conditions to a steady state, defined as showing no concentration changes greater than 1% over a period of 4000 minutes.

Table 5.1 Model v3.0/3.1 Species and Initial Concentrations

The model contains 32 species that represent the molecular species (mRNA and proteins) within the signaling module. Each species is given an initial concentration that is used as an input to the equilibrium (steady state) simulation. Species are localized to the cytoplasm or the nucleus. The initial concentrations of NF-κB, NEMO/IKK2, and NIK/IKK1 are set to 0.125, 0.1, and 0.1 μM, respectively, and are retained amongst free and bound complexes during all phases of the simulation.

	mRNA, Proteins and Protein Complexes	**Model Species**	**Initial μM**	**Location**
1	NEMO/IKK2	IKK2	0.1	Cytoplasm
2	NIK/IKK1	IKK1	0.1	Cytoplasm
3	NF-κB	NFkB	0.125	Cytoplasm
4	NF-κB	NFkBn	0	Nucleus
5	IκBα	IkBa	0	Cytoplasm
6	IκBα	IkBan	0	Nucleus
7	IκBβ	IkBb	0	Cytoplasm
8	IκBβ	IkBbn	0	Nucleus
9	IκBε	IkBe	0	Cytoplasm
10	IκBε	IkBen	0	Nucleus
11	IκBδ	IkBd	0	Cytoplasm
12	IκBδ	IkBdn	0	Nucleus
13	IκBα mRNA	IkBat	0	Cytoplasm
14	IκBβ mRNA	IkBbt	0	Cytoplasm
15	IκBε mRNA	IkBet	0	Cytoplasm
16	IκBδ mRNA	IkBdt	0	Cytoplasm
17	IKK2-IκBα	IKK2IkBa	0	Cytoplasm
18	IKK2-IκBβ	IKK2IkBb	0	Cytoplasm
19	IKK2-IκBε	IKK2IkBe	0	Cytoplasm
20	IKK1-IκBδ	IKK1IkBd	0	Cytoplasm
21	IκBα-NF-κB	IkBaNFkB	0	Cytoplasm
22	IκBα-NF-κB	IkBaNFkBn	0	Nucleus
23	IκBβ-NF-κB	IkBbNFkB	0	Cytoplasm
24	IκBβ-NF-κB	IkBbNFkBn	0	Nucleus
25	IκBε-NF-κB	IkBeNFkB	0	Cytoplasm
26	IκBε-NF-κB	IkBeNFkBn	0	Nucleus
27	IκBδ-NF-κB	IkBdNFkB	0	Cytoplasm
28	IκBδ-NF-κB	IkBdNFkBn	0	Nucleus
29	IKK2-IκBα-NF-κB	IKK2IkBaNFkB	0	Cytoplasm
30	IKK2-IκBβ-NF-κB	IKK2IkBbNFkB	0	Cytoplasm
31	IKK2-IκBε-NF-κB	IKK2IkBeNFkB	0	Cytoplasm
32	IKK1-IκBδ-NF-κB	IKK1IkBdNFkB	0	Cytoplasm

Table 5.2 Model v3.0 Reactions and Rate Constants

The model contains 98 reactions. Each reaction has a kinetic rate constant and is localized to either the cytoplasm (cyt) or nuclear (nuc) cellular compartments. The reactant or product 'null' represents a source (in the case of constitutive RNA synthesis) or a sink (in the case of RNA or protein degradation).

The transcription of IκBs is governed by multiple parameters and follows the form:

$$\frac{\mathbf{dmRNA}}{\mathbf{dt}} = \mathbf{k1 + k2^{*}\ NF\text{-}\kappa Bn^{H} - k3}$$

Where *k1* is the constitutive transcription rate, *k2* is the inducible transcription rate, *H* is the Hill Coefficient, and *k3* is the constitutive mRNA degradation rate.

Two assumptions were made to fit with experimental observations following LTβR stimulation: p100/IκBδ synthesis is diminished to account for p52 processing and nuclear IκB:NF-κB association rates are lowered to account for NF-κB post-translational modifications that affect canonical IκB binding. In modeling terms, following LTβR stimulation, the translation rate of p100/IκBδ and nuclear IκB:NF-κB association rates are divided by the fold NIK/IKK1 activity at that time point.

***Developmental IκBδ model (*Basak *et al.* 2007)**					
IκBα	**IκBβ**	**IκBε**	**IκBδ**	**Units**	**Description and Notes**
1.1848e-4	4.272e-5	6.1e-6	6.1e-6	min^{-1}	**Constitutive transcription** null => mRNA mRNA synthesis parameters were derived from mRNA and protein expression profiles measured by RPA and Western Blots in wild type and NF-κB-deficient cells
9.504	0.02	1.28	1.6	μM^{-2} min^{-1}	**Inducible transcription** null => mRNA *refer to Constitutive Transcription*
0	45	45	90	min^{-1}	**Inducible transcription delay** Component of the inducible transcription reaction that delays synthesis until this time point has been reached. Zero in equilibrium phase. Delays were measured via RPA as in (Kearns *et al*, 2006)
3	3	3	3	-	**Hill Coefficient** Component of the inducible transcription reaction that imparts cooperativity of NF-κB DNA binding and transactivation.

Table 5.2 Model v3.0 Reactions and Rate Constants, Continued.

0.0252	3.36e-3	6.72e-3	1.68e-3	min^{-1}	**mRNA degradation** mRNA => null (Werner *et al*, 2005) and estimation from RPA
0.2448	0.2448	0.2448	0.2448	min^{-1}	**Translation** mRNA => mRNA + IκB (Werner *et al*, 2005)
0.09	0.009	0.045	0.045	min^{-1}	**Free IκB Nuclear Import** IκB => IκBn (Werner *et al*, 2005)
0.012	0.012	0.012	0.012	min^{-1}	**Free IκB Nuclear Export** IκBn => IκB (Werner *et al*, 2005)
0.276	0.0276	0.138	0.276	min^{-1}	**IκB:NF-κB Nuclear Import** IκB:NF-κB => IκB:NF-κBn (Werner *et al*, 2005)
0.828	0.414	0.414	0.414	min^{-1}	**IκB:NF-κB Nuclear Export** IκB:NF-κBn => IκB:NF-κB (Werner *et al*, 2005)
IκB independent 5.4				min^{-1}	**NF-κB Nuclear Import** NF-κB => NF-κBn (Werner *et al*, 2005)
IκB independent 0.0048				min^{-1}	**NF-κB Nuclear Export** NF-κBn => NF-κB (Werner *et al*, 2005)
30	30	30	30	μM^{-1} min^{-1}	**IκB:NF-κB Association (cyt, nuc)** IκB + NF-κB => IκB:NF-κB (Werner *et al*, 2005)
6e-5	6e-5	6e-5	6e-5	min^{-1}	**IκB:NF-κB Dissociation (cyt, nuc)** IκB:NF-κB => IκB + NF-κB (Werner *et al*, 2005)
1.35	0.36	0.54	0	μM^{-1} min^{-1}	**IκB:IKK2 Association** IκB + IKK2 => IκB:IKK2 (Werner *et al*, 2005)
0.075	0.105	0.105	0	min^{-1}	**IκB:IKK2 Dissociation** IκB:IKK2 => IκB:IKK2 (Werner *et al*, 2005)
0	0	0	0.54	μM^{-1} min^{-1}	**IκB:IKK1 Association** IκB + IKK1 => IκB:IKK1 Assumed equal to canonical IκBs
0	0	0	0.105	min^{-1}	**IκB:IKK1 Dissociation** IκB:IKK1 => IκB:IKK1 Assumed equal to canonical IκBs
11.1	2.88	4.2	0	μM^{-1} min^{-1}	**IκB:NF-κB + IKK2 Association** IκB:NF-κB +IKK2 =>IκB:NF-κB:IKK2 (Werner *et al*, 2005)

Table 5.2 Model v3.0 Reactions and Rate Constants, Continued.

0	0	0	4.2	μM^{-1} min^{-1}	**IκB:NF-κB + IKK1 Association** IκB:NF-κB +IKK1 =>IκB:NF-κB:IKK1 Assumed equal to canonical IκBs
0.075	0.105	0.105	0	min^{-1}	**IκB:NF-κB + IKK2 Dissociation** IκB:NF-κB:IKK2 =>IκB:NF-κB+IKK2 (Werner *et al*, 2005)
0	0	0	0.105	min^{-1}	**IκB:NF-κB + IKK1 Dissociation** IκB:NF-κB:IKK1 =>IκB:NF-κB+IKK1 Assumed equal to canonical IκBs
30	30	30	0	μM^{-1} min^{-1}	**IκB:IKK2 + NF-κB Association** IκB:IKK2 +NF-κB =>IκB:NF-κB:IKK2 (Werner *et al*, 2005)
0	0	0	30	μM^{-1} min^{-1}	**IκB:IKK1 + NF-κB Association** IκB:IKK1 +NF-κB =>IκB:NF-κB:IKK1 Assumed equal to canonical IκBs
6e-5	6e-5	6e-5	0	μM^{-1} min^{-1}	**IκB:IKK2 + NF-κB Dissociation** IκB:IKK2:NF-κB =>IκB:IKK2 +NF-κB (Werner *et al*, 2005)
0	0	0	6e-5	μM^{-1} min^{-1}	**IκB:IKK1 + NF-κB Dissociation** IκB:IKK1:NF-κB =>IκB:IKK1 +NF-κB Assumed equal to canonical IκBs
0.12	0.18	0.18	0.12 cyt .18 nuc	min^{-1}	**Free IκB degradation (cyt, nuc)** IκB => null (Werner *et al*, 2005) IκBδ thought to have longer nuclear half-life than cytoplasmic.
6e-5	6e-5	6e-5	6e-5	min^{-1}	**Bound IκB degradation (cyt, nuc)** IκB:NF-κB => null + NF-κB (O'Dea *et al*, 2007) The IκBδ half-life was measured by quantitative Western Blot
1.8e-3	6e-4	1.2e-3	0	min^{-1}	**IKK2-mediated free IκB degradation** IκB:IKK2 => null + IKK2 (Werner *et al*, 2005)
0.36	0.12	0.18	0	min^{-1}	**IKK2-mediated bound IκB degradation** IκB:NF-κB:IKK2 => NF-κB + IKK2 (Werner *et al*, 2005)
0	0	0	1.2e-3	min^{-1}	**IKK1-mediated free IκB degradation** IκB:IKK1 => IKK1 Assumed equal to canonical IκBs
0	0	0	0.18	min^{-1}	**IKK1-mediated bound IκB degradation** IκB:NF-κB:IKK1 => NF-κB + IKK1 Assumed equal to canonical IκBs

Table 5.3 Model v3.1 Reactions and Rate Constants

The model contains 98 reactions. Each reaction has a kinetic rate constant and is localized to either the cytoplasm (cyt) or nuclear (nuc) cellular compartments. The reactant or product 'null' represents a source (in the case of constitutive RNA synthesis) or a sink (in the case of RNA or protein degradation).

The transcription of IκBs is governed by multiple parameters and follows the form:

$$\frac{\mathbf{dmRNA}}{\mathbf{dt}} = \mathbf{k1 + k2^{*}\ NF\text{-}\kappa B n^{H} - k3}$$

Where *k1* is the constitutive transcription rate, *k2* is the inducible transcription rate, *H* is the Hill Coefficient, and *k3* is the constitutive mRNA degradation rate.

***Inflammatory IκBδ model (*Shih *et al.* 2009)**					
IκBα	**IκBβ**	**IκBε**	**IκBδ**	**Units**	**Description and Notes**
2e-4	1e-5	3e-6	1e-7	min^{-1}	**Constitutive transcription** null => mRNA mRNA synthesis parameters were derived from mRNA and protein expression profiles measured by RPA and Western Blots in wild type and NF-κB-deficient cells
6	0.25	0.5	0.025	μM^{-2} min^{-1}	**Inducible transcription** null => mRNA *refer to Constitutive Transcription*
0	37	37	90	min^{-1}	**Inducible transcription delay** Component of the inducible transcription reaction that delays synthesis until this time point has been reached. Zero in equilibrium phase. Delays were measured via RPA as in (Kearns *et al*, 2006) and (Longo *et al*, in preparation)
3	3	3	3	-	**Hill Coefficient** Component of the inducible transcription reaction that imparts cooperativity of NF-κB DNA binding and transactivation.
0.035	3e-3	4e-3	2e-3	min^{-1}	**mRNA degradation** mRNA => null mRNA half-lives were determined by treating cells with Actinomycin-D and tracking the decay by RPA.
0.25	0.25	0.25	0.25	min^{-1}	**Translation** mRNA => mRNA + IκB (Werner *et al*, 2005)

Table 5.3 Model v3.1 Reactions and Rate Constants, Continued.

0.09	0.009	0.045	0.045	min^{-1}	**Free IκB Nuclear Import** IκB => IκBn (Werner *et al*, 2005)
0.012	0.012	0.012	0.012	min^{-1}	**Free IκB Nuclear Export** IκBn => IκB (Werner *et al*, 2005)
0.276	0.0276	0.138	0.276	min^{-1}	**IκB:NF-κB Nuclear Import** IκB:NF-κB => IκB:NF-κBn (Werner *et al*, 2005)
0.828	0.414	0.414	0.414	min^{-1}	**IκB:NF-κB Nuclear Export** IκB:NF-κBn => IκB:NF-κB (Werner *et al*, 2005)
IκB independent, 5.4				min^{-1}	**NF-κB Nuclear Import** NF-κB => NF-κBn (Werner *et al*, 2005)
IκB independent, 0.0048				min^{-1}	**NF-κB Nuclear Export** NF-κBn => NF-κB (Werner *et al*, 2005)
30	30	30	30	μM^{-1} min^{-1}	**IκB:NF-κB Association (cyt, nuc)** IκB + NF-κB => IκB:NF-κB (Werner *et al*, 2005)
6e-5	6e-5	6e-5	6e-5	min^{-1}	**IκB:NF-κB Dissociation (cyt, nuc)** IκB:NF-κB => IκB + NF-κB (Werner *et al*, 2005)
1.35	0.36	0.54	0	μM^{-1} min^{-1}	**IκB:IKK2 Association** IκB + IKK2 => IκB:IKK2 (Werner *et al*, 2005)
0.075	0.105	0.105	0	min^{-1}	**IκB:IKK2 Dissociation** IκB:IKK2 => IκB:IKK2 (Werner *et al*, 2005)
0	0	0	0.54	μM^{-1} min^{-1}	**IκB:IKK1 Association** IκB + IKK1 => IκB:IKK1 Assumed equal to canonical IκBs
0	0	0	0.105	min^{-1}	**IκB:IKK1 Dissociation** IκB:IKK1 => IκB:IKK1 Assumed equal to canonical IκBs
11.1	2.88	4.2	0	μM^{-1} min^{-1}	**IκB:NF-κB + IKK2 Association** IκB:NF-κB +IKK2 =>IκB:NF-κB:IKK2 (Werner *et al*, 2005)
0	0	0	4.2	μM^{-1} min^{-1}	**IκB:NF-κB + IKK1 Association** IκB:NF-κB +IKK1 =>IκB:NF-κB:IKK1 Assumed equal to canonical IκBs
0.075	0.105	0.105	0	min^{-1}	**IκB:NF-κB + IKK2 Dissociation** IκB:NF-κB:IKK2 =>IκB:NF-κB+IKK2 (Werner *et al*, 2005)

Table 5.3 Model v3.1 Reactions and Rate Constants, Continued.

0	0	0	0.105	min^{-1}	**IκB:NF-κB + IKK1 Dissociation** IκB:NF-κB:IKK1 =>IκB:NF-κB+IKK1 Assumed equal to canonical IκBs
30	30	30	0	μM^{-1} min^{-1}	**IκB:IKK2 + NF-κB Association** IκB:IKK2 +NF-κB =>IκB:NF-κB:IKK2 (Werner *et al*, 2005)
0	0	0	30	μM^{-1} min^{-1}	**IκB:IKK1 + NF-κB Association** IκB:IKK1 +NF-κB =>IκB:NF-κB:IKK1 Assumed equal to canonical IκBs
6e-5	6e-5	6e-5	0	μM^{-1} min^{-1}	**IκB:IKK2 + NF-κB Dissociation** IκB:IKK2:NF-κB =>IκB:IKK2 +NF-κB (Werner *et al*, 2005)
0	0	0	6e-5	μM^{-1} min^{-1}	**IκB:IKK1 + NF-κB Dissociation** IκB:IKK1:NF-κB =>IκB:IKK1 +NF-κB Assumed equal to canonical IκBs
0.12	0.18	0.18	1.4e-3	min^{-1}	**Free IκB degradation (cyt, nuc)** IκB => null (O'Dea *et al*, 2007) The IκBδ half-life was measured by quantitative Western Blot
6e-5	6e-5	6e-5	6e-5	min^{-1}	**Bound IκB degradation (cyt, nuc)** IκB:NF-κB => null + NF-κB (O'Dea *et al*, 2007) The IκBδ half-life was measured by quantitative Western Blot
1.8e-3	6e-4	1.2e-3	0	min^{-1}	**IKK2-mediated free IκB degradation** IκB:IKK2 => null + IKK2 (Werner *et al*, 2005)
0.36	0.12	0.18	0	min^{-1}	**IKK2-mediated bound IκB degradation** IκB:NF-κB:IKK2 => NF-κB + IKK2 (Werner *et al*, 2005)
0	0	0	1.2e-3	min^{-1}	**IKK1-mediated free IκB degradation** IκB:IKK1 => IKK1 Assumed equal to canonical IκBs
0	0	0	0.18	min^{-1}	**IKK1-mediated bound IκB degradation** IκB:NF-κB:IKK1 => NF-κB + IKK1 Assumed equal to canonical IκBs

Table 5.4 Model v3.0 NIK/IKK1 and NEMO/IKK2 Activity Profiles

IKK activity is defined by a numerical curve that correlates percent IKK activity (between 0 and 100%) with time. The NIK/IKK1 curves are based upon Western Blot analysis of NIK protein abundance in MEF cells following LTβR stimulation. The NEMO/IKK2 curves are based upon measurements performed in MEF cells via *in vitro* kinase assay, as in (Werner *et al*, 2005).

NIK/IKK1 (developmental)												
Basal only	**%**	1	1									
	Time (hr)	0	40									
LTβR starting at 20hr	**%**	1	1	1.2	1.4	1.9	2.4	2.6	2.6			
	Time (hr)	0	20	23	25	28	30	35	40			
LTβR	**%**	1	1.2	1.4	1.9	2.4	2.6	2.6	2.6			
	Time (hr)	0	3	5	8	10	15	20	40			

NEMO/IKK2 (inflammatory)												
Basal only	**%**	0.1	0.1									
	Time (hr)	0	40									
15' TNF pulse	**%**	0.1	60	100	65	50	36	21	16	10	0.1	0.1
	Time (min)	0	5	10	15	20	25	30	45	59	60	40 hr
45' LPS pulse	**%**	0.1	3	8	24	25	15	8	5	0.1	0.1	
	Time (min)	0	15	30	45	60	120	240	360	600	40 hr	

Table 5.5 Model v3.1 NIK/IKK1 and NEMO/IKK2 Activity Profiles

IKK activity is defined by a numerical curve that correlates percent IKK activity (between 0 and 100%) with time. The NIK/IKK1 activity is not modulated in this model and is left at a basal activity level for all simulations. The NEMO/IKK2 curves are based upon measurements performed in MEF cells via *in vitro* kinase assay, as in (Werner *et al*, 2005).

NIK/IKK1 (developmental)												
Basal only	**%**	1	1									
	Time (hr)	0	48									

NEMO/IKK2 (inflammatory)												
LPS chronic	**%**	1	2	4	12	8	8	5	5			
	Time (min)	0	10	15	60	90	120	24 hr	48 hr			

ACKNOWLEDGEMENTS

This chapter is adapted from two published research articles for which I am a co-author— IκBδ's role in developmental signaling (Basak *et al*, 2007) and in inflammatory signaling (Shih *et al*, 2009). Soumen Basak and Vincent Shih performed the experiments, wrote the manuscripts, and are the respective primary authors. I constructed the computational models and performed the simulations and also generated experimental reagents (probes used for RPA experiments). For the *Cell* manuscript, Hana Kim, Ellen O'Dea, Shannon Werner and professors Vinay Tergaonkar, Chris Benedict, Carl Ware, and Inder Verma provided experimental data, critical insights, and/or reagents. For the *PNAS* manuscript, Olga Savinova provided experimental data and Professor Gouri Ghosh provided insightful discussions. Professor Alexander Hoffmann is the corresponding author for both articles. The work presented in this chapter is not all inclusive of the findings of these research articles but rather describes only those findings that were informed through the computational modeling studies.

Chapter 6

IκBs as determinants of NF-κB dimer generation

ABSTRACT

The Nuclear Factor (NF) κB signaling pathway is central to a host of physiological responses and is controlled through a combinatorial and non-linear network of interactions. The primary NF-κB activator RelA is ubiquitously expressed as a homodimer and a RelA:p50 heterodimer. Four IκB isoforms are known to regulate RelA/NF-κB activities with different dynamics. Here we report computational modeling and experimental studies have delineated a novel function of IκBs as regulating the distribution of RelA dimers. We find that IκBβ preferentially stabilizes RelA homodimer. This stabilization is bidirectional, as cells deficient in RelA homodimer contain little IκBβ protein and cells that only express RelA homodimer contain IκBβ protein but are deficient in IκBα. Further, we find that IκBβ is required for efficient inflammatory activation of RelA homodimer. However, IκBβ does not regulate the dynamics of its post-induction repression.

INTRODUCTION

A series of mathematical models have been constructed to elucidate the stimulus-induced mechanisms regulating IκB proteins, and subsequently their control of NF-κB activity (Basak *et al*, 2007; Cheong *et al*, 2006; Hoffmann *et al*, 2002; Kearns *et al*, 2006; Krishna *et al*, 2006; Lipniacki *et al*, 2004; O'Dea *et al*, 2008; Shih *et al*, 2009; Werner *et al*, 2005). These models were critical for understanding the combinatorial roles IκBα, -ε, and -δ/p100 negative feedback mechanisms in regulating NF-κB transcriptional activity and complement experimental studies by providing analysis of emergent systems properties such as crosstalk and compensation effects (Kearns *et al*, 2009). More recently, modeling has examined the potent NF-κB regulation mediated by A20 deubiquitinase via its role in down-regulating signaling events upstream of NEMO-associated IKK2 that are proximal to the TNF receptor (Lipniacki *et al*, 2007; Werner *et al*, 2008). However, as constructed, these models are insufficient to explain homeostatic or stimulus-induced variability in the composition of the NF-κB dimer pool because they contain a singular NF-κB dimer, ostensibly the RelA:p50 heterodimer, whose concentration is defined as invariant.

NF-κB comprises fifteen observed hetero- and homo-dimeric associations of five NF-κB monomeric subunits—RelA/p65, RelB, cRel, p50, and p52—that regulate distinct but overlapping sets of genes (Hoffmann *et al*, 2006b). In the murine embryonic fibroblast (MEF) treated with an inflammatory stimulus, the representative cell type and condition from which the mathematical models have been derived, the predominantly expressed dimer is RelA:p50. This simplification enabled early

modeling efforts but does not account for the generation and function of other NF-κB dimers that are important for signaling in different cell types and/or conditions (Basak *et al*, 2008b). For example, developmental stimuli that activate the non-canonical NIK/IKK1 signaling axis drive RelB/NF-κB dimer activity in lymphocytes that is not subject to inhibition by the classical IκBα and IκBε negative feedback but rather IκBδ/p100 feedback (Solan *et al*, 2002). Further, the transcriptional syntheses of RelB, cRel, p105/p50, and p100/p52 are themselves positively regulated by RelA/NF-κB dimers that subsequently drive dynamic changes to the NF-κB dimer pool in response to stimuli (Basak *et al*, 2008b; Hoffmann *et al*, 2006b). The combinatorial complexity within the NF-κB signaling network—five IκB proteins, five NF-κB monomers, up to fifteen observed NF-κB dimers, and two stimulus-responsive IKK complexes—has been studied at the level of IKK (*system driver*) and IκB (*inhibitor*) dynamics, but less is known of the mechanisms controlling NF-κB dimer (*activator*) formation and activation (Basak *et al*, 2008b).

As an initial step towards understanding how dimer generation can affect the ability of the NF-κB system to respond to stimuli, we performed an integrated study utilizing mathematical modeling and experimental methodologies that focused on the generation and activation of the RelA dimers, RelA:p50 and RelA:RelA.

First, we developed a theoretical model to discern how NF-κB dimerization and IκB:NF-κB association kinetics can function to modulate the composition of the dimer pool in resting cells. Second, using the findings of this theoretical model together with an experimental finding that IκBβ expression, but not IκBα, is critically dependent upon RelA/NF-κB dimers as a motivation, we incorporated the NF-κB

stability model into the previously constructed IκB models. This experimentally validated model was used to examine the mechanisms that alter the homeostatic distribution and stimulus-responsive dynamics of RelA/NF-κB dimers.

RESULTS

Construction of a Multiple NF-κB Dimer Computational Model

A new computational model was constructed to address the homeostatic mechanisms that regulate NF-κB dimers—specifically the hetero- and homo-dimeric associations of RelA and p50 that comprise the bulk of the NF-κB dimer pool in MEFs. The model simulates synthesis of the three resulting dimers— RelA:RelA (A:A), RelA:p50 (A:50), and p50:p50 (50:50)—via sets of reactions that include a combined transcription/translation reaction and association/dissociation of monomeric subunits. A wiring diagram of this process consists of five molecular species and thirteen reactions that follow the principles of mass action kinetics (Figure 6.1A). The reaction rate constants are denoted symbolically as being (m) monomer-, or (d) dimer-specific.

The wiring diagram was used to write a set of five ordinary differential equations (ODE) that form the basis of the computational model. Each ODE calculates the steady-state abundance of one molecular species present in the model. Syntheses of RelA and p50 monomers (*A* and *50*, respectively) are treated as single-step reactions in which all biochemical mechanisms between initiation of transcription and cytoplasmic localization of protein are combined. Both NF-κB proteins are subject to constitutive synthesis (m1, m2) to produce protein that is then subject to a degradation reaction (m3, m4). The protein monomers combinatorially associate to form three NF-κB dimers through reversible reactions (d1-6). Both monomer and dimer proteins are subject to constitutive degradation (m7-8, d7-9).

While the set of ODEs describe the topology of the model, the parameters (rate constants) define this connectivity quantitatively. The full complement of reactions and rate constants are listed in the Supplementary Materials. Of note, key assumptions were made to inform the selection of parameter values. (i) NF-κB dimers proteolytically degrade via a ubiquitin proteasome dependent mechanism but with slow kinetics (Maine *et al*, 2007) (ii) Free NF-κB monomers are inherently unstable relative to NF-κB dimers as experiments using dimerization-deficient monomers show severely reduced monomer abundance (G. Ghosh, personal communication). (iii) Based upon analytical ultracentrifugation experiments, A:50 dimer has an 8x and 33x stronger affinity vs. 50:50 and A:A dimers, respectively (G. Ghosh, personal communication).

The model was simulated using MATLAB R2009a (The Mathworks, Inc.) to calculate the steady-state abundances of monomers and dimers. Keeping the ratio between dimer affinities fixed, the K_d of A:50 dimer was modulated between 10uM and 10pM to calculate the effect on monomer and dimer generation (Figure 6.1B). This same simulation data is also represented as color plots (Figure 6.1C). These simulations predict that the generations of both A:50 and A:A dimers to physiological levels requires nanomolar to sub-nanomolar affinities, respectively.

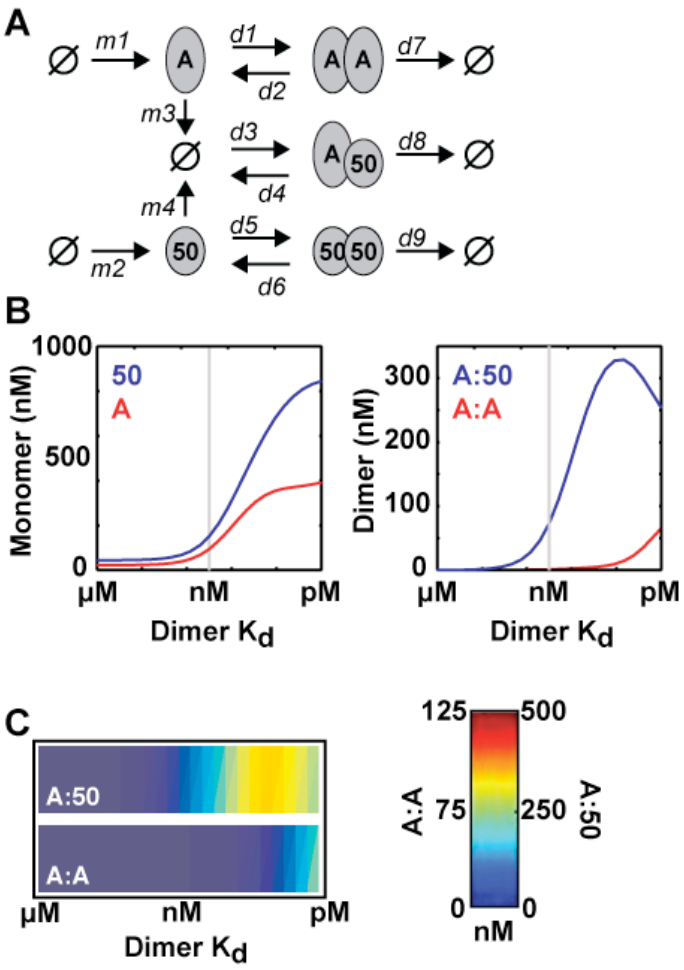

Figure 6.1 Construction of a multiple RelA/NF-κB Model

A. Wiring schematic for a computational model that simulates the generation of NF-κB dimers from RelA (A) and p50 (50) monomeric subunits. The model uses Mass Action kinetics, written as ordinary differential equations (ODEs), to simulate the equilibrium abundances of protein monomers and dimers. Rate constants governing each reaction are denoted symbolically as being (m)onomer- or (d)imer-specific.
B. The model was simulated with a range of dimer affinities to calculate the abundances of monomer and RelA-containing dimers. The association rate constants (d1, d3, d5) were held constant while the dissociation rate constants (d2, d4, d6) were modulated to satisfy the equilibrium dissociation constant expression $K_d = k_{off}/k_{on}$. Analytical ultracentrifugation data (G Ghosh, UCSD) was used to determine the ratio of dimer affinities such that A:50 K_d = 1/8 50:50 K_d = 1/33 A:A K_d. The X-axis scale denotes the A:50 K_d.
C. Color plot representation of the dimer abundances shown in (B) where blue and red denote low and high abundances, respectively. A:A and A:50 are plotted on separate color scales as shown on the color bar (right).

IκB Proteins Regulate the Generation of NF-κB Dimers

In the resting cell, NF-κB dimers are primarily localized to the cytoplasm via stoichiometric associations with IκB proteins. This interaction is known to stabilize IκB proteins (Mathes *et al*, 2008; O'Dea *et al*, 2007). To determine whether and to what degree IκB proteins can likewise affect the composition of the NF-κB dimer pool, the computational model was expanded to include association with a generic IκB (Figure 6.2A). In this expanded model, IκB is constitutively synthesized and degraded and reversibly associates with A:A and A:50 NF-κB dimers. IκBs have weak affinity to p50:p50 homodimer and thus these interaction reactions were excluded from the model (Ishikawa *et al*, 1998). Dimer and IκB can individually degrade while in the complex. The dissociation of dimer into monomers is not allowed while complexed to IκB as the IκB strongly associates along the monomer-monomer interface (Huxford *et al*, 1998). Thus, the function of IκB in this model is solely to inhibit dissociation of monomers from the dimer, but not to inhibit the degradation of the dimer.

Repeated simulations with a range of IκB:dimer affinities (1 uM … 1 nM … 1pM) were used to ascertain whether IκB can stabilize NF-κB dimer (Figure 6.2B). Indeed, the abundances of both NF-κB dimers are increased as a function of the IκB:dimer affinity. These simulations are also in line with previously published results (Mathes *et al*, 2008; O'Dea *et al*, 2007) that show experimentally that NF-κB dimers stabilize IκB proteins via direct protein interactions. This co-stabilization effect is also apparent in simulations in which the IκB:dimer and dimer affinities were modulated concomitantly (Figure 6.2C). Further, a model system in which IκB abundance is

invariant confirms that this IκB-induced stabilization of NF-κB dimers is independent of continued IκB synthesis (Figure 6.2D).

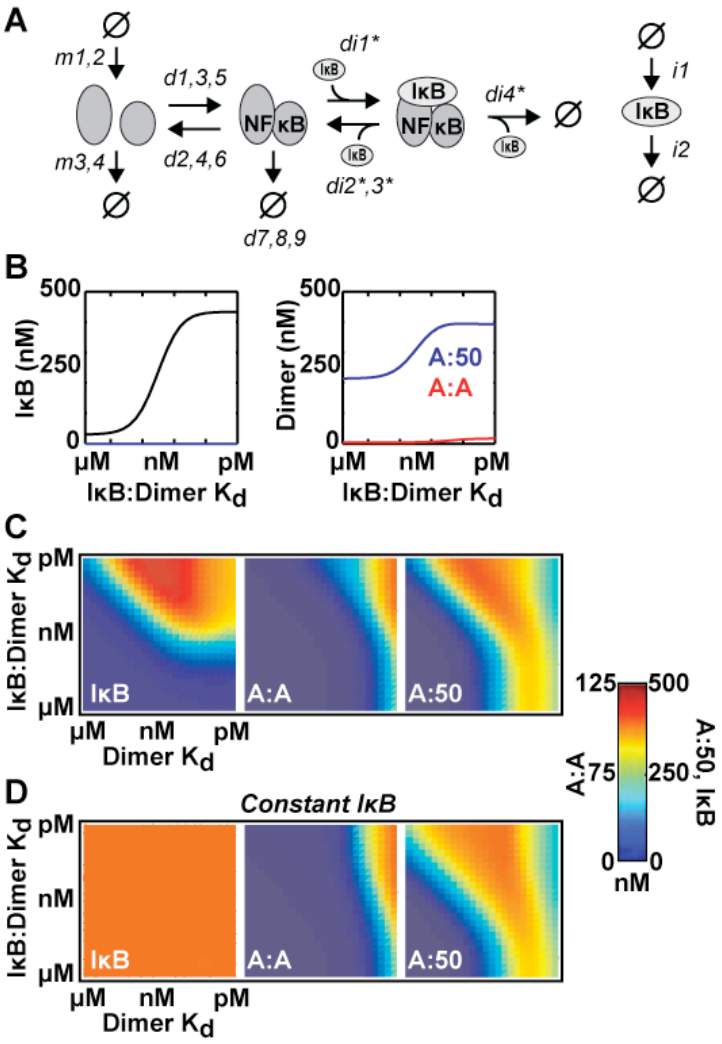

Figure 6.2 IκB and NF-κB proteins provide mutual stabilization

A. Wiring schematic for an expanded version of the computational model described in Figure 6.1A which includes synthesis and degradation of two IκB proteins and their interactions with RelA/NF-κB dimers. IκB-specific and IκB:dimer-specific rate constants are denoted with the prefixes ‘i’ and ‘di’, respectively. Asterisks indicate rate constants that have different values for each IκB:NF-κB complex.
B. The model was simulated with a range of IκB:NF-κB affinities to calculate the abundances of both IκB and the A:A and A:50 dimers.
C. IκB and dimer abundances were calculated in repeated simulations in which both the IκB:NF-κB and dimer affinities were modulated simultaneously. Abundances are represented in color plots.
D. Simulations were performed as in (C), but with IκB set to a constant abundance of 400 nM. IκB synthesis and degradation reactions were disabled.

IκB Proteins Require Specific NF-κB Dimers for Protein Stability

We next performed experiments to test whether the *in silico* prediction of a IκB:NF-κB costabilization relationship also exists in cells. First, motivated by earlier studies that observed the NF-κB-induced IκB stabilization component of this relationship (Mathes *et al*, 2008; O'Dea *et al*, 2007), we asked whether dimers differentially stabilize IκBs. There are two predominant NF-κB dimers observable by EMSA in unstimulated wild type MEF, RelA homodimer (A:A) and RelA:p50 heterodimer (A:50)(Figure 6.3A). Further, there are two predominant IκB proteins, IκBα and IκBβ. Measurement of IκBα and IκBβ abundances in wild type versus RelA-deficient cells recapitulated earlier findings that IκB expression is dependent upon NF-κB dimers (Mathes *et al*, 2008; O'Dea *et al*, 2007), but also revealed that the loss of the RelA monomeric subunit differentially affects these IκB isoforms (Figure 6.3B). While the abundance of IκBα is slightly reduced in *rela*$^{-/-}$ cells, IκBβ is reduced below the detection limit. The rich degree of combinatorial complexity within the IκB:NF-κB signaling pathway allows for compensation effects upon knockout or knock-down of system components (Basak *et al*, 2008b; Hoffmann *et al*, 2003; O'Dea *et al*, 2007). It was observed that *rela*$^{-/-}$ MEF contain an increased level of cRel:p50 dimer (Hoffmann *et al*, 2003) which can explain the remaining IκBα in these cells (Figure 6.3B).

We wanted to determine whether the reduction in IκBβ protein observed in RelA deficient cells was a consequence of protein synthesis or degradation kinetics. Consistent with the literature, MEFs deficient in the three canonical NF-κB monomer isoforms have severely reduced IκB protein levels (Figure 6.3C, middle) that are not associated with a similar decrease in mRNA levels (data not shown) and thus suggest

that homeostatic expression of IκBs is strongly modulated at the level of protein stability. This led us to question that if the abundance of IκBβ is modulated by its interaction with NF-κB, is its reduction in RelA deficient cells due to the loss of all RelA-containing dimers or a specific RelA/NF-κB dimer?

To remove any such compensation effects, a cell line was generated that contains only the RelA NF-κB monomer via genetic deletion of the remaining four subunits (*relb*$^{-/-}$*nfkb2*$^{-/-}$*nfkb1*$^{-/-}$*crel*$^{-/-}$). These cells contain only A:A dimer and, surprisingly, retain IκBβ expression while showing a severely reduced IκBα abundance (Figure 6.3C). This effect is not correlated with a significant change in RelA abundance, as the quadruple NF-κB knockouts maintain a similar, if not slightly reduced, level of RelA protein versus wild type (Figure 6.3D). Taken together, these results led us to conclude that the reduction of IκBβ in RelA deficient MEF is due to the specific loss of the RelA homodimer and not the loss of all RelA/NF-κB dimers as previously reported (Hertlein *et al*, 2005).

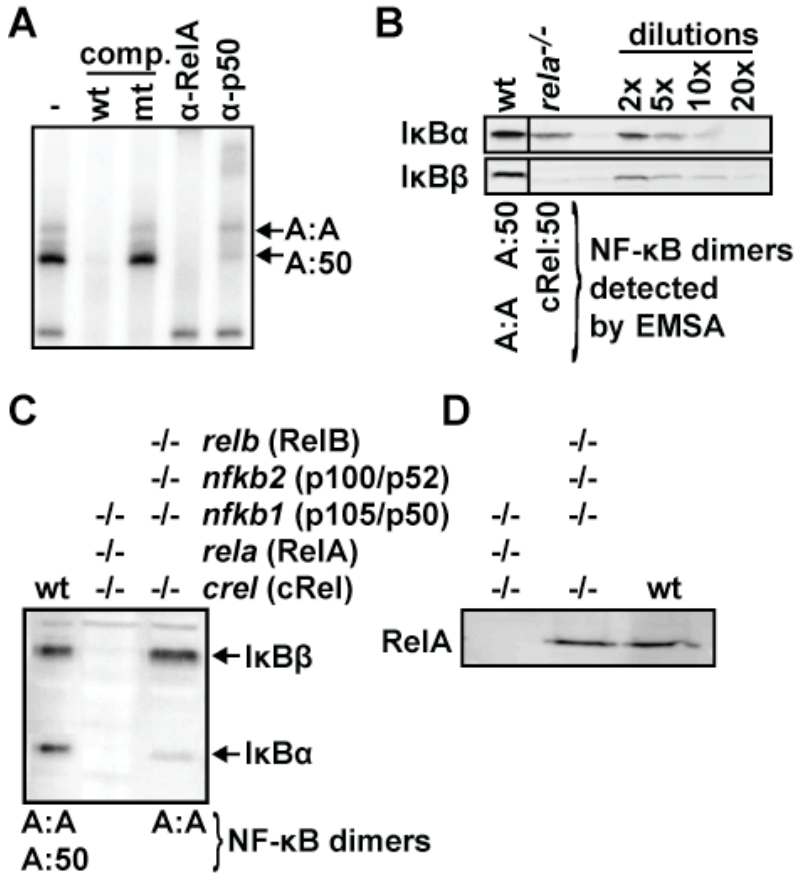

Figure 6.3 IκB proteins require specific NF-κB dimers for protein stability

A. NF-κB oligo-binding activity was measured by EMSA with wild type extracts. NF-κB-specific bands were revealed via competition assays with unlabeled/cold wild type (wt) and mutant (mt) oligos. Antibody supershifts revealed the primary NF-κB dimers to be RelA:RelA homodimer (A:A) and RelA:p50 heterodimer (A:50).
B. IκB protein levels were measured by Western blot in unstimulated wildtype of RelA-deficient cells. Dilutions of wild-type lysate are shown (right). The primary NF-κB dimers present in each cell-type were ascertained by EMSA (Hoffmann *et al*, 2003).
C. IκBα and IκBβ protein levels were measured by Western blot of wild type, cRel/RelA/p50-deficient, and cRel/p50/p52/RelB-deficient cells. The primary NF-κB dimers present in each cell-type are denoted.
D. RelA protein abundance was measured by Western blot as in (C).

IκB Interaction Specificities Can Regulate the Generation of NF-κB Dimers

We next sought to explore the reverse of the previous finding: do IκB proteins stabilize NF-κB dimers and do IκB isoforms provide dimer-specific stabilization? The model was expanded to include 2 IκB isoforms, now denoted IκBα and IκBβ, with equivalent rate constants. To enable direct comparison to the previous modeling results (Figure 6.2), the synthesis rates of both IκBs were set to 0.5x of the rate in the previous single IκB model. As a confirmation that the 2-IκB system behaves similarly, simulations were performed as in Figure 6.2B and C and the results reveal an identical NF-κB and IκB costabilization relationship (Figure 6.4A, B).

The IκB:dimer affinity rates were then adjusted to recapitulate the experimental observations that expression of IκBβ requires A:A dimer and that IκBα is severely reduced in the RelA-only cell line. Using the binding curves as a guide (Figure 6.4A), IκBβ was given a saturating 20pM K_d for A:A dimer and sub-saturating 200nM K_d for A:50 dimer. IκBα was given a sub-saturating 200nM K_d for A:A, while its affinity for A:50 was allowed to vary. Under this preferential IκBβ:A:A affinity scenario, A:A dimer was stabilized at nanomolar dimer affinity vs. picomolar in the non-preferential scenario (Figure 6.4C, D). The distribution of RelA into A:50 dimer was restored as the IκBα:A:50 interaction affinity was increased, as in the early results. These modeling simulations provide a simple mechanism through which IκBs can both stabilize dimers and alter the composition of the dimer pool.

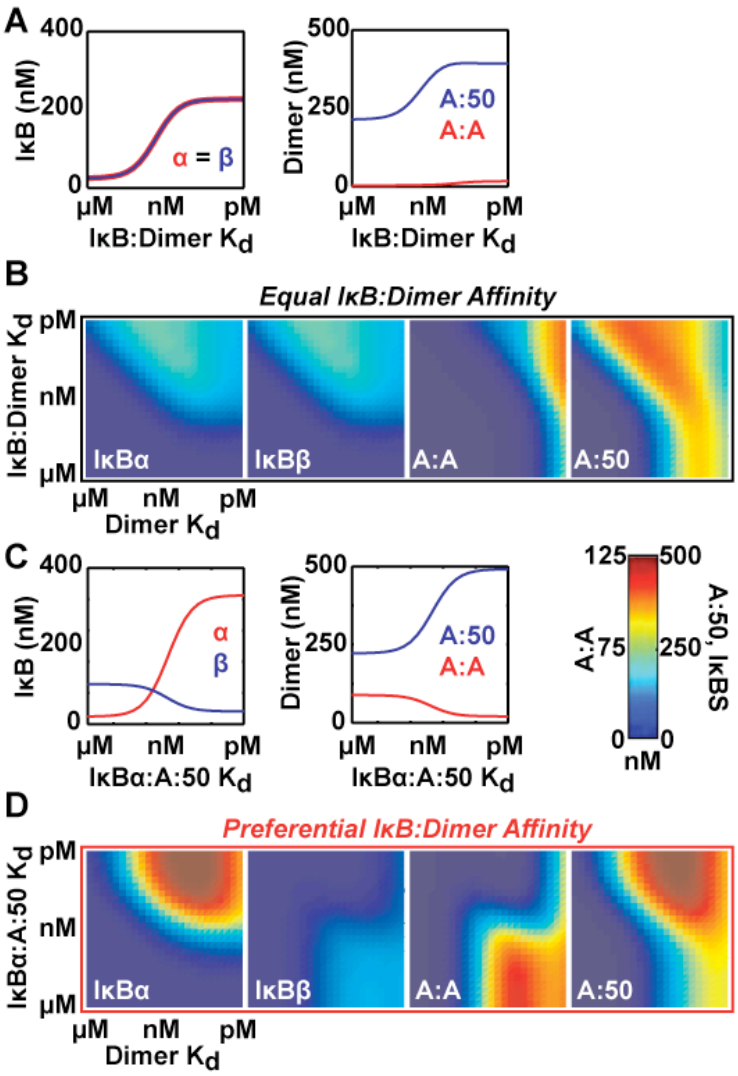

Figure 6.4 IκBs can regulate NF-κB dimer generation

A. The model was simulated with a range of IκB:NF-κB affinities to calculate the abundances of both IκBs and the A:A and A:50 dimers. IκBα and IκBβ have equivalent rate constants and thus behave identically.
B. IκB and dimer abundances were calculated in repeated simulations in which both the IκB:NF-κB and dimer affinities were modulated simultaneously. Abundances are represented in color plots.
C. Simulations were performed as in (A), but only the IκBα:A:50 K_d was varied. Using the binding curve data in (A), IκBβ:A:A was set to a saturating K_d (10pM) and IκBβ:A:50 and IκBα:A:A were set to a sub-saturing K_d (100nM).
D. Simulations were performed as in (B) using the IκB:Dimer affinities listed in (C).

Construction and Validation of a Combinatorial IκB:NF-κB Model

The NF-κB module, as described, simulates homeostatic distributions of IκBs and NF-κB dimers, but does not account for signaling dynamics and nucleo-cytoplasmic localization. The NF-κB module was interconnected with the previously modeled IκB signaling module to construct a new model capable of simulating stimulus-induced dynamics as well as the homeostatic state (Figure 6.5A). The *input* to the model is NEMO/IKK2 activity, represented by a numerical curve derived from the quantitation of experimental IKK kinase assay data (Werner *et al*, 2005), and the *outputs* are the temporal profiles of nuclear-localized, free NF-κB dimers. Using the principles of mass action kinetics, ordinary differential equations were written to account for synthesis, degradation, and localization, of IκB and NF-κB mRNA, protein, and protein complexes (Table 6.2).

The model was parameterized by selecting some rate constant values from the literature and determining others by experiment. For the selection of the remaining unknown parameters, such as the mRNA synthesis rates, a set of experimentally derived constraints was used to inform several rounds of computational parameter fitting/estimation (Table 6.6).

For further parameterization, the abundances of IκB and NF-κB monomers were quantitated by Western Blot using standard curves of respective recombinant protein. A representative example is shown for RelA protein (Figure 6.5B). Absolute molecule numbers were derived for each IκB and RelA within an estimated 25% error (Figure 6.5C). As a means of validation, the model was used to calculate the basal

abundances of IκB and NF-κB proteins (Figure 6.5D). The measured abundances are accounted for by the simulation results. As the model contains only two NF-κB dimers, a doubly p50- and IκBδ-deficient model system is comparable to the quadruple NF-κB knockout (*relb*$^{-/-}$*nfkb2*$^{-/-}$*nfkb1*$^{-/-}$*crel*$^{-/-}$) containing only RelA shown in Figure 6.3C. Importantly, simulation of this model reveals IκBα, IκBβ, and RelA protein levels that are comparable to the *in vitro* results.

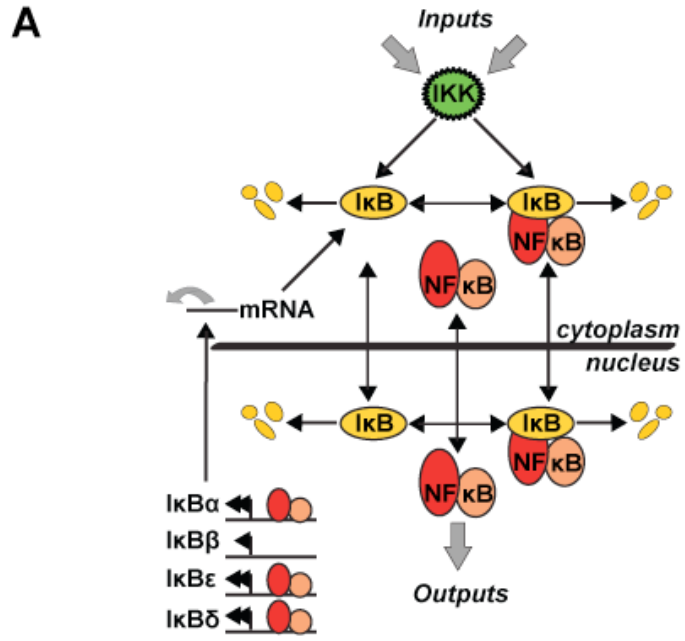

Figure 6.5 Construction and validation of a IκB:multi-dimer computational model

A. Wiring schematic for a computational model that contains 2 NF-κB monomers (p50 and RelA), 3 NF-κB dimers (RelA:RelA A:A, RelA:p50 A:50, and p50:p50), and 4 IκB proteins (IκBα, β, ε, and δ). The model uses Mass Action kinetics, written as ODEs, to calculate synthesis, degradation, localization, and protein:protein interaction reactions for each IκB and NF-κB. The *input* to the model is a numerical NEMO/IKK2 activity curve that corresponds to *in vitro* Kinase assay experiments (Werner Science 2005). NIK/IKK1 complex is contained within the model to drive IκBδ degradation, but has a constant, basal 1% activity. The *outputs* of the model are free NF-κB dimers in the nucleus. The model contains NF-κB and IκB isoform-specific reactions, but for simplicity the wiring diagram depicts a singular IκB and NF-κB species.

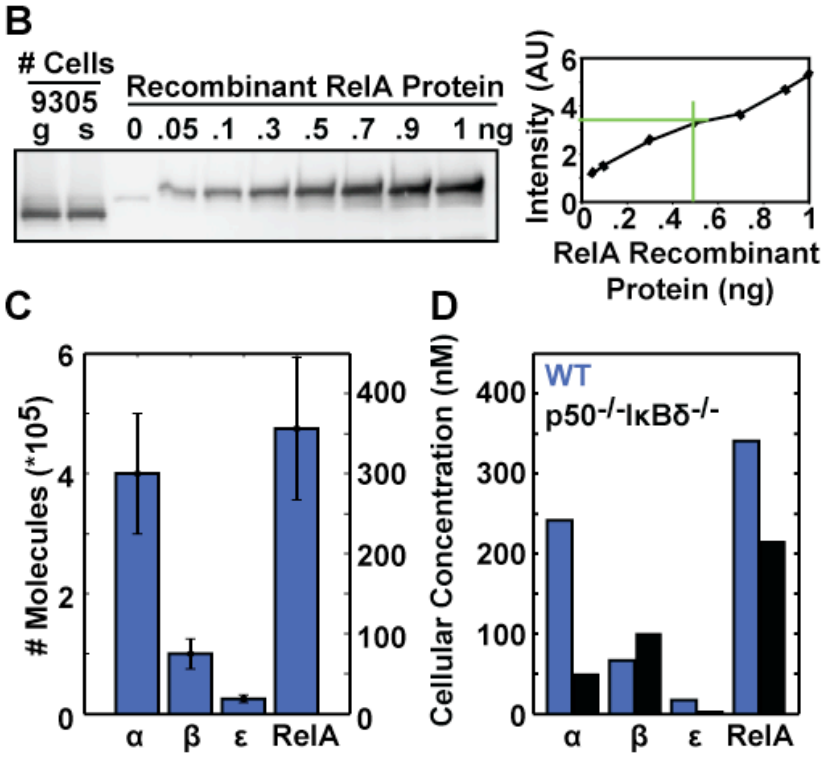

Figure 6.5 Construction and validation of a IκB:multi-dimer computational model, Continued.

B. To constrain the selection of model rate constant values, the cellular abundances of each IκB and NF-κB monomer were measured by Western Blot of wild type cells with standard curves of recombinant protein. Shown is a representative sample for the RelA Western blot and quantitation to determine the amount (ng) of RelA present in each cell. An equal number of cells from growing (g) and confluent-starved (s) plates were used to show that the abundance of protein does not vary between these conditions.
C. The measured amounts of each protein as measured in (B) were converted to # molecules via their respective molecular weights. These numbers were converted to concentrations (nM) by using the average volume of the fibroblast cell (2.2pL). Error bars represent an estimated 25% measurement error.
D. Results of simulations reveal that the model generates protein concentrations in the ranges defined in (C). Simulation of a model system deficient in p50 and IκBδ is comparable to *in vitro* results shown in Figure 6.3.

Simulations Predict that IκBβ Preferentially Stabilizes RelA Homodimer

The multi-dimer model was constructed to recapitulate the observed dependency of IκBβ protein stability on the RelA homodimer. We then used the model to explore the distribution of RelA-containing dimers in IκB-deficient model systems (Figure 6.6A). The simulations predicted that an IκBβ-deficient system has NF-κB dimer-specific effects. The abundance of A:A dimer is halved, suggesting a co-stabilization relationship between IκBβ and A:A. Further, A:50 abundance is increased due to elevated availability of RelA monomer that would have been sequestered as A:A dimer.

To test experimentally whether A:A dimer is primarily associated with IκBβ, cellular MEF extracts were assayed by EMSA following treatment with the detergent deoxycholate (DOC), which disrupts the IκB:NF-κB interaction and reveals total (latent) NF-κB dimers (Figure 6.6B). These results show that IκBβ deficiency significantly affects A:A abundance in a manner that is disproportional to the cellular abundance of IκBβ vs. IκBα. Further, immunodepletion of these extracts with IκB antibodies before addition of DOC revealed that the bulk of A:A dimer is associated with IκBβ (Figure 6.6C). Together, these simulations and experiments suggest a codependency between the induced stabilities of IκBβ and RelA homodimer.

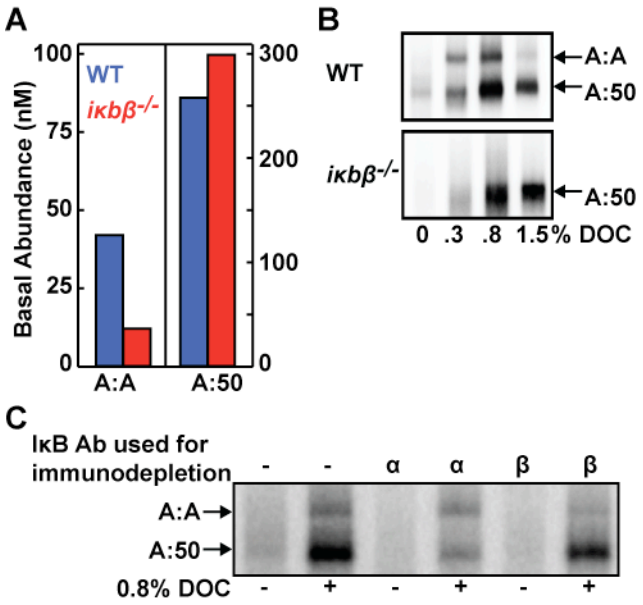

Figure 6.6 Simulations predict that IκBβ preferentially stabilizes RelA homodimer

A. Simulations of A:A and A:50 equilibrium concentrations in wild type and IκBβ-deficient model systems.
B. A:A and A:50 abundances were measured in cytoplasmic extracts from wild-type and IκBβ-deficient cells using a titration of the detergent deoxycholate (DOC) to disrupt the IκB:NF-κB interaction.
C. Wild-type cytoplasmic extracts were immunodepleted with IκBα, β, or ε antibody to remove free and NF-κB-bound IκB and treated with DOC to reveal the amount of A:A and A:50 dimers remaining.

IκBβ Selectively Regulates Activation, but not Dynamics, of RelA/NF-κB Dimers

To computationally probe the functional relevancy of the IκBβ:A:A costabilization relationship, a wild type system was simulated with a NEMO/IKK2 activity approximating chronic stimulation with the inflammatory TNF cytokine. IκBβ, unlike the other IκBs, is distinct in that its mRNA synthesis is not inducible by NF-κB activity and therefore IκBβ does not provide negative feedback.

Peak activities for A:A and A:50 dimers in the first hour are 14 and 148 nM, respectively (Figure 6.7A). A model system deficient in both IκBα and IκBε reduces both A:A and A:50 activities while a IκBβ-deficient model imparts specific regulation-- A:A activity is halved while A:50 activity is increased 24%. A p50-deficient system is used as a positive control and simulates 2-fold higher A:A activity. Together, these results predict that IκBβ differentially regulates the initial activation of specific RelA-containing dimers while IκBα and IκBε do not provide for this selectivity. This result is confirmed experimentally. Nuclear extracts from these cell-types were obtained after 30 min of TNF stimulation and assayed by EMSA (Figure 6.7B). Supershifts with RelA and p50 antibodies were used to reveal the activities of A:A and A:50 dimers.

We next used the model to determine whether IκBβ also provides dynamic regulation. A:A and A:50 were calculated in wild type, IκBα-deficient, and IκBβ-deficient cells during chronic TNF stimulation (Figure 6.7C). This revealed that IκBβ does not in fact regulate the post-induction dynamics of activity for either dimer. The temporal profiles of A:A and A:50 are preserved in the IκBβ-deficient system while the IκBα-deficient system shows dysregulation of both of these activities. While IκBβ

has preferential affinity for A:A, the inducible synthesis of IκBα that constitutes the primary negative feedback mechanism in the pathway produces sufficient IκBα protein to regulate the dynamics of the A:A dimer. These predictions are confirmed by experimental measurements A:A and A:50 activities in these cell types during chronic TNF stimulation (Figure 6.7D).

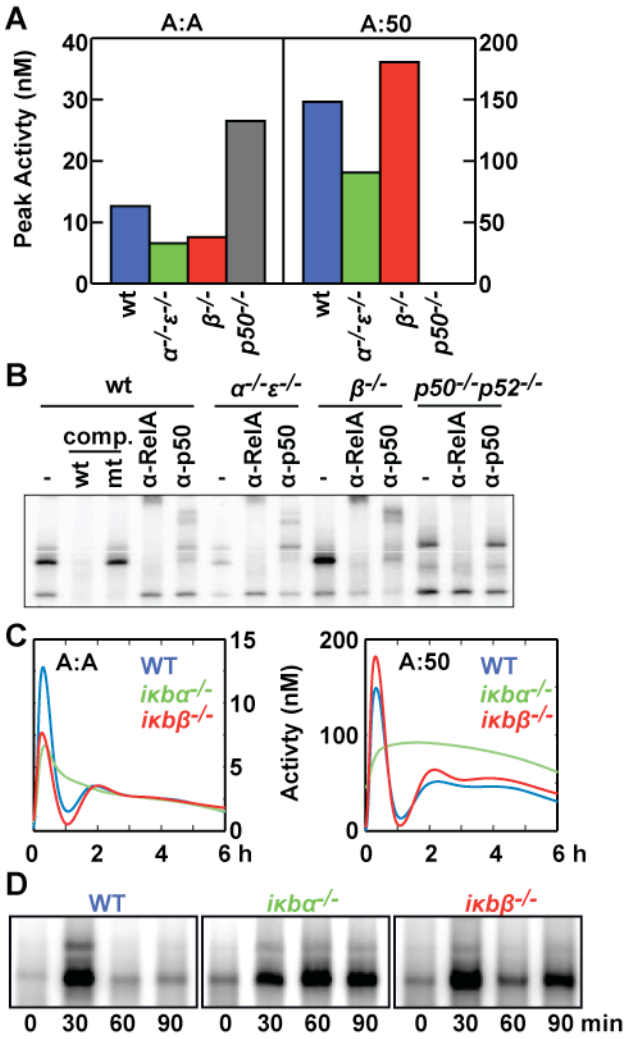

Figure 6.7 IκBβ is required for TNF-induced RelA homodimer activity, but does not regulate its dynamics

A. Wild type, IκBα/IκBε-, IκBβ-, and p50-deficient model systems were simulated with chronic TNF stimulation and the peaks of activity for A:A and A:50 in the first hour were recorded.
B. EMSA of nuclear extracts harvested at 30 min following cellular stimulation with 1ng/mL TNF of the denoted cell types. Oligo competition was performed with cold wild type (κB-site containint) and mutant probes to show specificity of the NF-κB:oligo binding. RelA and p50 antibodies were used to identify the composition of each NF-κB-bound oligo band.
C. Simulations of A:A and A:50 activity in wild-\ type, IκBα-deficient, and IκBβ-deficient model systems chronically stimulated with TNF.
D. A:A and A:50 activity measured by EMSA in chronically stimulated cells.

DISCUSSION

NF-κB transcription factors regulate distinct gene expression programs involving hundreds of genes in response to an expansive set of distinct cellular stresses and stimuli. NF-κB dimers are activated from a latent, IκB-bound, pool in the cytosol and the mechanisms that regulate their stimulus-induced dynamics are well studied and include temporal profiles of IKK activity, combinatorial negative feedback control by IκB proteins, and other regulatory mechanisms upstream of the IKK-NF-κB-IκB signaling module. Here, we utilized an integrated computational and experimental approach to discern the less well-understood mechanisms that regulate the abundance and distribution of NF-κB dimers in the latent pool.

The RelA/NF-κB dimers, RelA:p50 and RelA:RelA, represent the predominant fraction of NF-κB proteins within the MEF cell type and exploring their generation was therefore an attractive initial step towards addressing the combinatorial NF-κB dimer complexity. We took a stepwise approach in model construction. First, a computational model was constructed to simulate dimer formation as a function of monomer synthesis, degradation, and interaction. This model was analyzed using a range of values for dimer affinity rate constants to show the degrees to which dimer abundances are affected. IκB proteins were then added to this model and functioned in the experimentally-derived capacity to prevent dissociation of NF-κB monomers. Simulations of this model using ranges of IκB affinities revealed that this simple mode of action is sufficient to create a co-stabilization relationship in which the association of IκB and NF-κB proteins provides for mutual protein stabilization over several

orders of magnitude. Further simulation of the model with preferential binding specificities for certain IκBs and dimers demonstrated how differences in simple binding kinetics could substantially alter the distribution of NF-κB dimers. As NF-κB transcriptional activity is weak in resting cells, inducible expression of the IκB proteins that stabilize NF-κB is negligible, and therefore these findings suggest that protein stability and not protein synthesis is the prime determinant of the composition of the latent RelA/NF-κB dimer pool. Interestingly, this is in direct contrast to published results concerning RelB/NF-κB dimers in which stimulus-responsive RelA/NF-κB activity is required to induce synthesis of RelB monomer which then form RelB dimers (Basak *et al*, 2008b; Bren *et al*, 2001).

To translate these computational findings to a cell system, the NF-κB dimer model was coupled to the previously described IκB models (Kearns *et al*, 2009). This new model is capable of simulating the combinatorial interactions of four IκB proteins with two NF-κB dimers and is driven via a numerically-defined temporal profile of inflammatory NEMO/IKK2 activity. Results of these simulations were directly compared to experimental measurements in MEF cells to find that a co-stabilization relationship exists between IκBβ and RelA homodimer that allows for stable formation of RelA homodimer in resting cells. This finding was made possible via the novel generation of a novel MEF cell line, deficient in four of five NF-κB monomers (*relb*$^{-/-}$*nfkb2*$^{-/-}$*nfkb1*$^{-/-}$*crel*$^{-/-}$), that contains only RelA monomer. As the combinatorial nature of the NF-κB system ensures that a genetic knock-down or knock-out of an NF-κB monomer will be compensated for by the remaining monomers (Hoffmann *et al*, 2003), this is the first report to overcome this limitation. Future studies that aim to

elucidate the *in vivo* interaction specificities between specific NF-κB dimers and their IκB regulators via analysis of single or even double NF-κB knockout cells must delineate which findings are real and which are simply compensation artifacts.

While interaction specificities between IκB and RelA/NF-κB proteins regulate the distribution of NF-κB dimers in resting cells and thus define the poised system state, they have less effect on regulating the dynamics of stimulus-induced NF-κB activity. In response to stimuli, the strong negative feedback provided by IκBα, -ε, and -δ are sufficient to regulate A:A post-induction repression to a similar degree as their preferential binding partner, A:50. Further, both A:A and A:50 dimers activate a similar subset of NF-κB-inducible gene expression programs ((Hoffmann *et al*, 2003) and data not shown). So what, then, is the role of the IκBβ-stabilized A:A dimer if it follows similar temporal and functional dynamics as the more abundant A:50 dimer? Both RelA and IκBβ synthesis are not inducible by NF-κB activity (or are very weakly so) and it is interesting that the generation of the only non-inducible NF-κB monomer is preferentially regulated by the only non-inducible IκB protein. It is an attractive notion that perhaps A:A constitutes a buffer that limits the amount of A:50 generation and that IκBβ, whose synthesis is not affected by A:50 activity, is the regulator of this mechanism.

It is clear that the analysis of NF-κB activity must contend with the generation and functional roles of multiple NF-κB dimers. The finding that IκB proteins have both an inhibitory role to regulate dynamics of NF-κB activation as well as a stabilization role in mediating dimer generation adds another level of complexity. Deciphering this dual functionality may explain the combinatorial functions of the NF-

κB signaling in cell types such as macrophages and B-cells that show enhanced expression of and differential requirements for the activities of the ‘alternative’ RelB and cRel dimers.

MATERIALS AND METHODS

Experimental Studies:

Immortalized MEFs were prepared and cultured as previously described (*Methods*, Chapter 2). Experimental assays were performed by my collaborators and are previously described—DOC EMSA (Basak *et al*, 2007), cold oligo competition EMSA (Hoffmann *et al*, 2003), antibody supershift EMSA (Hoffmann *et al*, 2003), and immunodepletion (Basak *et al*, 2007). The cell lines used were: wild-type (Hoffmann *et al*, 2002), *ikbβ*$^{-/-}$ (Kearns *et al*, 2006), *ikbα*$^{-/-}$*ikbε*$^{-/-}$ (Hoffmann *et al*, 2002), *ikbα*$^{-/-}$*ikbβ*$^{-/-}$*ikbε*$^{-/-}$ (O'Dea *et al*, 2007), *rela*$^{-/-}$ (Hoffmann *et al*, 2003), *rela*$^{-/-}$*crel*$^{-/-}$*nfkb1*$^{-/-}$ (O'Dea *et al*, 2007), *nfkb1*$^{-/-}$*nfkb2*$^{-/-}$ (Hoffmann *et al*, 2003). *crel*$^{-/-}$*relb*$^{-/-}$*nfkb1*$^{-/-}$*nfkb2*$^{-/-}$ knockouts were generated from E12.5-14.5 embryos (Alexander Hoffmann). IκBα (sc-371), IκBβ (sc-946 for Western blot and sc-969 for immunodepletion), RelA (sc-372) antibodies were provided by Santa Cruz Biotechnology. p50 N-terminal antisera was a generous gift from Nancy Rice (NIH).

Computational Studies:

Description of the Computational Model

Two computational models were constructed for this chapter. The first is a simplified model that simulates the homeostatic generation of NF-κB dimers from RelA and p50 NF-κB monomers and the effect of the interactions with two IκB isoforms on their stabilities. This model is shown graphically in panel A of Figure 6.1 and Figure 6.2. The model contains 11 species and 33 reactions that are listed in Table

6.1 and Table 6.2, respectively. All species are given an initial concentration of zero nM and allowed to reach a steady state. The results shown in the chapter figures are the final steady state concentrations.

The second computational model appends the previously published IκB models (Kearns *et al*, 2009), with the reactions that govern RelA/NF-κB dimer generation (Figure 6.5A). The *input* to this model is a numerical curve for IKK activity (Table 6.5) and the *outputs* are free, nuclear RelA:RelA homodimer and Rel:p50 heterodimer. The complete new model contains 40 species (Table 6.3) and 110 reactions governed by 122 parameters (Table 6.4).

Computational Simulations

The ODEs were solved numerically using MATLAB version R2009a (The MathWorks, Inc.) with subroutine *ode15s*, a variable order, multi-step solver. Prior to stimulation, the system was allowed to equilibrate from starting conditions to a steady state, defined as showing no concentration changes greater than 1% over a period of 4000 minutes. Stimulus-induced perturbation from the equilibrium state was accomplished by direct modulation of IKK activity via a numerical input curve representing TNF stimulation (as in Werner et al., 2005).

Table 6.1 Simplified RelA/Dimer Model Species and Initial Concentrations

The model contains 11 species that are all contained within a single cellular compartment. As this is a model of the steady state, the IKK input used as the driver in the IκB:NF-κB models and the shuttling between cytoplasm and nucleus are excluded. Further, synthesis of proteins is simplified into a singular reaction that encompasses both transcription and translation.

	Proteins and Protein Complexes	**Model Species**	**Initial nM**
1	RelA monomer	A	0
2	p50 monomer	50	0
3	RelA:RelA homodimer	AA	0
4	p50:p50 homodimer	5050	0
5	RelA:p50 heterodimer	A50	0
6	IκBα	IkB1	0
7	IκBαAA	IkB1AA	0
8	IκBαA50	IkB1A50	0
9	IκBβ	IkB2	0
10	IκBβAA	IkB2AA	0
11	IκBβA50	IkB2A50	0

Table 6.2 Simplified RelA/Dimer Model Reactions and Rate Constants

The model contains 33 reactions. The reactant or product 'null' represents a source (in the case synthesis) or a sink (in the case degradation). The values listed here treat both IκB isoforms as equivalent.

	Reaction	**Parameter Value**	**Parameter Name**	**Category**
1	null => A	2.1e-3 nM sec^{-1}	m1	Synthesis
2	A => null	9.5e-5 sec^{-1}	m2	Degradation
3	null => 50	4.2e-3 nM sec^{-1}	m3	Synthesis
4	50 => null	9.5e-5 sec^{-1}	m4	Degradation
5	A + A => AA	4e-6 nM^{-1} sec^{-1}	d1	Association
6	AA => A + A	2e-4 sec^{-1}	d2	Dissociation
7	50 + 50 => 5050	1.7e-5 nM^{-1} sec^{-1}	d5	Association
8	5050 => 50 + 50	2e-4 sec^{-1}	d6	Dissociation
9	A + 50 => A50	1.6e-5 nM^{-1} sec^{-1}	d3	Association
10	A50 => A + 50	2.4e-5 sec^{-1}	d4	Dissociation
11	AA => null	4e-6 sec^{-1}	d7	Degradation
12	5050 => null	4e-6 sec^{-1}	d9	Degradation
13	A50 => null	4e-6 sec^{-1}	d8	Degradation
14	null => IkB1	0.6 nM sec^{-1}	i1_1	Synthesis
15	IkB1 => null	2e-3 sec^{-1}	I2_1	Degradation
16	null => IkB2	0.6 nM sec^{-1}	i1_2	Synthesis
17	IkB2 => null	2e-3 sec^{-1}	i2_2	Degradation
18	IkB1 + AA => IkB1AA	3.3e-3 nM^{-1} sec^{-1}	di1_AA_1	Association
19	IkB1AA => IkB1 + AA	1.4e-4 sec^{-1}	di2_AA_1	Dissociation
20	IkB2 + AA => IkB2AA	3.3e-3 nM^{-1} sec^{-1}	di1_AA_2	Association
21	IkB2AA => IkB2 + AA	1.4e-4 sec^{-1}	di2_AA_2	Dissociation
22	IkB1 + A50 => IkB1A50	3.3e-3 nM^{-1} sec^{-1}	di1_A50_1	Association
23	IkB1A50 => IkB1 + A50	1.4e-4 sec^{-1}	di2_A50_1	Dissociation
24	IkB2 + A50 => IkB2A50	3.3e-3 nM^{-1} sec^{-1}	di1_A50_2	Association
25	IkB2A50 => IkB2 + A50	1.4e-4 sec^{-1}	di2_A50_2	Dissociation
26	IkB1AA => IkB1 + null	4e-6 sec^{-1}	di3_AA_1	Degradation
27	IkB1AA => null + AA	2.65e-5 sec^{-1}	di4_AA_1	Degradation
28	IkB2AA => IkB2 + null	4e-6 sec^{-1}	di3_AA_2	Degradation
29	IkB2AA => null + AA	2.65e-5 sec^{-1}	di4_AA_2	Degradation
30	IkB1A50 => IkB1 + null	4e-6 sec^{-1}	di3_A50_1	Degradation
31	IkB1A50 => null + A50	2.65e-5 sec^{-1}	di4_A50_1	Degradation
32	IkB2A50 => IkB2 + null	4e-6 sec^{-1}	di3_A50_2	Degradation
33	IkB2A50 => null + A50	2.65e-5 sec^{-1}	di4_A50_2	Degradation

Table 6.3 Model v5.0 Species and Initial Concentrations

The model contains 40 molecular species that include mRNA, protein, and protein complexes for 4 IκB isoforms, 2 NF-κB monomers, 3 NF-κB dimers, and combinatorial IκB:NF-κB complexes. All species are given an initial concentration of 0 nM and the model is then simulated to compute steady state concentrations. IKK1/NIK and IKK2/NEMO are not counted as molecular species because they are given an initial concentration (140 nM) that does not vary with respect to time and do not associate with other model species. The IKKs act as non-binding catalysts for IκB degradation. Complexes of IκB with p50:p50 homodimer are included in the model (for technical reasons) but not in this table because these complexes never form during simulations due null rate values for IκB:(5050) association.

	mRNA, Proteins and Protein Complexes	**Model Species**	**Location**
1	IκBα mRNA	IkBat	Cyt
2	IκBα	IkBa	Cyt
3	IκBα	IkBan	Nuc
4	IκBβ mRNA	IkBbt	Cyt
5	IκBβ	IkBb	Cyt
6	IκBβ	IkBbn	Nuc
7	IκBε mRNA	IkBet	Cyt
8	IκBε	IkBe	Cyt
9	IκBε	IkBen	Nuc
10	IκBδ mRNA	IkBdt	Cyt
11	IκBδ	IkBd	Cyt
12	IκBδ	IkBdn	Nuc
13	RelA mRNA	RelAt	Cyt
14	RelA monomer	RelA	Cyt
15	RelA monomer	RelAn	Nuc
16	p50 mRNA	p50t	Cyt
17	p50 monomer	p50	Cyt
18	p50 monomer	p50n	Nuc
19	RelA:RelA homodimer	AA	Cyt
20	RelA:RelA homodimer	AAn	Nuc
21	IκBα:(RelA:RelA)	IkBaAA	Cyt
22	IκBα:(RelA:RelA)	IkBaAAn	Nuc
23	IκBβ:(RelA:RelA)	IkBbAA	Cyt
24	IκBβ:(RelA:RelA)	IkBbAAn	Nuc
25	IκBε:(RelA:RelA)	IkBeAA	Cyt
26	IκBε:(RelA:RelA)	IkBeAAn	Nuc
27	IκBδ:(RelA:RelA)	IkBdAA	Cyt
28	IκBδ:(RelA:RelA)	IkBdAAn	Nuc
29	RelA:p50 heterodimer	A50	Cyt

Table 6.3 Model v5.0 Species and Initial Concentrations, Continued.

30	RelA:p50 heterodimer	A50n	Nuc
31	IκBα:(RelA:p50)	IkBaA50	Cyt
32	IκBα:(RelA:p50)	IkBaA50n	Nuc
33	IκBβ:(RelA:p50)	IkBbA50	Cyt
34	IκBβ:(RelA:p50)	IkBbA50n	Nuc
35	IκBε:(RelA:p50)	IkBeA50	Cyt
36	IκBε:(RelA:p50)	IkBeA50n	Nuc
37	IκBδ:(RelA:p50)	IkBdA50	Cyt
38	IκBδ:(RelA:p50)	IkBdA50n	Nuc
39	p50:p50 homodimer	5050	Cyt
40	p50:p50 homodimer	5050n	Nuc
*	IKK1/NIK	-	Cyt
*	IKK2/NEMO	-	Cyt

Table 6.4 Model v5.0 Reactions and Rate Constants
The model contains 4 lists of reactions and rate constants (parameters). Each list is associated with a category of reactions—those that involve IκBs only (i), NF-κB monomers only (m), NF-κB dimers only (d), and associations of NF-κB dimers and IκBs (di).

The inducible transcription of IκBs is governed by multiple parameters:

$$\frac{dmRNA}{dt} = k1 * \frac{1 + (k2 * (AA/K_d)^H) + (k3 * (A50/K_d)^H)}{1 + ((AA/K_d)^H) + ((A50/K_d)^H)} - k4$$

Where *k1* is the constitutive transcription rate, K_d is the NF-κB affinity to the IκB promoter, and *H* is the Hill Coefficient. These 3 parameters are assumed to be irrespective of the specific NF-κB dimer and are thus defined once in the IκB reaction category. The parameters *k2* and *k3* are the inducibility factors (unitless) that govern the amplitude of the mRNA induction fold driven by AA and A50 dimers, respectively. These are dimer specific and are defined combinatorially in the NF-κB:IκB reaction category. IκBβ is not induced by NF-κB and its transcription is simply defined by the constitutive rate constant. *K4* is the constitutive mRNA degradation rate.

IκB reactions and rate constants (i)					
IκBα	**IκBβ**	**IκBε**	**IκBδ**	**Units**	**Description and Notes**
2.1e-4	1.2e-5	2e-6	6e-8	nM sec^{-1}	**Constitutive transcription** null => mRNA Fit to measured protein abundance levels (C. Lynch and S. Basak)
0	-	2200	5400	sec	**Inducible transcription delay** Component of the transcription reaction that delays synthesis until this time point has been reached. (Basak *et al*, 2007; Kearns *et al*, 2006) (Longo *et al*, in preparation) *Assumed to be equal for all NF-κB dimers and, as such, is listed once in the IκB parameter table.*
3	-	3	3	-	**Hill Coefficient** Component of the transcription reaction that imparts cooperativity of NF-κB DNA binding and transactivation. (Basak *et al*, 2007; Werner *et al*, 2005) *Assumed to be equal for all NF-κB dimers and, as such, is listed once in the IκB parameter table.*

Table 6.4 Model v5.0 Reactions and Rate Constants, Continued.

150	-	150	150	nM	**NF-κB dimer K_d to IκB promoter** Component of the transcription reaction that enables saturation of the reaction via DNA binding affinity of NF-κB to the IκB promoters. The value was fit such that the mRNA induction profiles matched experimental data. *Assumed to be equal for all NF-κBs.*
7.3e-4	4.8e-5	6.4e-5	3.2e-5	sec^{-1}	**mRNA degradation** mRNA => null mRNA half lives were measured by RPA in cellss treated with actinomycinD (transcription inhibitor) (Shih *et al*, 2009)
0.2	0.2	0.2	0.2	sec^{-1}	**Translation** mRNA => mRNA + IκB Assumed to be equal for all IκBs. Derived from the elongation rate of the ribosome and corrected for the nucleotide spacing between adjacent ribosomes on the same transcript. (30nt/sec) / (150nt) = 0.2 sec^{-1}
1e-3	7.5e-4	7.5e-4	7.5e-4	sec^{-1}	**Free IκB Nuclear Import** Adapted from (Basak *et al*, 2007; Hoffmann *et al*, 2002)
2e-4	2e-4	2e-4	2e-4	sec^{-1}	**Free IκB Nuclear Export** Adapted from (Basak *et al*, 2007; Hoffmann *et al*, 2002)
2e-3	3e-3	3e-3	2.4e-5	sec^{-1}	**Free IκB degradation (cyt, nuc)** IκB => null (Basak *et al*, 2007; O'Dea *et al*, 2007)
4e-6	4e-6	4e-6	4e-6	sec^{-1}	**Bound IκB degradation (cyt, nuc)** IκB:NF-κB => null + NF-κB (Basak *et al*, 2007; O'Dea *et al*, 2007)
2.25e-5	7.5e-5	1.5e-5	0	sec^{-1}	**IKK2-mediated free IκB degradation** IκB + IKK2 => null + IKK2 Adapted from (Hoffmann *et al*, 2002)
2.25e-5	7.5e-5	1.5e-5	0	sec^{-1}	**IKK2-mediated bound IκB degradation** IκB:NF-κB + IKK2 => NF-κB + IKK2 *Assumed that bound IκB degradation is equal to free IκB.* (Mathes *et al*, 2008)
0	0	0	1.5e-5	sec^{-1}	**IKK1-mediated free IκB degradation** IκB + IKK1 => null + IKK2
0	0	0	1.5e-5	sec^{-1}	**IKK1-mediated bound IκB degradation** IκB:NF-κB + IKK1 => NF-κB + IKK1 *Assumed free and bound degradation is equal* (Mathes *et al*, 2008)

Table 6.4 Model v5.0 Reactions and Rate Constants, Continued.

NF-κB monomer reactions and rate constants (m)			
RelA	**p50**	**Units**	**Description and Notes**
5e-7	1e-6	nM sec^{-1}	**Constitutive transcription** null => mRNA Fit to measured protein abundance levels (C. Lynch and S. Basak)
4.8e-5	4.8e-5	sec^{-1}	**mRNA degradation** mRNA => null mRNA half lives were measured by RPA in samples treated with actinomycinD (transcription inhibitor) (Shih *et al*, 2009)
0.2	0.2	sec^{-1}	**Translation** mRNA => mRNA + monomer Assumed to be equal for both monomers. Derived from the elongation rate of the ribosome and corrected for the nucleotide spacing between adjacent ribosomes on the same mRNA transcript. (30nt/sec) / (150nt) = 0.2 sec^{-1}
9.5e-5	9.5e-5	sec^{-1}	**Free monomer degradation (cyt,nuc)** monomer => null Fit to measured abundance levels (C Lynch and S Basak). Assumed to be short because free monomer is not experimentally observable in wild type conditions or in cells transfected with dimerization-deficient NF-κB constructs (G. Ghosh, private communication)

Table 6.4 Model v5.0 Reactions and Rate Constants, Continued.

NF-κB dimer reactions and rate constants (d)				
AA	**A50**	**5050**	**Units**	**Description and Notes**
4e-6	1.6e-5	1.7e-5	nM^{-1} sec^{-1}	**Dimer Association (cyt, nuc)** Mon1 + Mon2 => NF-κB Dimer affinities were measured using recombinant proteins via Analytical Ultracentrifugation (G Ghosh, private communication). These values were 50 nM (AA), 1.5 nM (A50), and 12 nM (5050). Using the equilibrium state expression [$K_d = k_{off}/k_{on}$], the association and dissociation rates were fit such that they satisfied this ratio. The simplified model informed the selection of these values.
2e-4	2.4e-5	2e-4	sec^{-1}	**Dimer Dissociation (cyt, nuc)** NF-κB => Mon1 + Mon2
9e-2	9e-2	9e-2	sec^{-1}	**Free NF-κB Nuclear Import** Import and export rates were adapted from the single NF-κB model (Hoffmann *et al*, 2002) and assumed to be equal for all dimers. Dimers import with fast kinetics and export slowly.
8e-5	8e-5	8e-5	sec^{-1}	**Free NF-κB Nuclear Export**
4e-6	4e-6	4e-6	sec^{-1}	**Free NF-κB degradation (cyt, nuc)** NF-κB => null Dimers were assumed to have equally slow degradation kinetics. (Basak *et al*, 2007; O'Dea *et al*, 2007)
4e-6	4e-6	4e-6	sec^{-1}	**Bound NF-κB degradation (cyt, nuc)** IκB:NF-κB => IκB + null *Assumed that IκB-bound NF-κB degrades with similar kinetics to free NF-κB.*

Table 6.4 Model v5.0 Reactions and Rate Constants, Continued.

IκB:NF-κB dimer reactions and rate constants (di)				
	AA	**A50**	**Units**	**Description and Notes**
IκBα	3.3e-3	3.3e-3	$nM^{-1}\ sec^{-1}$	**Association (Cyt, Nuc)** IκB + NF-κB => IκB:NF-κB
IκBβ	3.3e-3	3.3e-4		
IκBε	3.3e-3	3.3e-3		
IκBδ	3.3e-3	3.3e-3		
IκBα	7e-4	1.3e-4	sec^{-1}	**Dissociation (Cyt, Nuc)** IκB:NF-κB => IκB + NF-κB
IκBβ	7e-5	1.3e-4		
IκBε	7e-4	1.3e-4		
IκBδ	7e-4	1.3e-4		
IκBα	4.6e-3	4.6e-3	sec^{-1}	**Nuclear Import** IκB:NF-κB => IκB:NF-κBn Import and export rates were adapted from the single NF-κB model (Basak *et al*, 2007; Hoffmann *et al*, 2002) and assumed to be governed by the IκB.
IκBβ	4.6e-4	4.6e-4		
IκBε	2.3e-3	2.3e-3		
IκBδ	2.3e-3	2.3e-3		
IκBα	1.4e-2	1.4e-2	sec^{-1}	**Nuclear Export** IκB:NF-κBn => IκB:NF-κB
IκBβ	7e-3	7e-3		
IκBε	7e-3	7e-3		
IκBδ	7e-3	7e-3		
IκBα	25	25	-	**NF-κB-inducible transcription** Component of the transcription reaction that enables NF-κBn to induce IκB transcription. The value was fit such that the mRNA induction profiles matched experimental data. Assumed that AA and A50 share the same values.
IκBβ	-	-		
IκBε	125	125		
IκBδ	200	200		

Table 6.5 Model v5.0 Numerical IKK Activity Profiles

IKK activity is defined by a numerical curve that correlates percent IKK activity (between 0 and 100%) with time. These curves are based upon measurements performed in MEF cells via *in vitro* kinase assay (Werner *et al*, 2005). IKK1/NIK activity is not modulated by TNF stimulation and thus a basal (1%) activity curve is utilized for all simulations.

Basal activity	**%**	1	1										
	Time (min)	0	360										
15' TNF pulse activity	**%**	1	60	100	65	50	36	21	16	10	1	1	1
	Time (min)	0	5	10	15	20	25	30	45	59	60	90	360
Chronic TNF activity	**%**	1	60	100	65	50	36	21	20	18	15	15	10
	Time (min)	0	5	10	15	20	25	30	60	90	120	240	360

Table 6.6 Model v5.0 Constraints

Eight constraints (or sets of), based upon experimental measurements, were developed that capture the important characteristics of basal (steady state) and TNF-induced signaling responses.

	Description	**Source**
C1	Basal AA and A50 activities are less than 5% of the total abundances of these proteins	EMSA
C2	Basal AA abundance is 0.1 to 0.5 of A50 abundance	EMSA
C3	Basal free IκB protein (IκBα, -β, -ε) is 5- 25% of the total IκB, respectively.	(O'Dea et al, 2007)
C4	Basal abundance of IκBα > IκBβ > IκBε	(O'Dea et al, 2007)
C5	15' TNF Pulse: Both AA and A50 activities are > 10 fold basal activity within the first hour	EMSA (Cheong et al, 2006)
C6	TNF Chronic: Both AA and A50 activities are > 10 fold basal activity within the first hour	EMSA (Cheong et al, 2006)
C7	TNF Chronic: Both AA and A50 activities are > 4 fold basal and > 20% of peak activity at 240 min	EMSA (Cheong et al, 2006)
C8	Basal IκB and RelA monomer levels are within 25% of the measured abundances *Assume 70nM = 100k molecules* (2.2pL cell volume) IκBα: 400k molecules, 280 nM IκBβ: 100k molecules, 70 nM IκBε: 25k molecules, 17.5 nM RelA: 480k molecules, 336 nM	C. Lynch and S. Basak performed Western blots of wild type MEF samples using recombinant protein standards to calculate cellular abundances.

ACKNOWLEDGEMENTS

This chapter is adapted from a manuscript in preparation for submission for which I am the primary author. Candace Lynch, Soumen Basak, and Kim Ngo performed the experiments and are co-authors. I constructed and analyzed the two computational models and wrote the manuscript. Professor Alexander Hoffmann is the corresponding author. Professors Gouri Ghosh (UCSD), Betsy Komives (UCSD), and Simpson Joseph (UCSD) provided insightful discussions.

Chapter 7

Conclusions and Future Directions

CONCLUSIONS

The fundamental goal of my integrated experimental and computational studies of NF-κB signaling is to increase our understanding of how cells utilize this pathway to sense and react to changes in their environment. Using a *Bottom-Up* approach—starting from molecular parts lists and defined modules of interactions and iteratively expanding the complexity and scope of interest—I have revealed the roles of several key regulatory mechanisms that encode NF-κB signaling dynamics and are responsible for generating emergent system properties.

The starting point for my research was a similarly integrated study that examined the role of negative feedback on NF-κB mediated by the dominant IκB isoform, IκBα (Hoffmann *et al*, 2002)(Chapter 1). At this point in time, IκBα was the only known direct negative regulator of NF-κB activity. An open question following this study was how IκBα-driven oscillations in NF-κB activity during chronic inflammatory stimulation, observed experimentally in cells doubly deficient in the IκBβ and IκBε isoforms, were dampened in wild type cells. The remaining IκB isoforms, IκBβ and IκBε, were thought to be constitutive regulators and it was confounding how this type of non-responsive regulation could impart such specific dynamical control. I found that IκBε is in fact not a constitutive regulator, but rather provides negative feedback via its NF-κB-inducible synthesis. The strength of this feedback coupled with a temporal delay at the level of mRNA synthesis are optimally tuned to create asynchronous IκBα and IκBε dynamics that results in dampened NF-κB oscillations. While both IκBs have the same functionality and are therefore

redundant in the absence of stimulus, their specific kinetic properties assign specific regulatory functions in the presence of stimulus.

The analysis of the role of A20 deubiquitinase in negatively regulating NF-κB activity provided the opportunity to examine the importance of network topology in signaling dynamics. Both IκBα and A20 are strongly inducible immediate-early NF-κB response genes, but while IκBα directly inhibits NF-κB activity, A20 provides regulation upstream of IKK by catalyzing the removal of activating ubiquitin chains from the RIP component of the TNF receptor associated signaling complex. Through a collaborative study, I determined that A20 and IκBα have very specific functions that are determined by their locations within the NF-κB signaling network. The direct interaction between IκBα and NF-κB couples the regulatory dynamics of IκBα feedback very closely to the NF-κB activation dynamics. The upstream function of A20 provides for very diffuse negative regulation that is largely decoupled from NF-κB dynamics and more dependent upon the strength of the stimulus and past cellular history. The difference between IκBα and A20 functions explains the non-redundant phenotypes observed in IκBα- and A20-deficient mice.

IκBα, IκBε, and A20 regulatory mechanisms encode inflammatory TNF-induced NF-κB activity in very specific ways (Figure 7.1A). IκBα encodes a 'hardwired' first phase (~1 h) of NF-κB activity and, with chronic TNF stimulation, a second oscillatory phase (Hoffmann *et al*, 2002). IκBε, which provides weaker and temporally delayed feedback with respect to IκBα, functions to regulate the amplitude of second phase oscillatory NF-κB activity. Inducible feedback by A20 deubiquitinase is actually dispensable for its role in regulating the duration of the

second phase of NF-κB activity and can be fully compensated for by elevated constitutive synthesis. The inducibility, coupled to stable A20 protein degradation kinetics, constitutes a transient (< 24 h) cellular memory mechanism that can serve to dampen first phase NF-κB activity in cells previously challenged with inflammatory stimulus.

NF-κB is also activated by developmental stimuli, including LTβR and B cell activating factor (BAFF) via the NIK/IKK1 signaling axis. In contrast to many inflammatory stimuli that induce acute and strong NF-κB activity, these developmental responses are prolonged (> 24 h) and lower amplitude. The discovery that p100 can form an asynchronous homodimer with IκB activity (IκBδ), led me to expand the computational model, in collaboration with experimentalists in the laboratory, to include both canonical (NEMO/IKK2) and non-canonical (NIK/IKK1) inputs (Basak *et al*, 2007). First, I showed that pre-challenge with a short pulse of inflammatory TNF stimulation can increase the fraction of NF-κB bound to IκBδ and thereby lead to elevated "inflammatory-like" NF-κB activity in response to subsequent developmental challenge. The long half-life of IκBδ, 8 h versus the < 10 min for canonical IκBs, constitutes a cellular memory that enables IκBδ to mediate crosstalk between inflammatory and developmental signaling pathways. Second, I showed that IκBδ also plays an important role as a negative feedback regulator of persistent inflammatory LPS-induced NF-κB signaling. Under this condition, IκBδ is immune from the chronic NEMO/IKK2 activity that degrades the canonical IκBs and, coupled to its long half-life, serves to dampen long-lasting inflammatory NF-κB activity (Figure 7.1B). Thus, the same kinetic properties that allow IκBδ to regulate

developmental responses also enable it to modulate the subset of inflammatory stimuli that drive persistent NF-κB signaling.

In resting cells, IκB proteins are stabilized by their interaction with NF-κB (O'Dea *et al*, 2007) and these complexes create a poised state in the cytoplasm that enables stimulus-responsive NF-κB activity. The regulatory mechanisms that govern the formation and stabilization of NF-κB dimers are less clear. As a first step, I undertook a collaborative project to explore the generation of RelA/NF-κB dimers—RelA homodimer and RelA:p50 heterodimer. This study revealed that IκB proteins do have a positive role in NF-κB dimer generation and that differences in IκB:dimer interaction specificities prescribe specific functions to individual IκB isoforms. IκBβ was found to have a role in the generation of RelA homodimer, but due to its constitutive synthesis kinetics, no role in the regulation of stimulus-induced dimer dynamics. This finding expands our understanding of IκB proteins to include a second, novel function as determinants of NF-κB dimer generation.

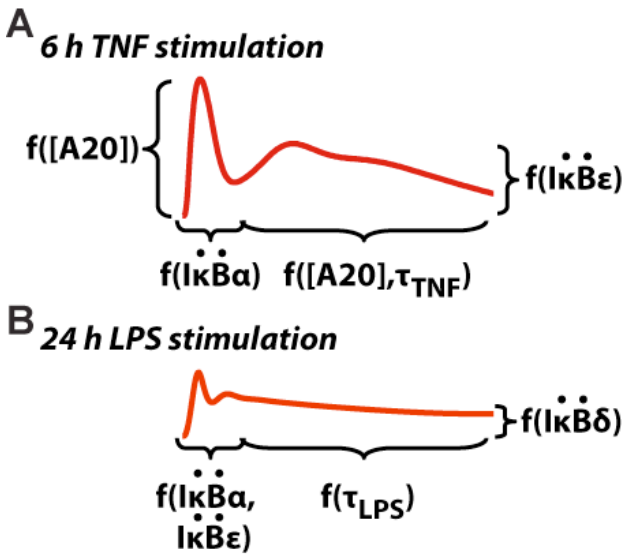

Figure 7.1 Negative regulators impart specific control of NF-κB dynamics

(A) TNF stimulation produces a typically biphasic NF-κB activity that is encoded by the differential functions of IκBα, IκBε, and A20. The duration of the first phase is a function of the inducibility (change in synthesis rate, or second-order derivative, denoted by "˙˙") of IκBα, but is not a function of the TNF stimulus duration or concentration. The duration of the second phase is a function of the concentration of the A20 protein at that time. High concentrations of A20 protein during the early phase (as a result of prior NF-κB activity) may also affect the amplitude of the first phase, but not its duration. The amplitude of NF-κB oscillations in the second phase is regulated by delayed IκBε negative feedback.

(B) LPS stimulation drives persistent NF-κB activity. IκBα and IκBε, due to their fast degradation kinetics and susceptibility to LPS-induced NEMO/IKK2 activity, mediate only the early NF-κB dynamics. IκBδ, due to its slow degradation kinetics and immunity from NEMO/IKK2 activity, mediates the amplitude of the chronic NF-κB response.

FUTURE DIRECTIONS

Beyond the NF-κB signaling module

The original computational studies of NF-κB signaling exploited the inherent modularity in the pathway to define the model boundaries as the network of reactions between IKK activity and nuclear localization of free NF-κB dimer (Chapter 1). While NF-κB is a pleiotropic transcription factor that responds to hundreds of stimuli (Pahl, 1999) to elicit stimulus-specific gene expression programs (Werner *et al*, 2005), the reactions upstream of IKK and downstream of NF-κB nuclear localization that are responsible for these behaviors have yet to be fully addressed.

The comparative study of IκBα with A20 deubiquitinase required an expansion of the model scope to include reactions upstream of IKK activation within the TNF pathway (Chapter 4). This was an initial step that appended a 'TNF receptor module' onto the existing IKK-IκB-NF-κB module. Future studies will append further receptor modules that include Interferon(IFN)β-, IL-1β-, and LPS-induced signaling, for example, which activate both NF-κB and other transcription factor responses. These studies are ongoing within the laboratory and are structured to enable analysis of individual as well as the combinatorial engagement of multiple signaling pathways.

The construction of additional signaling modules will also require the separation of the upstream pathways into receptor-dependent and receptor-independent modules. As IKK is the central mediator, or hub, of NF-κB activation, the first step is to construct an IKK module that receptor modules will impinge upon. The activation of IKK in the TNF receptor model (Chapter 4) includes reactions that

cycle IKK through poised, activated, and transiently inactivated states (Figure 7.2, left). A new 5-state model that includes association of the inflammatory signaling-responsive NEMO adapter protein and is activated at two reaction steps by upstream signaling (Figure 7.2, right) is currently being explored both experimentally and computationally. This work aims to address the signal processing characteristics of the IKK cycle that transfer, filter, or transform upstream signaling information into downstream NF-κB activity.

Analysis of signaling downstream of NF-κB is also an important future direction. Our current studies relate specific stimuli, by way of specific temporal profiles of IKK activity, to nuclear localization of free NF-κB dimers. The role of NF-κB dynamics in driving transcription of target genes has not been addressed beyond the coarse-grained reactions that relate NF-κB nuclear localization to IκB negative feedback activity. Studies are ongoing within the laboratory to discern NF-κB DNA binding dynamics and target sequence specificities in both cellular and biophysical contexts. These will inform the construction of 'gene modules' for key NF-κB target genes that will include reactions between explicit NF-κB recruitment to the promoter and PolII-induced mRNA synthesis. Such modules are especially important for analysis of combinatorial stimulations in which the dynamics of multiple transcription factor pathways converge to drive, or repress, transcription from these genes.

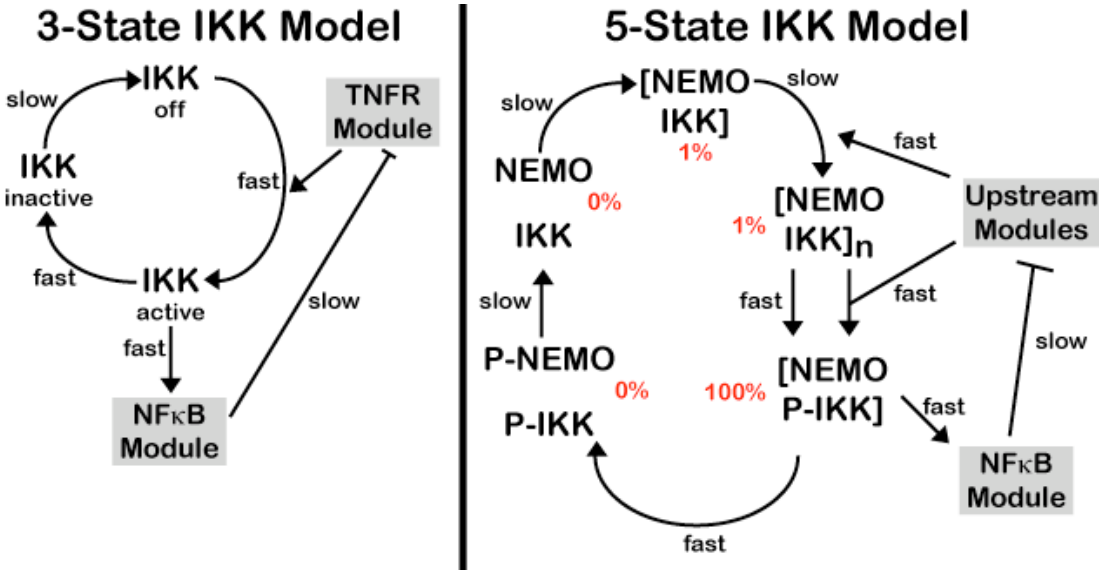

Figure 7.2 Expansion of the NEMO/IKK2 activation cycle

The activation of canonical IKK was computationally modeled in Chapter 4 as a 3-state process driven by upstream engagement of the TNF receptor by TNF ligand. In simulations, IKK is primarily in the 'off' state in resting cells and quickly activates upon TNF stimulation. Once 'active', IKK drives NF-κB activation and is cycled into an 'inactive' state by an auto-regulatory mechanism. Recycling of inactive IKK back to the poised off state is achieved by slow constitutive kinetics. Future work will expand this 3-state IKK model into an experimentally validated 5-state model that includes association of IKK with the NEMO adapter and explicit phosphorylation, de-phosphorylation, and dis/association reactions. The input to this model will be upstream signaling modules, such as TNF receptor pathway. Specific NF-κB-inducing activities for each of the 5 states are denoted as percentages (red).

Multiple NF-κB dimer models

The RelA/NF-κB model (Chapter 6) was an initial step towards addressing the role of multiple NF-κB dimers in the IKK:IκB:NF-κB signaling module and their combinatorial interactions with IκB proteins. The next step is to expand the scope of the integrated computational and experimental studies to include further dimers. Such work is in currently underway and is focused upon RelB/NF-κB dimers and their activation via the non-canonical NIK/IKK1 signaling pathway.

Wiring diagrams of the combined RelA/NF-κB and RelB/NF-κB signaling network have been proposed (Basak and Hoffmann, 2008a; Basak *et al*, 2008b). These expand the scope of the network to include four NF-κB monomers and four IκB isoforms and, like previous work (Basak *et al*, 2007), are responsive to both canonical NEMO/IKK2 and NIK/IKK1 activities. The aims of this research may be to discern the dynamics of RelA-inducible synthesis of RelB and p100/p52 monomers (and subsequently dimeric associations) and the effects of crosstalk between canonical and non-canonical pathways.

A first version of a computational model has been constructed that incorporates the expanded signaling module (Figure 7.3). In its current state, this model expands the RelA/NF-κB model (Chapter 6) from 40 to 98 molecular species and from 110 to 256 reactions. The first stage of model construction, developing the computer code, was enabled by taking advantage of the modularity built into the original RelA/NF-κB model (Figure 7.4). This new model has some fundamental differences from the earlier RelA/NF-κB model. Of note, the mechanisms through which inflammatory and developmental signaling are achieved are different. Unlike NEMO/IKK2 signaling

where the complex is in a poised state before stimulation (and thus simulated at a constant abundance), NIK protein is continually degraded in resting cells and is stabilized upon upstream developmental signaling. A numerically defined NEMO/IKK2 profile (% activity over time) is used as an inflammatory pathway input. The developmental input is a temporal modulation of the NIK degradation rate whereby NIK abundance increases with stimulation. Further, to match experimental data, p100 and RelB are inducibly synthesized via RelA/NF-κB (A:50, A:A, A:52) activity and the generations of IκBδ and p52 involve the p100 precursor protein to homodimerize or to get proteolytically processed via NIK/IKK1, respectively. The rate constants were given initial values derived from the RelA/NF-κB model, experimental measurements, and from our best estimates.

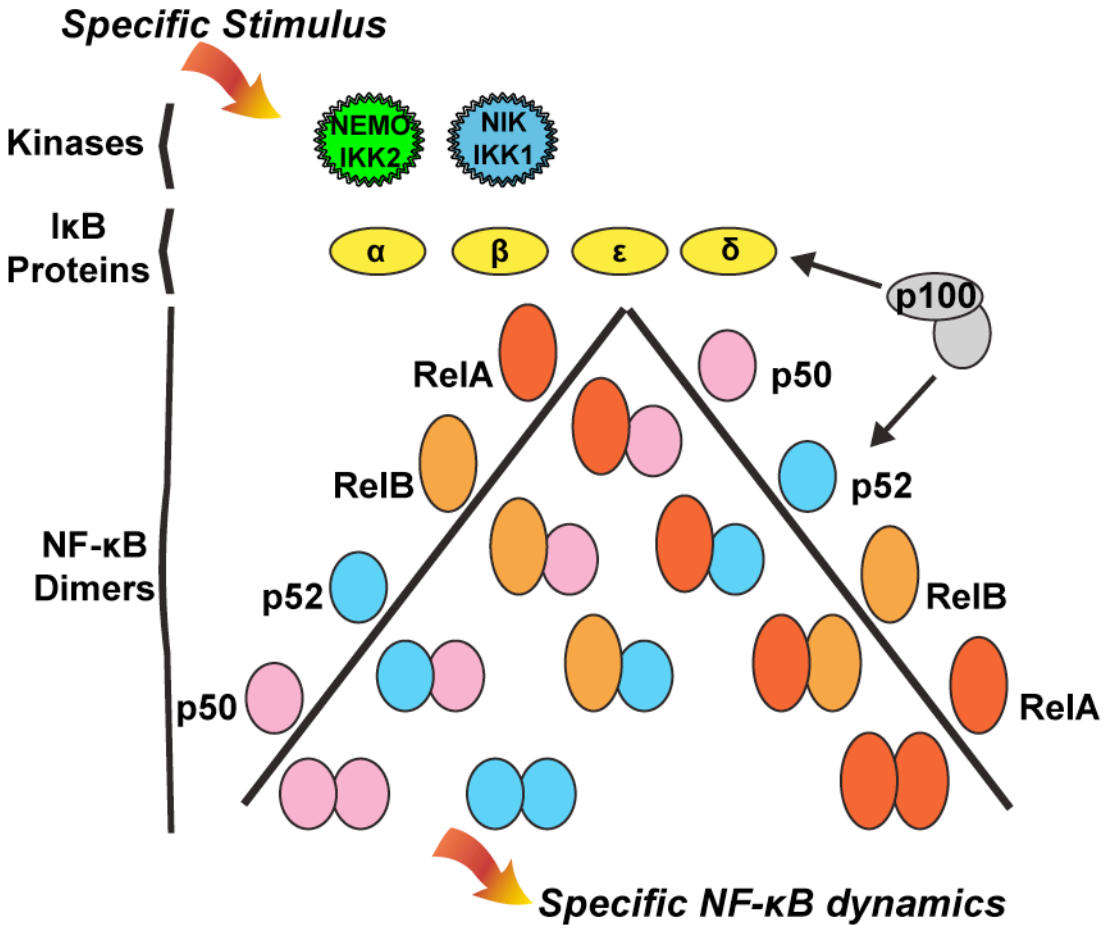

Figure 7.3 Molecular species in a RelA/NF-κB and RelB/NF-κB signaling module

RelA and RelB protein monomers form homo- and hetero-dimeric complexes with p50 and p52. Up to nine NF-κB dimers are generated and the abundance of each is cell type and stimulus-dependent. RelB:RelB homodimer has not been experimentally observed. These dimers are regulated via stoichiometric associations with IκBα, -β, -ε, -δ/p100 inhibitor proteins. Cellular stimuli and stresses activate NEMO-dependent IKK2 or NIK-dependent IKK1 complexes that drive IκB protein degradation and subsequent stimulus-specific NF-κB dimer activity. In this module, IκBδ and p52 are generated by homodimerization or NIK/IKK1-mediated processing of p100 precursor protein, respectively.
(Adapted with permission from (Hoffmann *et al*, 2006b))

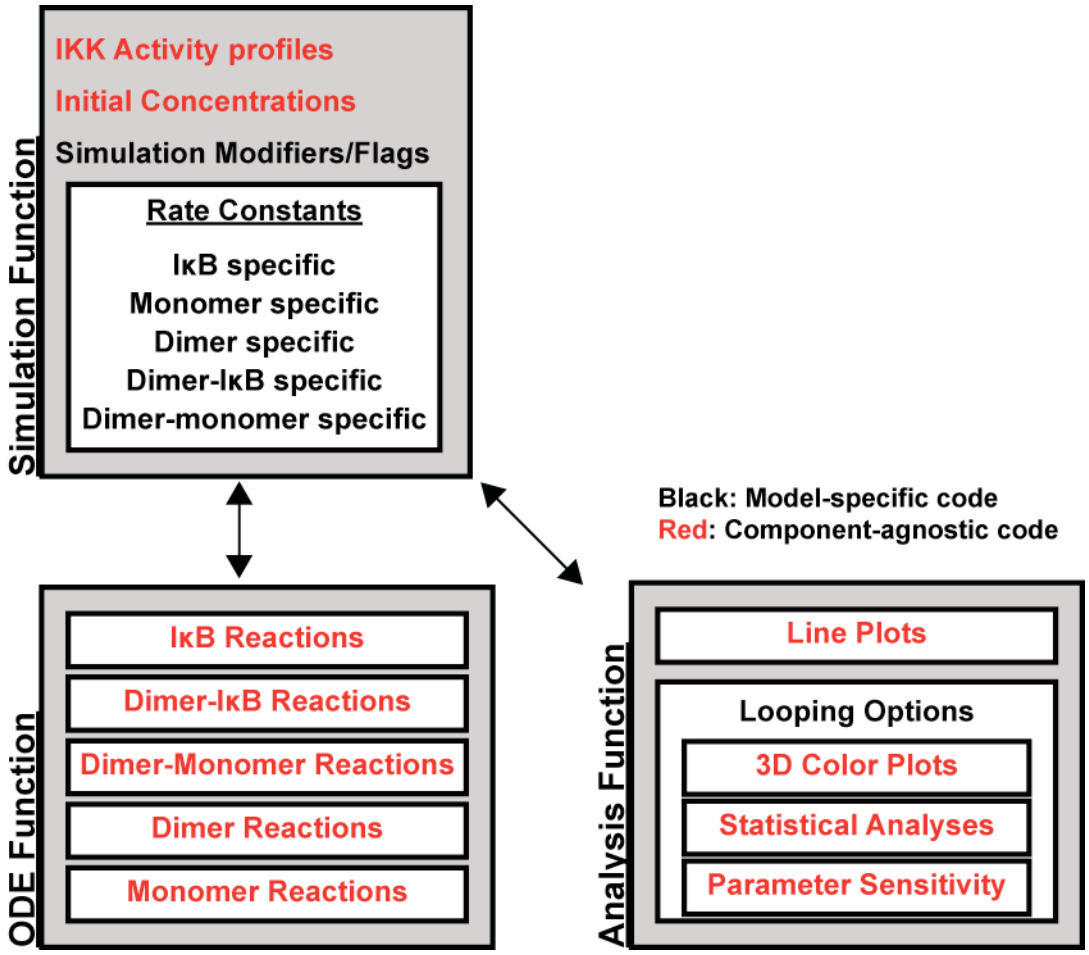

Figure 7.4 Development of future, expanded multiple NF-κB dimer models

The 3-dimer model (Chapter 6) contains 40 components (molecular species) and 110 reactions. Future models containing more NF-κB dimers and IκBs are expected to grow to > 100 components and > 400 reactions. To facilitate this, the MATLAB programming code was structured to be as 'component agnostic' as possible. The ODE function can handle variable numbers of IκBs, monomers, and dimers without user intervention. The analysis function requires only minimal intervention to adapt it for larger models.

Simulations were performed to probe the model's capacity to transduce inflammatory (NEMO/IKK1) and developmental (NIK/IKK1) signals. First, a chronic inflammatory TNF stimulation was run using a numerically defined NEMO/IKK2 activity profile (Werner *et al*, 2005)(Figure 7.5A). Under this condition, NIK/IKK1 is not perturbed from its steady state value. RelA/NF-κB dimers are robustly activated in response to TNF stimulation while RelB/NF-κB dimers are only marginally affected. Next, a chronic developmental LTβR stimulation was run by temporally modulating the NIK/IKK1 degradation rate constant (Figure 7.5C). In contrast to the inflammatory simulations, NIK/IKK1 activity only induces RelB/NF-κB and does so via its role in processing latent p100 precursor to p52 monomer that subsequently associates to form RelB:p52 dimer. Then, co-stimulation of both pathways was simulated via combinations of NEMO/IKK2 and NIK/IKK1 inputs and RelB/NF-κB activity following 24 h of stimulation plotted as a heat map (Figure 7.5C). These results suggest that co-stimulation leads to synergistic generation and activation of RelB/NF-κB dimers.

The simulations of single stimulations match, qualitatively, some of the trends observed in initial experiments. Further refinements of the rate constant values as well as the wiring diagram itself are required to bring the model into quantitative agreement with these experiments. In addition, key experimental studies are required to derive constraints—measurements of protein abundances (RelB, p100, p52, NIK) at resting and stimulus-induced states, development of a better detection assay for nuclear RelB/NF-κB dimers, analysis of the combinatorial monomer:monomer and IκB:NF-κB interaction affinities, etc. These constraints can be directly utilized in the

computational model to guide the selection of rate constant values and to test the validity of the reaction wiring diagram. This methodology has been used in earlier studies (Chapters 4 and 6).

Once the model has been quantitatively fit to experimental constraints, it will be used to form experimentally testable hypotheses. It is hoped that this will reveal both the emergent properties (crosstalk, compensation effects, dose responses, etc.) that the signaling module is capable of generating as well as the regulatory mechanisms that encode them. Further, this model can then be used as a building block towards translating from the MEF cell type to others in which the full complement of NF-κB dimers are known to play important physiological roles. Studies are underway within the laboratory to discern the function of NF-κB signaling in B cells, macrophages, and dendritic cells and can certainly benefit from an integrated experimental/modeling approach.

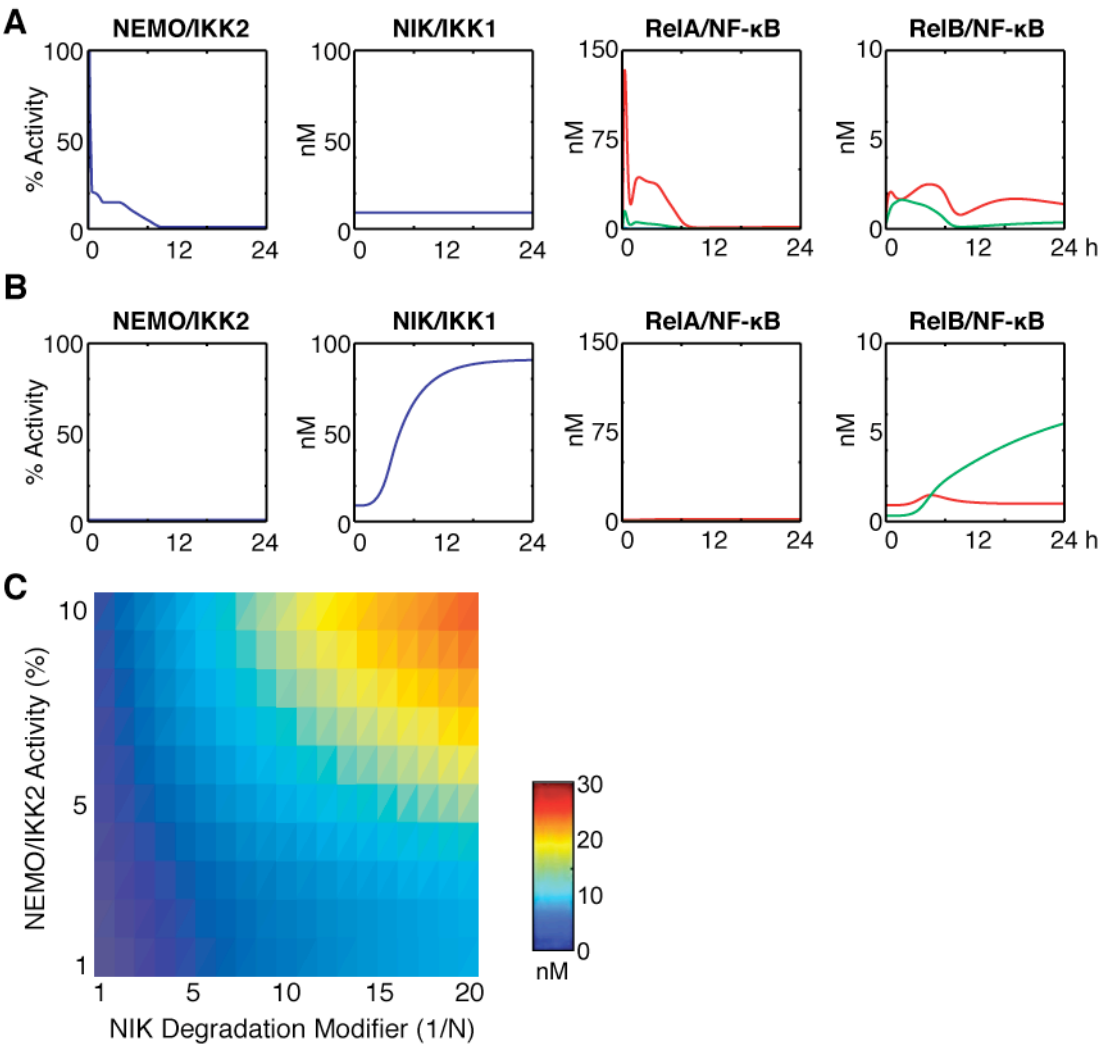

Figure 7.5 Preliminary simulation results of an expanded multiple NF-κB dimer model

(A) Chronic inflammatory TNF stimulation of a wild type model system. The activities of NEMO/IKK2 (%) and NIK/IKK1 (nM) drive activation of RelA/NF-κB (A:50, red ; A:A, green ; A:52, blue) and RelB/NF-κB (B:50, red ; B:52, green) dimers. NIK/IKK1 is not regulated by TNF stimulation.

(B) Chronic developmental LTβR stimulation of a wild type model system. Plots are as in (A). NEMO/IKK2 is not regulated by LTβR stimulation.

(C) The total activity of RelB/NF-κB dimers (B:50 and B:52) was calculated in repeated simulations with increasing co-stimulation activities of NEMO/IKK2 and NIK/IKK1. NEMO/IKK2 is modulated by a step function with the indicated % activity. NIK/IKK1 is modulated by decreasing the degradation rate by the indicated denominator, which has the effect of increasing [NIK] as in (B). RelB/NF-κB activity is represented as a heat map.

REFERENCES

Aggarwal BB, Shishodia S, Ashikawa K, Bharti AC (2002) The role of TNF and its family members in inflammation and cancer: lessons from gene deletion. *Curr Drug Targets Inflamm Allergy* **1:** 327-341.

Alon U (2007) *An introduction to systems biology : design principles of biological circuits*. Boca Raton, FL: Chapman & Hall/CRC.

Altschul SF, Madden TL, Schaffer AA, Zhang J, Zhang Z, Miller W, Lipman DJ (1997) Gapped BLAST and PSI-BLAST: a new generation of protein database search programs. *Nucleic acids research* **25:** 3389-3402.

Banner DW, D'Arcy A, Janes W, Gentz R, Schoenfeld HJ, Broger C, Loetscher H, Lesslauer W (1993) Crystal structure of the soluble human 55 kd TNF receptor-human TNF beta complex: implications for TNF receptor activation. *Cell* **73:** 431-445.

Barken D, Wang CJ, Kearns J, Cheong R, Hoffmann A, Levchenko A (2005) Comment on "Oscillations in NF-kappaB signaling control the dynamics of gene expression". *Science (New York, NY* **308:** 52; author reply 52.

Barnes PJ, Karin M (1997) Nuclear factor-kappaB: a pivotal transcription factor in chronic inflammatory diseases. *N Engl J Med* **336:** 1066-1071.

Basak S, Hoffmann A (2008a) Crosstalk via the NF-kappaB signaling system. *Cytokine Growth Factor Rev* **19:** 187-197.

Basak S, Kim H, Kearns JD, Tergaonkar V, O'Dea E, Werner SL, Benedict CA, Ware CF, Ghosh G, Verma IM, Hoffmann A (2007) A fourth IkappaB protein within the NF-kappaB signaling module. *Cell* **128:** 369-381.

Basak S, Shih VF, Hoffmann A (2008b) Generation and activation of multiple dimeric transcription factors within the NF-kappaB signaling system. *Mol Cell Biol* **28:** 3139-3150.

Beg AA, Sha WC, Bronson RT, Baltimore D (1995) Constitutive NF-kappa B activation, enhanced granulopoiesis, and neonatal lethality in I kappa B alpha-deficient mice. *Genes Dev* **9:** 2736-2746.

Beutler BA, Milsark IW, Cerami A (1985) Cachectin/tumor necrosis factor: production, distribution, and metabolic fate in vivo. *J Immunol* **135:** 3972-3977.

Beyer A, Bandyopadhyay S, Ideker T (2007) Integrating physical and genetic maps: from genomes to interaction networks. *Nat Rev Genet* **8:** 699-710.

Bren GD, Solan NJ, Miyoshi H, Pennington KN, Pobst LJ, Paya CV (2001) Transcription of the RelB gene is regulated by NF-kappaB. *Oncogene* **20:** 7722-7733.

Buchler NE, Gerland U, Hwa T (2003) On schemes of combinatorial transcription logic. *Proc Natl Acad Sci.* **100:** 5136-5141.

Cabannes E, Khan G, Aillet F, Jarrett RF, Hay RT (1999) Mutations in the IkBa gene in Hodgkin's disease suggest a tumour suppressor role for IkappaBalpha. *Oncogene* **18:** 3063-3070.

Cheong R, Bergmann A, Werner SL, Regal J, Hoffmann A, Levchenko A (2006) Transient IkappaB kinase activity mediates temporal NF-kappaB dynamics in response to a wide range of tumor necrosis factor-alpha doses. *The Journal of biological chemistry* **281:** 2945-2950.

Cho KH, Shin SY, Lee HW, Wolkenhauer O (2003) Investigations into the analysis and modeling of the TNF alpha-mediated NF-kappa B-signaling pathway. *Genome research* **13:** 2413-2422.

Covert MW, Knight EM, Reed JL, Herrgard MJ, Palsson BO (2004) Integrating high-throughput and computational data elucidates bacterial networks. *Nature* **429:** 92-96.

Covert MW, Leung TH, Gaston JE, Baltimore D (2005) Achieving stability of lipopolysaccharide-induced NF-kappaB activation. **309:** 1854-1857.

Davidson EH, Rast JP, Oliveri P, Ransick A, Calestani C, Yuh CH, Minokawa T, Amore G, Hinman V, Arenas-Mena C, Otim O, Brown CT, Livi CB, Lee PY, Revilla R, Rust AG, Pan Z, Schilstra MJ, Clarke PJ, Arnone MI, Rowen L, Cameron RA, McClay DR, Hood L, Bolouri H (2002) A genomic regulatory network for development. *Science* **295:** 1669-1678.

Dejardin E, Droin NM, Delhase M, Haas E, Cao Y, Makris C, Li ZW, Karin M, Ware CF, Green DR (2002) The lymphotoxin-beta receptor induces different patterns of gene expression via two NF-kappaB pathways. *Immunity* **17:** 525-535.

Delhase M, Hayakawa M, Chen Y, Karin M (1999) Positive and negative regulation of IkappaB kinase activity through IKKbeta subunit phosphorylation. *Science* **284:** 309-313.

Dibrov BF, Zhabotinsky AM, Kholodenko BN (1982) Dynamic stability of steady states and static stabilization in unbranched metabolic pathways. *J Math Biol* **15:** 51-63.

Dixit VM, Green S, Sarma V, Holzman LB, Wolf FW, O'Rourke K, Ward PA, Prochownik EV, Marks RM (1990) Tumor necrosis factor-alpha induction of novel gene products in human endothelial cells including a macrophage-specific chemotaxin. *The Journal of biological chemistry* **265:** 2973-2978.

Doerre S, Mesires KP, Daley KM, McCarty T, Knoetig S, Corley RB (2005) Reductions in I kappa B epsilon and changes in NF-kappa B activity during B lymphocyte differentiation. *J Immunol* **174:** 983-991.

Emmerich F, Theurich S, Hummel M, Haeffker A, Vry MS, Dohner K, Bommert K, Stein H, Dorken B (2003) Inactivating I kappa B epsilon mutations in Hodgkin/Reed-Sternberg cells. *J Pathol* **201:** 413-420.

Eungdamrong NJ, Iyengar R (2004) Computational approaches for modeling regulatory cellular networks. *Trends in Cell Biology* **14:** 661-669.

Fuss H, Dubitzky W, Downes CS, Kurth MJ (2005) Mathematical models of cell cycle regulation. *Briefings in bioinformatics* **6:** 163-177.

Ghosh S, May MJ, Kopp EB (1998) NF-kappa B and Rel proteins: evolutionarily conserved mediators of immune responses. *Annu Rev Immunol* **16:** 225-260.

Grell M, Wajant H, Zimmermann G, Scheurich P (1998) The type 1 receptor (CD120a) is the high-affinity receptor for soluble tumor necrosis factor. *Proc Natl Acad Sci.* **95:** 570-575.

Hartwell LH, Hopfield JJ, Leibler S, Murray AW (1999) From molecular to modular cell biology. *Nature* **402:** C47-52.

Hayden MS, Ghosh S (2008) Shared principles in NF-kappaB signaling. *Cell* **132:** 344-362.

Hayot F, Jayaprakash C (2006) NF-kappaB oscillations and cell-to-cell variability. *J Theor Biol* **240:** 583-591.

Heinrich R, Neel BG, Rapoport TA (2002) Mathematical models of protein kinase signal transduction. *Molecular cell* **9:** 957-970.

Hertlein E, Wang J, Ladner KJ, Bakkar N, Guttridge DC (2005) RelA/p65 regulation of IkappaBbeta. *Mol Cell Biol* **25:** 4956-4968.

Hitotsumatsu O, Ahmad RC, Tavares R, Wang M, Philpott D, Turer EE, Lee BL, Shiffin N, Advincula R, Malynn BA, Werts C, Ma A (2008) The ubiquitin-editing enzyme A20 restricts nucleotide-binding oligomerization domain containing 2-triggered signals. *Immunity* **28:** 381-390.

Hoffmann A, Baltimore D (2006a) Circuitry of nuclear factor kappaB signaling. *Immunological Reviews* **210:** 171-186.

Hoffmann A, Leung TH, Baltimore D (2003) Genetic analysis of NF-kappaB/Rel transcription factors defines functional specificities. *Embo J* **22:** 5530-5539.

Hoffmann A, Levchenko A, Scott ML, Baltimore D (2002) The IkappaB-NF-kappaB signaling module: temporal control and selective gene activation. *Science* **298:** 1241-1245.

Hoffmann A, Natoli G, Ghosh G (2006b) Transcriptional regulation via the NF-kappaB signaling module. *Oncogene* **25:** 6706-6716.

Huxford T, Huang DB, Malek S, Ghosh G (1998) The crystal structure of the IkappaBalpha/NF-kappaB complex reveals mechanisms of NF-kappaB inactivation. *Cell* **95:** 759-770.

Ingolia NT (2004) Topology and robustness in the Drosophila segment polarity network. *PLoS biology* **2:** e123.

Ishikawa H, Claudio E, Dambach D, Raventos-Suarez C, Ryan C, Bravo R (1998) Chronic inflammation and susceptibility to bacterial infections in mice lacking the polypeptide (p)105 precursor (NF-kappaB1) but expressing p50. *J Exp Med* **187:** 985-996.

Islam A, Adamik B, Hawari FI, Ma G, Rouhani FN, Zhang J, Levine SJ (2006) Extracellular TNFR1 release requires the calcium-dependent formation of a nucleobindin 2-ARTS-1 complex. *The Journal of biological chemistry* **281:** 6860-6873.

Jiang X, Takahashi N, Matsui N, Tetsuka T, Okamoto T (2003) The NF-kappa B activation in lymphotoxin beta receptor signaling depends on the phosphorylation of p65 at serine 536. *The Journal of biological chemistry* **278:** 919-926.

Karin M, Greten FR (2005) NF-kappaB: linking inflammation and immunity to cancer development and progression. *Nat Rev Immunol* **5:** 749-759.

Kaufman DR, Choi Y (1999) Signaling by tumor necrosis factor receptors: pathways, paradigms and targets for therapeutic modulation. *Int Rev Immunol* **18:** 405-427.

Kearns JD, Basak S, Werner SL, Huang CS, Hoffmann A (2006) IkappaBepsilon provides negative feedback to control NF-kappaB oscillations, signaling dynamics, and inflammatory gene expression. *J Cell Biol* **173:** 659-664.

Kearns JD, Hoffmann A (2009) Integrating Computational and Biochemical Studies to Explore Mechanisms in NF-{kappa}B Signaling. *The Journal of biological chemistry* **284:** 5439-5443.

Kholodenko BN (2006) Cell-signalling dynamics in time and space. *Nature reviews* **7:** 165-176.

Klement JF, Rice NR, Car BD, Abbondanzo SJ, Powers GD, Bhatt PH, Chen CH, Rosen CA, Stewart CL (1996) IkappaBalpha deficiency results in a sustained NF-kappaB response and severe widespread dermatitis in mice. *Mol Cell Biol* **16:** 2341-2349.

Krappmann D, Emmerich F, Kordes U, Scharschmidt E, Dorken B, Scheidereit C (1999) Molecular mechanisms of constitutive NF-kappaB/Rel activation in Hodgkin/Reed-Sternberg cells. *Oncogene* **18:** 943-953.

Krishna S, Jensen MH, Sneppen K (2006) Minimal model of spiky oscillations in NF-kappa B signaling. *Proceedings of the National Academy of Sciences of the United States of America* **103:** 10840-10845.

Laberge MA, Moore KJ, Freeman MW (2005) Atherosclerosis and innate immune signaling. *Ann Med* **37:** 130-140.

Lee EG, Boone DL, Chai S, Libby SL, Chien M, Lodolce JP, Ma A (2000) Failure to regulate TNF-induced NF-kappaB and cell death responses in A20-deficient mice. *Science* **289:** 2350-2354.

Leloup JC, Goldbeter A (2003) Toward a detailed computational model for the mammalian circadian clock. *Proc Natl Acad Sci.* **100:** 7051-7056.

Lipniacki T, Paszek P, Brasier AR, Luxon B, Kimmel M (2004) Mathematical model of NF-kappaB regulatory module. *J Theor Biol* **228:** 195-215.

Lipniacki T, Puszynski K, Paszek P, Brasier AR, Kimmel M (2007) Single TNFalpha trimers mediating NF-kappaB activation: stochastic robustness of NF-kappaB signaling. *BMC bioinformatics* **8:** 376.

Longo DM, Kearns JD, Hoffmann A, Hasty J, Tsimring LS (in preparation) Dual delayed feedback provides sensitivity and robustness to the NF-kappaB signaling module.

Maine GN, Mao X, Komarck CM, Burstein E (2007) COMMD1 promotes the ubiquitination of NF-kappaB subunits through a cullin-containing ubiquitin ligase. *Embo J* **26:** 436-447.

Mathes E, O'Dea EL, Hoffmann A, Ghosh G (2008) NF-kappaB dictates the degradation pathway of IkappaBalpha. *Embo J* **27:** 1357-1367.

Memet S, Laouini D, Epinat JC, Whiteside ST, Goudeau B, Philpott D, Kayal S, Sansonetti PJ, Berche P, Kanellopoulos J, Israel A (1999) I kappa B epsilon-deficient mice: Reduction of one T cell precursor subspecies and enhanced Ig isotype switching and cytokine synthesis. *J Immunol* **163:** 5994-6005.

Mercurio F, Zhu H, Murray BW, Shevchenko A, Bennett BL, Li J, Young DB, Barbosa M, Mann M, Manning A, Rao A (1997) IKK-1 and IKK-2: cytokine-activated IkappaB kinases essential for NF-kappaB activation. *Science* **278:** 860-866.

Monaco C, Paleolog E (2004) Nuclear factor kappaB: a potential therapeutic target in atherosclerosis and thrombosis. *Cardiovasc Res* **61:** 671-682.

Nelson DE, Ihekwaba AE, Elliott M, Johnson JR, Gibney CA, Foreman BE, Nelson G, See V, Horton CA, Spiller DG, Edwards SW, McDowell HP, Unitt JF, Sullivan E, Grimley R, Benson N, Broomhead D, Kell DB, White MR (2004) Oscillations in NF-kappaB signaling control the dynamics of gene expression. *Science* **306:** 704-708.

Ng A, Bursteinas B, Gao Q, Mollison E, Zvelebil M (2006) Resources for integrative systems biology: from data through databases to networks and dynamic system models. *Briefings in bioinformatics* **7:** 318-330.

Novick A, Weiner M (1957) Enzyme Induction as an All-or-None Phenomenon. *Proc Natl Acad Sci.* **43:** 553-566.

O'Dea EL, Barken D, Peralta RQ, Tran KT, Werner SL, Kearns JD, Levchenko A, Hoffmann A (2007) A homeostatic model of IkappaB metabolism to control constitutive NF-kappaB activity. *Mol Syst Biol* **3:** 111.

O'Dea EL, Kearns JD, Hoffmann A (2008) UV as an amplifier rather than inducer of NF-kappaB activity. *Molecular cell* **30:** 632-641.

Pahl HL (1999) Activators and target genes of Rel/NF-kappaB transcription factors. *Oncogene* **18:** 6853-6866.

Palsson B (2006) *Systems biology : properties of reconstructed networks*. Cambridge ; New York: Cambridge University Press.

Phillips RJ, Ghosh S (1997) Regulation of IkappaB beta in WEHI 231 mature B cells. *Mol Cell Biol* **17:** 4390-4396.

Ramakrishnan P, Wang W, Wallach D (2004) Receptor-specific signaling for both the alternative and the canonical NF-kappaB activation pathways by NF-kappaB-inducing kinase. *Immunity* **21:** 477-489.

Rao CV, Wolf DM, Arkin AP (2002) Control, exploitation and tolerance of intracellular noise. *Nature* **420:** 231-237.

Raser JM, O'Shea EK (2005) Noise in gene expression: origins, consequences, and control. *Science* **309:** 2010-2013.

Robertson SH, Smith CK, Langhans AL, McLinden SE, Oberhardt MA, Jakab KR, Dzamba B, Desimone DW, Papin JA, Peirce SM (2007) Multiscale computational analysis of Xenopus laevis morphogenesis reveals key insights of systems-level behavior. *BMC Syst Biol* **1:** 46.

Saccani S, Pantano S, Natoli G (2001) Two waves of nuclear factor kappaB recruitment to target promoters. *J Exp Med* **193:** 1351-1359.

Savinova OV, Hoffmann A, Ghosh G (2009) The Nfkb1 and Nfkb2 proteins p105 and p100 function as the core of high-molecular-weight heterogeneous complexes. *Molecular cell* **DOI: 10.1016/j.molcel.2009.04.033**.

Schneider-Brachert W, Tchikov V, Neumeyer J, Jakob M, Winoto-Morbach S, Held-Feindt J, Heinrich M, Merkel O, Ehrenschwender M, Adam D, Mentlein R, Kabelitz D, Schutze S (2004) Compartmentalization of TNF receptor 1 signaling: internalized TNF receptosomes as death signaling vesicles. *Immunity* **21:** 415-428.

Scott ML, Fujita T, Liou HC, Nolan GP, Baltimore D (1993) The p65 subunit of NF-kappa B regulates I kappa B by two distinct mechanisms. *Genes Dev* **7:** 1266-1276.

Senftleben U, Cao Y, Xiao G, Greten FR, Krahn G, Bonizzi G, Chen Y, Hu Y, Fong A, Sun SC, Karin M (2001) Activation by IKKalpha of a second, evolutionary conserved, NF-kappa B signaling pathway. *Science* **293:** 1495-1499.

Shih VF, Kearns JD, Basak S, Savinova OV, Ghosh G, Hoffmann A (2009) Kinetic control of negative feedback regulators of NF-{kappa}B/RelA determines their pathogen- and cytokine-receptor signaling specificity. *Proc Natl Acad Sci.* (in press)

Simeonidis S, Liang S, Chen GY, Thanos D (1997) Cloning and functional characterization of mouse I kappa B epsilon. *Proc Natl Acad Sci U S A* **94:** 14372-14377.

Solan NJ, Miyoshi H, Carmona EM, Bren GD, Paya CV (2002) RelB cellular regulation and transcriptional activity are regulated by p100. *The Journal of biological chemistry* **277:** 1405-1418.

Song HY, Rothe M, Goeddel DV (1996) The tumor necrosis factor-inducible zinc finger protein A20 interacts with TRAF1/TRAF2 and inhibits NF-kappaB activation. *Proc Natl Acad Sci* **93:** 6721-6725.

Song XT, Kabler KE, Shen L, Rollins L, Huang XF, Chen SY (2008) A20 is an antigen presentation attenuator, and its inhibition overcomes regulatory T cell-mediated suppression. *Nat Med* **14:** 258-265.

Spiecker M, Darius H, Liao JK (2000) A functional role of I kappa B-epsilon in endothelial cell activation. *J Immunol* **164:** 3316-3322.

Stelling J, Sauer U, Szallasi Z, Doyle FJ, 3rd, Doyle J (2004) Robustness of cellular functions. *Cell* **118:** 675-685.

Stilo R, Varricchio E, Liguoro D, Leonardi A, Vito P (2008) A20 is a negative regulator of BCL10- and CARMA3-mediated activation of NF-kappaB. *J Cell Sci*. **121:** 1165-1171

Suyang H, Phillips R, Douglas I, Ghosh S (1996) Role of unphosphorylated, newly synthesized I kappa B beta in persistent activation of NF-kappa B. *Mol Cell Biol* **16:** 5444-5449.

Tergaonkar V (2006) NFkappaB pathway: a good signaling paradigm and therapeutic target. *Int J Biochem Cell Biol* **38:** 1647-1653.

Tian B, Nowak DE, Jamaluddin M, Wang S, Brasier AR (2005) Identification of direct genomic targets downstream of the nuclear factor-kappaB transcription factor mediating tumor necrosis factor signaling. *The Journal of biological chemistry* **280:** 17435-17448.

Turer EE, Tavares RM, Mortier E, Hitotsumatsu O, Advincula R, Lee B, Shifrin N, Malynn BA, Ma A (2008) Homeostatic MyD88-dependent signals cause lethal inflammation in the absence of A20. *J Exp Med* **205:** 451-464.

Wallach D, Varfolomeev EE, Malinin NL, Goltsev YV, Kovalenko AV, Boldin MP (1999) Tumor necrosis factor receptor and Fas signaling mechanisms. *Annu Rev Immunol* **17:** 331-367.

Wang C, Deng L, Hong M, Akkaraju GR, Inoue J, Chen ZJ (2001) TAK1 is a ubiquitin-dependent kinase of MKK and IKK. *Nature* **412:** 346-351.

Watanabe N, Kuriyama H, Sone H, Neda H, Yamauchi N, Maeda M, Niitsu Y (1988) Continuous internalization of tumor necrosis factor receptors in a human myosarcoma cell line. *The Journal of biological chemistry* **263:** 10262-10266.

Werner S, Barken D, Hoffmann A (2005) Stimulus specificity of gene expression programs determined by temporal control of IKK activity. *Science* **309:** 1857-1861.

Werner SL, Kearns JD, Zadorozhnaya V, Lynch C, O'Dea E, Boldin MP, Ma A, Baltimore D, Hoffmann A (2008) Encoding NF-kappaB temporal control in response to TNF: distinct roles for the negative regulators IkappaBalpha and A20. *Genes Dev* **22:** 2093-2101.

Wertz IE, O'Rourke KM, Zhou H, Eby M, Aravind L, Seshagiri S, Wu P, Wiesmann C, Baker R, Boone DL, Ma A, Koonin EV, Dixit VM (2004) De-ubiquitination and ubiquitin ligase domains of A20 downregulate NF-kappaB signalling. *Nature* **430:** 694-699.

Whiteside ST, Epinat JC, Rice NR, Israel A (1997) I kappa B epsilon, a novel member of the I kappa B family, controls RelA and cRel NF-kappa B activity. *Embo J* **16:** 1413-1426.

Wolfrum S, Teupser D, Tan M, Chen KY, Breslow JL (2007) The protective effect of A20 on atherosclerosis in apolipoprotein E-deficient mice is associated with reduced expression of NF-{kappa}B target genes. *Proc Natl Acad Sci.* **47:** 18601-18606